

JPTM

**Journal of Pathology
and Translational Medicine**

March 2019
Vol. 53 / No.2
jpatholm.org
pISSN: 2383-7837
eISSN: 2383-7845



*Frozen Cytology
of CNS Neoplasm*

Aims & Scope

The *Journal of Pathology and Translational Medicine* is an open venue for the rapid publication of major achievements in various fields of pathology, cytopathology, and biomedical and translational research. The Journal aims to share new insights into the molecular and cellular mechanisms of human diseases and to report major advances in both experimental and clinical medicine, with a particular emphasis on translational research. The investigations of human cells and tissues using high-dimensional biology techniques such as genomics and proteomics will be given a high priority. Articles on stem cell biology are also welcome. The categories of manuscript include original articles, review and perspective articles, case studies, brief case reports, and letters to the editor.

Subscription Information

To subscribe to this journal, please contact the Korean Society of Pathologists/the Korean Society for Cytopathology. Full text PDF files are also available at the official website (<http://jpathol.tn.org>). *Journal of Pathology and Translational Medicine* is indexed by Emerging Sources Citation Index (ESCI), PubMed, PubMed Central, Scopus, KoreaMed, KoMCI, WPRIM, Directory of Open Access Journals (DOAJ), and CrossRef. Circulation number per issue is 700.

Editors-in-Chief

Jung, Chan Kwon, MD (*The Catholic University of Korea, Korea*) <https://orcid.org/0000-0001-6843-3708>
Park, So Yeon, MD (*Seoul National University, Korea*) <https://orcid.org/0000-0002-0299-7268>

Senior Editors

Hong, Soon Won, MD (*Yonsei University, Korea*) <https://orcid.org/0000-0002-0324-2414>
Kim, Chong Jai, MD (*University of Ulsan, Korea*) <http://orcid.org/0000-0002-2844-9446>

Associate Editors

Shin, Eunah, MD (*CHA University, Korea*) <http://orcid.org/0000-0001-5961-3563>
Kim, Haeryoung, MD (*Seoul National University, Korea*) <http://orcid.org/0000-0002-4205-9081>

Editorial Board

Avila-Casado, Maria del Carmen (*University of Toronto, Toronto General Hospital UHN, Canada*)

Bae, Young Kyung (*Yungnam University, Korea*)

Bongiovanni, Massimo (*Lausanne University Hospital, Switzerland*)

Choi, Yeong-Jin (*The Catholic University, Korea*)

Chung, Jin-Haeng (*Seoul National University, Korea*)

Fadda, Guido (*Catholic University of Rome-Foundation Agostino Gemelli University Hospital, Italy*)

Gong, Gyungyub (*University of Ulsan, Korea*)

Ha, Seung Yeon (*Gachon University, Korea*)

Han, Jee Young (*Inha University, Korea*)

Jang, Se Jin (*University of Ulsan, Korea*)

Jeong, Jin Sook (*Dong-A University, Korea*)

Kang, Gyeong Hoon (*Seoul National University, Korea*)

Kim, Aeree (*Korea University, Korea*)

Kim, Jang-Hee (*Ajou University, Korea*)

Kim, Jung Ho (*Seoul National University, Korea*)

Kim, Kyu Rae (*University of Ulsan, Korea*)

Kim, Se Hoon (*Yonsei University, Korea*)

Kim, Woo Ho (*Seoul National University, Korea*)

Ko, Young Hyeh (*Sungkyunkwan University, Korea*)

Koo, Ja Seung (*Yonsei University, Korea*)

Lee, C. Soon (*University of Western Sydney, Australia*)

Lee, Hye Seung (*Seoul National University, Korea*)

Lkhagvadorj, Sayamaa (*Mongolian National University of Medical Sciences, Mongolia*)

Moon, Woo Sung (*Chonbuk University, Korea*)

Park, Chan-Sik (*University of Ulsan, Korea*)

Park, Young Nyun (*Yonsei University, Korea*)

Shahid, Pervez (*Aga Khan University, Pakistan*)

Sung, Chang Ohk (*University of Ulsan, Korea*)

Than, Nandor Gabor (*Semmelweis University, Hungary*)

Tse, Gary M. (*The Chinese University of Hong Kong, Hong Kong*)

Tan, Puay Hoon (*National University of Singapore, Singapore*)

Yatabe, Yasushi (*Aichi Cancer Center, Japan*)

Yoon, Sun Och (*Yonsei University, Korea*)

Bychkov, Andrey (*Chulalongkorn University, Thailand Kameda Medical Center, Japan Nagasaki University Hospital, Japan*)

Chong, Yo Sep (*The Catholic University of Korea, Korea*)

Jain, Deepali (*All India Institute of Medical Sciences, India*)

Jun, Sun-Young (*The Catholic University of Korea, Korea*)

Lai, Chiung-Ru (*Taipei Veterans General Hospital, Taiwan*)

Liu, Zhiyan (*Shandong University, China*)

Paik, Jin Ho (*Seoul National University, Korea*)

Song, Joon Seon (*University of Ulsan, Korea*)

Zhu, Yun (*Jiangsu Institution of Nuclear Medicine, China*)

Consulting Editors

Huh, Sun (*Hallym University, Korea*)

Kakudo, Kennichi (*Kindai University, Japan*)

Ro, Jae Y. (*Cornell University, The Methodist Hospital, U.S.A.*)

Ethic Editors

Choi, In-Hong (*Yonsei University, Korea*)

Statistics Editors

Kim, Dong Wook (*National Health Insurance Service Ilsan Hospital, Korea*)

Lee, Hye Sun (*Yonsei University, Korea*)

Layout Editor

Chang, Soo-Hee (*InfoLumi Co., Korea*)

Website and JATS XML File Producer

Cho, Yoonsang (*M2Community Co., Korea*)

Im, Jeonghee (*M2Community Co., Korea*)

Administrative Assistant

Jung Ji Young (*The Korean Society Of Pathologists*)

Jeon Annmi (*The Korean Society Of Cytopathology*)

Contact the Korean Society of Pathologists/the Korean Society for Cytopathology

Publishers: Lee, Kyo Young, MD, Hong, Soon Won, MD

Editors-in-Chief: Jung, Chan Kwon, MD, Park, So Yeon, MD

Published by the Korean Society of Pathologists/the Korean Society for Cytopathology

Editorial Office

Room 1209 Gwanghwamun Officia, 92 Saemunan-ro, Jongno-gu, Seoul 03186, Korea

Tel: +82-2-795-3094 Fax: +82-2-790-6635 E-mail: office@jpathol.tn.org

#1508 Renaissancetower, 14 Mallijae-ro, Mapo-gu, Seoul 04195, Korea

Tel: +82-2-593-6943 Fax: +82-2-593-6944 E-mail: office@jpathol.tn.org

Printed by iMiS Company Co., Ltd. (JMC)

Jungang Bldg. 18-8 Wonhyo-ro 89-gil, Yongsan-gu, Seoul 04314, Korea

Tel: +82-2-717-5511 Fax: +82-2-717-5515 E-mail: ml@smileml.com

Manuscript Editing by InfoLumi Co.

210-202, 421 Pangyo-ro, Bundang-gu, Seongnam 13522, Korea

Tel: +82-70-8839-8800 E-mail: infolumi.chang@gmail.com

Front cover image: Cytologic features of central nervous system neoplasms (Fig. 1). p106.

© Copyright 2019 by the Korean Society of Pathologists/the Korean Society for Cytopathology

© Journal of Pathology and Translational Medicine is an Open Access journal under the terms of the Creative Commons Attribution Non-Commercial License (<https://creativecommons.org/licenses/by-nc/4.0>).

Ⓢ This paper meets the requirements of KS X ISO 9706, ISO 9706-1994 and ANSI/NISO Z.39.48-1992 (Permanence of Paper).

This journal was supported by the Korean Federation of Science and Technology Societies Grant funded by the Korean Government.

CONTENTS

ORIGINAL ARTICLES

- 75 **Loss of Human Leukocyte Antigen Class I Expression Is Associated with Poor Prognosis in Patients with Advanced Breast Cancer**
Hong Sik Park, Uiju Cho, So Young Im, Chang Young Yoo, Ji Han Jung, Young Jin Suh, Hyun Joo Choi
- 86 **Human Leukocyte Antigen Class I and Programmed Death-Ligand 1 Coexpression Is an Independent Poor Prognostic Factor in Adenocarcinoma of the Lung**
Yeon Bi Han, Hyun Jung Kwon, Soo Young Park, Eun-Sun Kim, Hyojin Kim, Jin-Haeng Chung
- 94 **Guanabenz Acetate Induces Endoplasmic Reticulum Stress-Related Cell Death in Hepatocellular Carcinoma Cells**
Hyo Jeong Kang, Hyang Sook Seol, Sang Eun Lee, Young-Ah Suh, Jihun Kim, Se Jin Jang, Eunsil Yu
- 104 **Intraoperative Frozen Cytology of Central Nervous System Neoplasms: An Ancillary Tool for Frozen Diagnosis**
Myunghee Kang, Dong Hae Chung, Na Rae Kim, Hyun Yee Cho, Seung Yeon Ha, Sangho Lee, Jungsuk An, Jae Yeon Seok, Gie-Taek Yie, Chan Jong Yoo, Sang Gu Lee, Eun Young Kim, Woo Kyung Kim, Seong Son, Sun Jin Sym, Dong Bok Shin, Hee Young Hwang, Eung Yeop Kim, Kyu Chan Lee

CASE REPORTS

- 112 **Squamous Cell Carcinoma of the Extrahepatic Common Hepatic Duct**
Myunghee Kang, Na Rae Kim, Dong Hae Chung, Hyun Yee Cho, Yeon Ho Park
- 119 **Primary Malignant Melanoma of the Breast**
Jiwon Koh, Jihyeon Lee, So Youn Jung, Han Sung Kang, Tak Yun, Youngmee Kwon
- 125 **Coexisting Mucinous Cystic Neoplasm of the Pancreas and Type 1 Autoimmune Pancreatitis**
Mee-Jeong Kim, Tae Jun Song, Hyoung Jung Kim, Song-Cheol Kim, Myung-Hwan Kim, Seung-Mo Hong
- 129 **Adrenal Cortical Neoplasm with Uncertain Malignant Potential Arising in the Heterotopic Adrenal Cortex in the Liver of a Patient with Beckwith-Wiedemann Syndrome**
Eun Na Kim, Dong Eun Song, Hee Mang Yoon, Beom Hee Lee, Chong Jai Kim

-
- 136 **Encapsulated Papillary Thyroid Tumor with Delicate Nuclear Changes and a *KRAS* Mutation as a Possible Novel Subtype of Borderline Tumor**
Kenji Ohba, Norisato Mitsutake, Michiko Matsuse, Tatiana Rogounovitch, Nobuhiko Nishino, Yutaka Oki, Yoshie Goto, Kennichi Kakudo
- 142 **Crystal-Storing Histiocytosis with Plasma Cell Neoplasm in the Setting of Chronic Carbamazepine Exposure**
Woo Cheal Cho, Safina Hafeez, Peter Shen
- 145 **Wharton Jelly Hair in a Case of Umbilical Cord Stricture and Fetal Death**
Eun Na Kim, Jae-Yoon Shim, Chong Jai Kim
- 148 **Metastatic Insulinoma Presenting as a Liver Cyst**
Hua Li, Tony El Jabbour, Ankesh Nigam, Hwajeong Lee

Instructions for Authors for *Journal of Pathology and Translational Medicine* are available at <http://jpatholm.org/authors/authors.php>

Loss of Human Leukocyte Antigen Class I Expression Is Associated with Poor Prognosis in Patients with Advanced Breast Cancer

Hong Sik Park · Uiju Cho
So Young Im · Chang Young Yoo
Ji Han Jung · Young Jin Suh¹
Hyun Joo Choi

Departments of Hospital Pathology and ¹Surgery, St. Vincent's Hospital, College of Medicine, The Catholic University of Korea, Seoul, Korea

Received: August 9, 2018
Revised: September 21, 2018
Accepted: October 11, 2018

Corresponding Author

Hyun Joo Choi, MD
Department of Hospital Pathology, St. Vincent's Hospital, College of Medicine, The Catholic University of Korea, 93 Jungbu-daero, Paldal-gu, Suwon 16247, Korea
Tel: +82-31-249-7592
Fax: +82-31-244-6786
E-mail: chj0103@catholic.ac.kr

Background: Human leukocyte antigen class I (HLA-I) molecules play important roles in regulating immune responses. Loss or reduction of HLA-I expression has been shown to be associated with prognosis in several cancers. Regulatory T-cells (Tregs) also play critical functions in immune response regulation. Evaluation of HLA-I expression status by the EMR8-5 antibody and its clinical impact in breast cancer have not been well studied, and its relationship with Tregs remains unclear. **Methods:** We evaluated HLA-I expression and Treg infiltration by immunohistochemistry in 465 surgically resected breast cancer samples. We examined the correlation between HLA-I expression and Treg infiltration and clinicopathologic characteristics and survival analyses were performed. **Results:** Total loss of HLA-I expression was found in 84 breast cancer samples (18.1%). Univariate survival analysis revealed that loss of HLA-I expression was significantly associated with worse disease-specific survival (DSS) ($p = .029$). HLA-I was not an independent prognostic factor in the entire patient group, but it was an adverse independent prognostic factor for DSS in patients with advanced disease (stage II-IV) ($p = .031$). Treg numbers were significantly higher in the intratumoral stroma of HLA-I-positive tumors than in HLA-I-negative tumors (median 6.3 cells/high power field vs 2.1 cells/high power field, $p < .001$). However, Tregs were not an independent prognostic factor in our cohort. **Conclusions:** Our findings suggest that the loss of HLA-I expression is associated with poor prognosis in breast cancer patients, highlighting the role of HLA-I alterations in immune evasion mechanisms of breast cancer. HLA-I could be a promising marker that enables the application of more effective and precise immunotherapies for patients with advanced breast cancer.

Key Words: Breast neoplasms; HLA antigens; Major histocompatibility complex; Lymphocytes, tumor-infiltrating; T-lymphocytes, regulatory

Host immune systems can recognize and eliminate cells presenting abnormal tumor antigens, such as those against mutated oncoproteins. However, genomic instability and cancer-promoting inflammation can accelerate the acquisition of genetic and epigenetic alterations that allow cancer cells to evade the innate and adaptive immune systems.¹ One alteration that helps cancer cells escape from cytotoxic T lymphocyte recognition is the down-regulation or complete loss of human leukocyte antigen class I (HLA-I) expression, which is induced by changes in HLA-A, -B, and -C variants and the β -2-microglobulin chain.² Aberrant expression of HLA-I on cancer cells has been frequently observed in cancers of various histological types and is associated with clinical outcome.³ Aberrant expression of HLA-I ranges from loss of a single allele to complete loss of HLA-I expression.⁴ Down-regulation of HLA-I expression has also been observed in breast cancer^{2,3,5,6} and was reported in up to 85% of the primary tumors. The destruction of HLA-I-positive can-

cer cells by a specific T cell-mediated immune reaction, "T-cell immune selection," is thought to underlie HLA-I down-regulation in breast cancer.⁷

Few studies have examined the clinical implications of HLA-I expression in breast cancer, and the results have been conflicting in different subsets.^{5,8,9} Among these analyses, even fewer studies used the recently developed anti-pan HLA-I monoclonal antibody (EMR8-5), which has shown improved suitability for immunostaining formalin-fixed paraffin-embedded (FFPE) tissue.^{6,9-12}

Regulatory T cells (Tregs) are a subset of helper T lymphocytes that play an important role in tumor-induced tolerance to immune surveillance.¹³ Tregs were found to be significantly increased in the tumor stroma of several cancer types and act as immune suppressors.^{14,15} Tregs were initially characterized as CD4- and CD25-expressing cells. Further investigation demonstrated that Tregs express forkhead box protein P3 (FOXP3) and hold essential role in their development and function.¹⁶ Tregs can be specifically

detected in tissue sections by FOXP3 staining. Several studies showed that an increased number of intratumoral Tregs was associated with poor clinical outcome in breast cancer,^{8,17} while other investigations found no prognostic significance.¹⁶ Therefore, its prognostic value still remains controversial. Furthermore, few studies have examined Treg number and HLA-I expression in breast cancer.

Here we examined HLA-I expression in primary invasive breast cancer and some matched metastatic breast cancer tissues using the anti-pan HLA-I antibody EMR8-5 and investigated the possible relationship between Treg infiltration and HLA-I expression in tumors. We also explored the association between HLA-I expression with clinicopathological factors and the clinical implications of HLA-I loss in breast cancer.

MATERIALS AND METHODS

Patients and tissue samples

We collected 465 cases of invasive breast cancer from the archives of St. Vincent's Hospital, Suwon between January 2003 and December 2011. Among them, 18 cases had paired tissues of metastatic breast cancer that developed after the initial surgery. All patients underwent surgical resection and were treated according to standard treatment guidelines, as outlined during that time-frame, regarding chemotherapy and radiotherapy. Data regarding patient demographics, clinicopathological parameters and survival were retrospectively collected from hospital medical records. Pathologic stages were categorized according to the seventh edition of the TNM classification by the American Joint Committee on Cancer.¹⁸ According to the clinical characteristics, tumors in stage I were defined as early cases and those in stages II, III and IV were defined as advanced cases. All samples and medical record data were anonymized before use in this study. Formal written informed consent was not required based on a waiver by the Institutional Review Board (IRB) of St. Vincent's Hospital. The use of medical record data and tissue samples for this study was approved by the IRB (VC16SISI0214).

Construction of tissue microarray

We constructed tissue microarrays (TMAs) from 465 FFPE breast cancer blocks. A morphologically representative tumor area in each of the donor blocks was selected based on the hematoxylin and eosin (H&E)-stained sections and the site corresponding to the confirmed tumor site in the paraffin block was marked. The selected area was harvested using a 2-mm Quick-Ray tissue microarrayer device (Micro Digital Co., Seoul, Korea) and then trans-

ferred to a recipient TMA mold. One core per case was used for the construction of the TMA. One slide from each of the TMA blocks was stained with H&E to confirm the presence of tumor tissue.

Immunohistochemistry and evaluation of immunohistochemical staining

The TMA blocks were cut into 4- μ m-thick sections and mounted on precoated glass slides. Briefly, TMA sections were dried, deparaffinized and rehydrated following standard procedures. Immunohistochemistry (IHC) for HLA-I (HLA-ABC, clone EMR8-5, mouse monoclonal, 1:200 dilution, Abcam, Cambridge, MA, USA) and FOXP3 (clone 236A/E7, mouse monoclonal, 1:100 dilution, Abcam) was carried out using a Ventana NX automated IHC system (Ventana Medical Systems, Tucson, AZ, USA). Heat-induced antigen retrieval was performed using cell conditioning solution (CC1, a proprietary buffer). Normal tonsil tissues served as a positive control for all the antibodies. HLA-I expression was categorized as "negative" when there was a complete absence of HLA-I expression in the tumor cells and as "positive" when HLA-I expression was observed in any of the tumor cell membranes. HLA-I expression was also assessed according to the percentage of HLA-I positive cells in a given field: low (< 25%), intermediate (25%–75%) or high (> 75%) expression. Tregs were identified by FOXP3 staining. Lymphocytes with nuclear FOXP3 expression regardless of the intensity were counted as FOXP3-positive cells. The number of FOXP3-positive T cells was counted at the entire peritumoral area in five high power fields (HPF) per case, and the average number of cells per a HPF was calculated. Treg infiltration was categorized as "absent" when there were no FOXP3-positive T cells and as "present" when more than one FOXP3-positive T cell was observed. All slides were evaluated by two pathologists blinded to patient information.

A combination of HLA-I expression status and Treg infiltration status yielded four immunologic groups (group 1, HLA-I^{negative}/Treg^{absent}; group 2, HLA-I^{negative}/Treg^{present}; group 3, HLA-I^{positive}/Treg^{absent}; and group 4, HLA-I^{positive}/Treg^{present}) and they were analyzed for clinical significance.

Definition of breast cancer subtypes

Expressions of standard biomarkers including estrogen receptor (ER), progesterone receptor (PR), human epidermal growth factor receptor 2 (HER2), and Ki67 were evaluated from whole sections at the time of diagnosis and the results were obtained from the pathology reports. For ER and PR, an Allred method

was used for scoring and a score ≥ 3 was considered positive.¹⁹ For HER2, a score of 3+ on IHC or the presence of gene amplification on in situ hybridization was considered positive for amplification. Each of the intrinsic breast cancer subtypes was classified as follows: luminal A type (ER+ and/or PR+, HER2-, Ki67 < 14%); luminal B type (ER+ and/or PR+, HER2-, Ki67 $\geq 14\%$ or ER+ and/or PR+, HER2+); HER2-positive type (ER-/PR-/HER2+); and triple-negative type (ER-/PR-/HER2-).

Statistical analysis

The chi-square test or Fisher exact test was used to analyze the correlation between HLA-I expression and clinicopathological parameters and Student's t test was used to analyze the differences in mean values. Disease-specific survival (DSS) time was measured from the time of initial diagnosis until death specifically caused by breast cancer or until the end of follow-up. Disease-free survival (DFS) time was measured from the time of initial diagnosis until disease recurrence, progression or metastasis. Survival data were analyzed using Kaplan-Meier survival curves and the differences between curves were analyzed using log-rank tests. Multivariate analysis for the DSS and DFS were performed using the Cox proportional hazards model. Two-tailed p-values of < .05 were considered significant. Analysis and data graphing listed above were performed using SPSS ver. 21.0 (IBM Corp., Armonk, NY, USA).

RESULTS

HLA-I expression and Treg infiltration in primary tumors and their correlation with clinicopathologic factors in breast cancer patients

A total of 465 cases of invasive breast cancer were included in this study. Patients and their clinicopathological characteristics are described in Table 1. The median age of patients was 53.2 years (standard deviation, 11.8; range, 30 to 86 years). The median follow-up of patients was 62 months (range, 1 to 172 months), and 32 patients (6.9%) died from breast cancer. A total of 63 patients (13.5%) had disease progression, recurrence or metastasis after the initial diagnosis.

HLA-I expression in primary tumor cells was positive in 381 patients (81.9%) and negative in 84 patients (18.1%) (Fig. 1). In the 381 patients with positive HLA-I expression, 101 patients (26.5%) had low expression (< 25%), 74 patients (19.4%) had mid expression (25%–75%) and 206 patients (54%) had high expression (> 75%). HLA-I expression was uniformly strong in stromal cells of all the cases.

Infiltration of Tregs was generally absent or low in all 465 tumors. The median number of tumor-infiltrating Tregs was 1.8 cells/HPF (range, 0 to 91), and 123 cases (26.5%) had no Tregs.

We analyzed the correlation between HLA-I expression and Treg presence with clinicopathological features (Table 1). Loss of HLA-I expression was associated with old age, low histologic grade, low nuclear grade and luminal A intrinsic type (all $p < .05$). Presence of Treg infiltration was significantly correlated with tumors with high histologic grade, high nuclear grade, negative hormone receptor (HR) status and triple negative intrinsic type (all $p < .05$).

HLA-I expression and Treg infiltration in metastatic tumors

Of the 63 patients who developed progression, recurrence or metastasis after the primary surgery, paired metastatic tumor materials were available for 18 patients and these tissues were evaluated for HLA-I expression. Notably, patients were not treated with immunotherapy during the course of metastatic disease. In the metastatic subset, HLA-I expression was positive in 16 patients (89%) and negative in two (11%). All HLA-I positive cases showed strong expression on tumor cell membranes. Loss of HLA-I expression occurred more frequently in the primary tumor than the metastatic tumor (18.1% vs 11%, respectively), but this difference was not statistically significant ($p = .441$). There was little change in HLA-I expression between the paired primary and metastatic lesions. Only one case with loss of HLA-I expression in the primary lesion showed HLA-I expression in the metastatic lesion.

We also examined Tregs in the metastatic subset. The median number of infiltrating Tregs was 2 cells/HPF (range, 0 to 25.8) and four cases (22%) had no Tregs in the tumor microenvironment. There was no significant difference in the number of Tregs between primary and metastatic tumors ($p = .641$).

Correlation of HLA-I expression and Treg infiltration

We evaluated the correlation between HLA-I expression and Treg infiltration in primary tumors and metastatic tumors. In the primary tumors, HLA-I–negative tumors had a significantly lower number of Tregs in their tumor microenvironment than HLA-I–positive tumors (median, 2.1 cells/HPF vs 6.3 cells/HPF; $p < .001$) (Fig. 2). Likewise, when cases were categorized into absent and present Treg infiltration, the loss of HLA-I expression was significantly correlated with the absence of Treg infiltration (Table 1).

Table 1. Baseline characteristics of the patients according to the HLA-I expression and regulatory T-cell infiltration

Characteristic	Total (n=465)	HLA-I		p-value	Regulatory T cell		p-value
		Negative (n=84)	Positive (n=381)		Absent (n=123)	Present (n=342)	
Age at diagnosis (yr) ^a	53.2±11.8	55.7±12.0	52.6±11.8	.030	54.4±12.3	52.7±11.7	.190
No. of Tregs (cells/HPF) ^a	5.5±10.0	2.1±4.5	6.3±10.7	<.001	-	-	-
Sex							
Female	464 (99.8)	84 (100)	380 (99.7)	.999 ^b	122 (99.2)	342 (100)	.265 ^b
Male	1 (0.2)	0	1 (0.3)		1 (0.8)	0	
Operation							
Lumpectomy	294 (63.2)	46 (54.8)	248 (65.1)	.081	76 (61.8)	218 (63.7)	.700
Mastectomy ^c	171 (36.8)	38 (45.2)	133 (34.9)		47 (38.2)	124 (36.3)	
Multiplicity							
Solitary tumor	407 (87.5)	73 (86.9)	334 (87.7)	.856	110 (89.4)	296 (86.8)	.456
Multiple tumor	58 (12.5)	11 (13.1)	47 (12.3)		13 (10.6)	45 (13.2)	
Histologic grade							
Low (grade 1)	123 (26.5)	36 (42.9)	87 (22.8)	<.001	53 (43.1)	70 (20.5)	<.001
High (grade 2, 3)	342 (73.5)	48 (57.1)	294 (77.2)		70 (56.9)	272 (79.5)	
Nuclear grade							
Low (grade 1)	43 (9.2)	17 (20.2)	26 (6.8)	<.001	19 (15.4)	24 (7.0)	<.001
High (grade 2, 3)	422 (90.8)	67 (79.8)	355 (93.2)		104 (84.6)	318 (93.0)	
Lymphovascular invasion							
Absent	342 (73.5)	66 (78.6)	276 (72.4)	.249	91 (74.0)	251 (73.4)	.898
Present	123 (26.5)	18 (21.4)	105 (27.6)		32 (26.0)	91 (26.6)	
Perineural invasion							
Absent	424 (91.2)	78 (92.9)	346 (90.8)	.550	110 (89.4)	314 (91.8)	.424
Present	41 (8.8)	6 (7.1)	35 (9.2)		18 (10.6)	28 (8.2)	
T category							
T1	245 (52.7)	50 (59.5)	195 (51.2)	.544	72 (58.5)	172 (50.3)	.110
T2	200 (43.0)	30 (35.7)	170 (44.6)		47 (38.2)	154 (45.0)	
T3	19 (4.1)	4 (4.8)	15 (3.9)		3 (2.4)	16 (4.11)	
T4	1 (0.2)	0	1 (0.3)		1 (0.8)	0	
N category							
N0	313 (67.3)	59 (70.2)	254 (66.7)	.610	81 (65.9)	232 (67.8)	.787
N1	106 (22.8)	15 (17.9)	91 (23.9)		28 (22.8)	78 (22.8)	
N2	30 (6.5)	6 (7.1)	24 (6.3)		8 (6.5)	22 (73.3)	
N3	16 (3.4)	6 (4.8)	12 (3.1)				
Lymph node metastasis							
Absent	313 (67.3)	59 (70.2)	254 (66.7)	.528	81 (65.9)	232 (67.8)	.688
Present	152 (32.7)	25 (29.8)	127 (33.3)		42 (34.1)	110 (32.2)	
Distant metastasis							
Absent	453 (97.4)	80 (95.2)	373 (97.9)	.164	119 (96.7)	334 (97.7)	.396 ^c
Present	12 (2.6)	4 (4.8)	8 (2.1)		4 (3.3)	8 (2.3)	
AJCC stage							
I	188 (40.4)	41 (48.8)	147 (38.6)	.163	53 (43.1)	135 (39.5)	.849
II	220 (47.3)	31 (36.9)	189 (49.6)		54 (43.7)	166 (48.5)	
III	47 (10.1)	9 (10.7)	38 (10.0)		13 (10.6)	34 (9.95)	
IV	10 (2.2)	3 (3.6)	7 (1.8)		3 (2.4)	7 (2.0)	
ER status							
Negative	182 (39.1)	33 (39.3)	149 (39.1)	.976	35 (28.5)	147 (43.0)	.005
Positive	283 (60.9)	51 (60.7)	232 (60.9)		88 (71.5)	195 (57.0)	
PR status							
Negative	213 (45.8)	37 (44.0)	176 (46.2)	.721	45 (36.6)	168 (49.1)	.017
Positive	252 (54.2)	47 (56.0)	205 (53.8)		78 (63.4)	174 (50.9)	
HER2 status							
Negative	333 (71.6)	64 (76.2)	269 (70.6)	.304	94 (76.4)	239 (69.9)	.168
Positive	132 (28.4)	20 (23.8)	112 (29.4)		29 (23.6)	103 (30.1)	

(Continued to the next page)

Table 1. Continued

Characteristic	Total (n=465)	HLA-I		p-value	Regulatory T cell		p-value
		Negative (n=84)	Positive (n=381)		Absent (n=123)	Present (n=342)	
Intrinsic subtype							
Luminal A	194 (41.7)	46 (54.8)	148 (38.8)	.014	69 (56.1)	125 (36.5)	.001
Luminal B	116 (24.9)	11 (9.5)	105 (27.6)		25 (20.3)	91 (26.6)	
HER2	70 (15.1)	14 (16.7)	56 (14.7)		16 (13.0)	54 (15.8)	
Triple negative	85 (18.3)	13 (15.5)	72 (18.9)		13 (10.6)	72 (21.1)	
Hormone receptor							
Negative	155 (33.3)	27 (32.1)	128 (33.6)	.798	29 (23.6)	126 (36.8)	.007
Positive	310 (66.7)	57 (67.9)	253 (66.4)		94 (76.4)	216 (63.2)	
Treatment							
Neo-adjuvant chemotherapy	16 (3.4)	82 (97.6)	367 (96.3)	.748 ^b	116 (94.3)	333 (97.4)	.099 ^b
Surgery alone	449 (96.6)	2 (2.4)	14 (3.7)		7 (5.7)	9 (2.6)	
Regulatory T cell							
Absent	123 (26.5)	37 (44.0)	86 (22.6)	<.001	-	-	
Present	342 (73.5)	47 (56.0)	295 (77.4)		-	-	

Values are presented as mean±standard deviation or number (%).

HLA-I, human leukocyte antigen class I; Treg, regulatory T cell; HPF, high-power field; AJCC, American Joint Committee on Cancer; ER, estrogen receptor; PR, progesteron receptor; HER2, human epidermal growth factor receptor 2.

^aStudent's t test was used for comparison between the two group; ^bFisher exact test was used for comparison of between the two groups; ^cThis variable includes modified radical mastectomy and radical mastectomy.

Prognostic significance of HLA-I expression and Treg infiltration in the total patient group

Univariate analysis demonstrated that lymphovascular invasion ($p = .001$), perineural invasion ($p = .002$), distant metastasis ($p < .001$), T category ($p < .001$), N category ($p < .001$), lymph node metastasis ($p = .002$), and HLA-I expression ($p = .029$) (Fig. 3A) were associated with DSS. The presence of Tregs and immunologic group by HLA/Treg status were not associated with DSS ($p = .102$ and $p = .080$, respectively). In the multivariate analysis, only distant metastasis ($p = .032$) was an independent prognostic factor for DSS (Table 2). In the univariate analysis for DFS, lymphovascular invasion ($p = .034$), distant metastasis ($p < .001$), T category ($p < .001$), N category ($p < .001$), and histologic grade ($p = .003$) were significantly associated among the clinicopathological features. In the multivariate analysis for DFS, distant metastasis ($p = .001$), T category ($p = .003$), and histologic grade ($p = .015$) remained as independent prognostic factors (Table 2). HLA-I ($p = .863$) (Fig. 3B), Treg ($p = .347$), and immunologic group by HLA/Treg ($p = .695$) were not associated with DFS.

Prognostic significance of HLA-I expression and Treg infiltration in the advanced disease group

Of the 277 patients with advanced disease (American Joint Committee on Cancer stage II–IV), 27 patients (9.7%) died of breast cancer and 53 (19.1%) experienced disease recurrence or progression during the follow-up period. Positive HLA-I expres-

sion and Treg infiltration was observed in 84.5% (234/277) and 74.7% (207/277) of the cases, respectively. Among the clinicopathological features, HLA-I expression ($p = .007$) (Fig. 3C), perineural invasion ($p = .001$), distant metastasis ($p < .001$), T category ($p < .001$), and N category ($p < .001$) were associated with DSS in the univariate analysis. Based on the multivariate analysis, patients with negative HLA-I expression ($p = .034$), distant metastasis ($p = .026$), and high N category ($p = .034$) had worse DSS (Table 2). However, in the univariate analysis for DFS, perineural invasion ($p = .005$), distant metastasis ($p < .001$), T category ($p < .001$), and N category ($p < .001$) were the only features that were significantly associated with the survival (Table 2), and HLA-I showed no prognostic significance ($p = .506$) (Fig. 3D).

Prognostic significance of HLA-I expression and Treg infiltration in intrinsic subtypes

We also performed subgroup analysis according to HR status and intrinsic subtypes. In the 155 patients with HR-negative tumors, 18.7% (29/155) had no peritumor Treg infiltration. Univariate analysis showed that tumors with Treg infiltration had better DSS than tumors without Treg infiltration (mean survival duration, 158.6 months vs. 106.3 months, respectively; $p = .044$). Other clinicopathological features that were significantly associated with DSS were perineural invasion ($p = .001$), distant metastasis ($p < .001$), T category ($p < .001$), and N category ($p = .032$). HLA-I expression ($p = .227$) and the immunologic

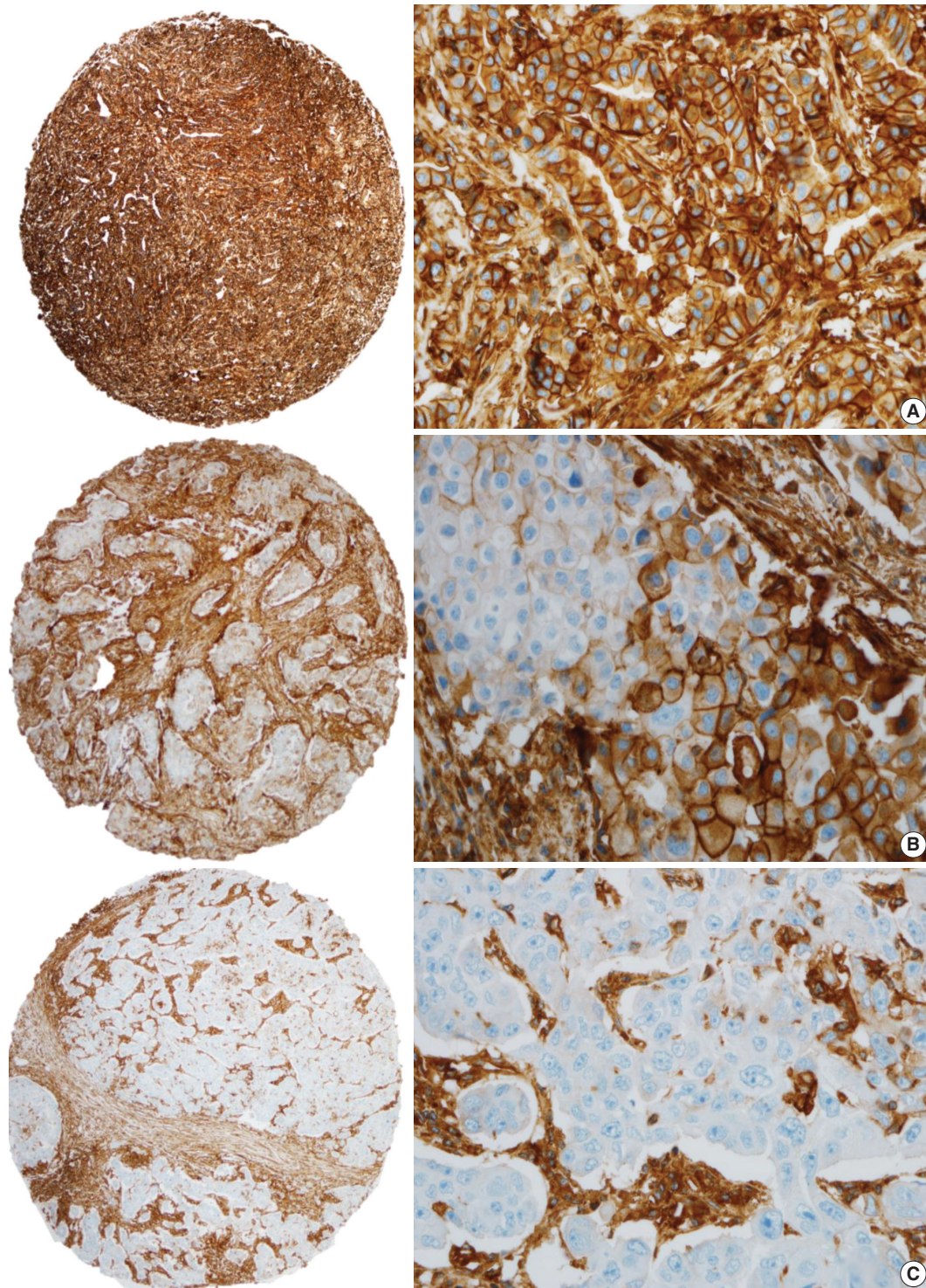


Fig. 1. Immunohistochemical staining of breast cancer tissues with anti-human leukocyte antigen class I (HLA-I) antibody. (A) Most of the HLA-I-positive cases showed a strong and diffuse membranous expression of HLA-I in breast cancer. In a HLA-I-positive case, the tumor cell membranes are completely stained with HLA-I. (B) A tumor with intermediate HLA-I expression (25%–75%) shows a heterogeneous staining pattern with a range of intensity. Partial loss of HLA-I expression in tumor cells is observed. (C) HLA-I-negative cases showed complete loss of HLA-I in breast cancer cells. Only the stromal cells are strongly stained and tumor cells are absent for HLA-I expression in cell membranes.

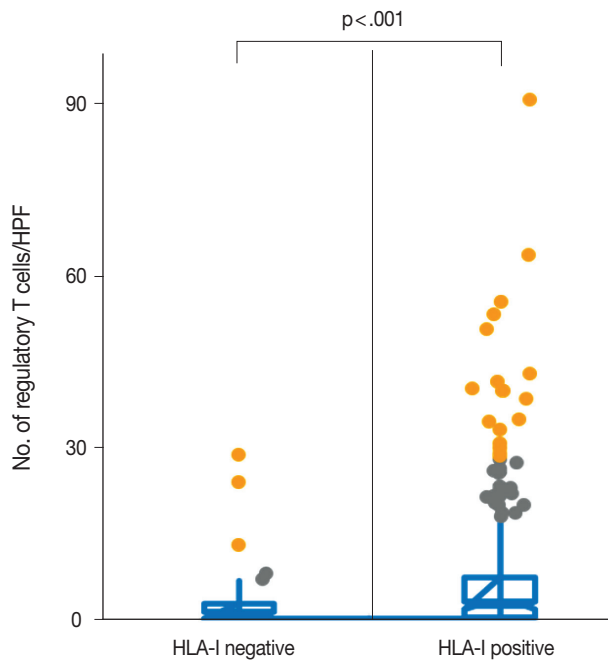


Fig. 2. The mean number of regulatory T lymphocytes in the human leukocyte antigen class I (HLA-I)-negative and HLA-I-positive tumors was 2.1 cells/high-power field (HPF) and 6.3 cells/HPF, respectively. There was a statistically significant difference in the regulatory T cell infiltration between the two groups ($p < .001$).

group by combination of HLA/Treg status ($p = .080$) were not associated with DSS in the HR-negative group. In the multivariate analysis, Treg infiltration had no statistically significant association with DSS after adjusting for other clinicopathological factors ($p = .317$). In univariate analysis for DFS, only nuclear grade ($p = .010$), lymphovascular invasion ($p = .004$), perineural invasion ($p < .001$), distant metastasis ($p = .001$), and T category ($p < .001$) were significantly associated with clinical outcome, but immunologic markers (e.g., HLA-I, Treg, immunologic group by combination of HLA/Treg status) had no prognostic significance.

When the HR-negative group was categorized into the HER2-positive subtype and triple negative subtype, HLA-I status and Treg infiltration had no significant impact on clinical outcomes in both groups (all $p > .05$ for DSS and DFS). The DSS of the patients with HER2-positive breast cancer based on HLA/Treg was not statistically evaluable due to non-occurrence of patient death during the study period in some subgroups. There was no difference between the HLA/Treg groups for other clinical outcomes in patients with the HER2-positive subtype and triple negative subtype (all $p > .05$).

In the HR-positive group, Treg infiltration and HLA-I expression had no prognostic significance with respect to DSS and DFS (all $p > .05$). In both luminal A and luminal B subtypes, Treg

infiltration and HLA-I expression also had no prognostic significance with respect to DSS and DFS (all $p > .05$).

DISCUSSION

Several fundamental changes in cell physiology are considered hallmarks of cancer. One of these hallmarks is the ability of cancer cells to evade the host immune response. The host immune system can recognize and eliminate cells presenting abnormal tumor antigens, such as those against mutated oncoproteins. Altered HLA-I expression in tumor cells is one of the mechanisms that contributes to immune system evasion.³ The infiltration of Tregs is a host response to abnormal tumor antigens.¹⁶

In the present study, we found that 18.1% of the 465 primary breast cancer tissues showed total loss of HLA-I expression, which was correlated with decreased Treg infiltration. We found that a total loss of HLA-I expression was an unfavorable prognostic factor in the overall patient group as well as in the advanced disease group. A negative prognostic role for Tregs in breast cancer has been reported.¹⁷ However, Treg infiltration was not a significant prognostic factor in our study.

Little is known about the utility of the anti-pan HLA class I antibody EMR8-5 in breast cancer. EMR8-5 was first developed by a group led by Sato and can recognize denatured antigens in FFPE tissues.⁶ Most anti-HLA antibodies detect the heterodimeric structure of a β -microglobulin with a heavy chain or the native, allele-specific structure of HLA-I molecules. Unlike other anti-HLA-I antibodies (e.g., HC10 and HCA2) that show specificity to either HLA-A or -B/-C alleles, EMR8-5 reacts with all 17 types of HLA-A, -B, and -C alleles in FFPE tissues.⁶ The conflicting results on the prognostic impact of HLA-I could arise from the different anti-HLA-I antibodies and varying specificity.⁵ In the present study, we provide compelling evidence using the EMR8-5 antibody that loss of HLA-I expression is a marker of poor prognosis in breast cancer patients. Patients with HLA-I-negative breast cancers had significantly worse prognosis compared with the patients with positive HLA-I expression ($p = .029$) as determined by univariate analysis. Furthermore, HLA-I itself was a significant prognostic factor for DSS without association of TNM factors in patients with advanced disease stages (stage II, III, and IV). Two of the four previous studies conducted with EMR8-5 demonstrated a significant association of HLA-I expression and DFS in breast cancer.^{9,10} However, after adjusting for other clinicopathological features in these studies, HLA-I was not a significant prognostic marker. Along with the previous results, our data suggest that the negative prognostic impact of

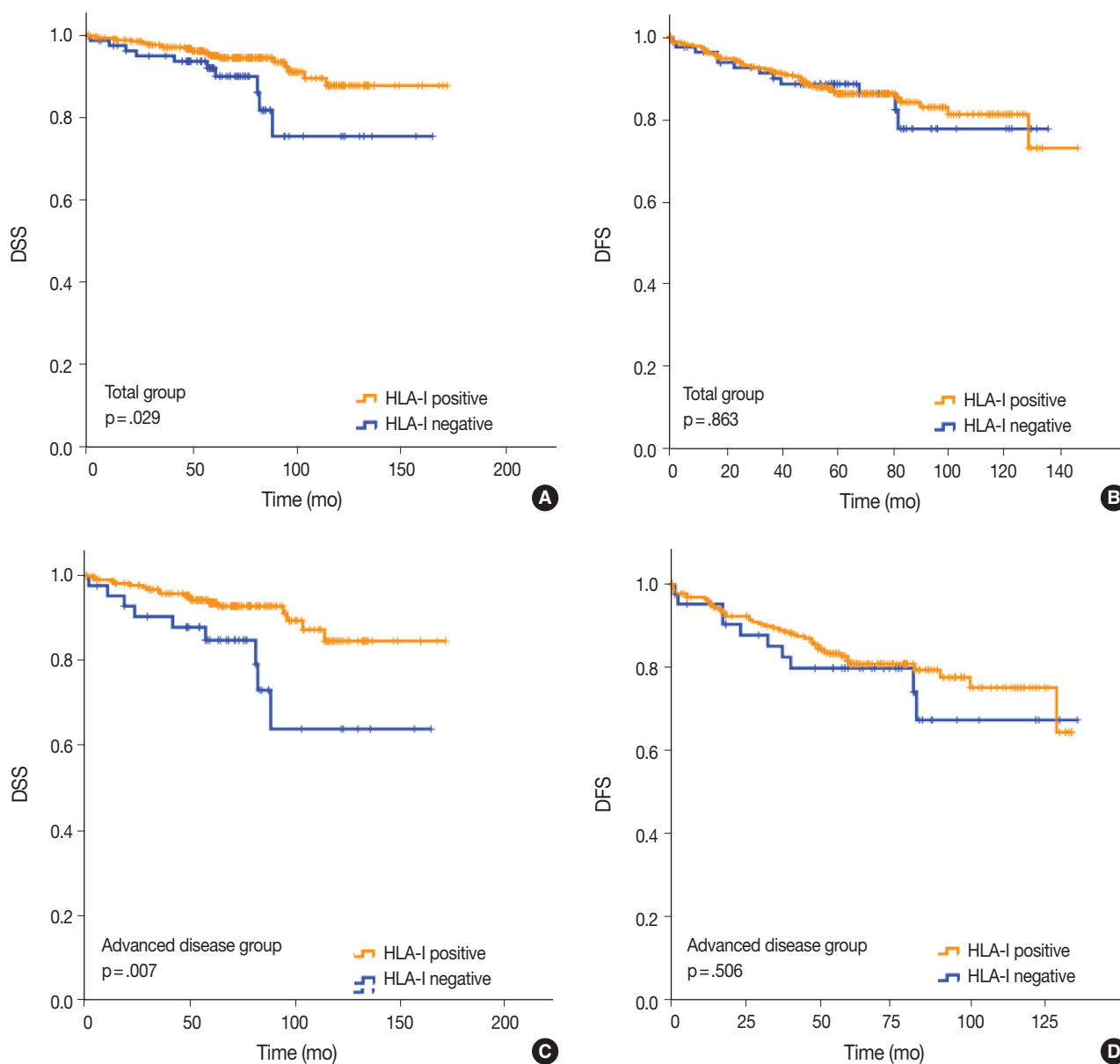


Fig. 3. (A) Disease-specific survival (DSS) of all patients with breast cancer based on human leukocyte antigen class I (HLA-I) expression ($p = .029$). (B) Disease-free survival (DFS) of all patients with breast cancer based on HLA-I expression ($p = .863$). (C) DSS of the patient subgroup with stage II–IV breast cancer based on HLA-I expression ($p = .007$). (D) DFS of the patient subgroup with stage II–IV breast cancer based on HLA-I expression ($p = .506$).

HLA-I alteration may not be sufficient to alter the clinical course in the stage I group, which has good prognosis and with a 5-year relative survival rate of nearly 100%. However, HLA-I expression was significantly associated with prognosis in the advanced stage group.¹⁰ The exact mechanism of HLA-I down-regulation and its association with prognosis is still unclear, and clarifying of the underlying mechanism in future studies may lead to novel therapeutic strategies for breast cancer.

In the current study, we also examined the relationship between

HLA-I expression and Treg infiltration, as this has not been explored. The number of tumor-infiltrating lymphocytes, although not specifically Tregs, was positively correlated with HLA expression in breast cancer.⁹ Immune-suppressing Tregs might consider HLA-I–positive tumor cells as normal cells and infiltrate to suppress immune attack, or tumor cells may influence Tregs to evade immune attack by effector T cells.⁸ In our study, the number of infiltrating Tregs was positively correlated with HLA-I expression in tumor cells. Regarding an association between loss of

Table 2. Multivariate analysis for disease-specific survival and disease-free survival

Variable	Total patient group (n=465)						Advanced breast cancer group (stage II, III, IV) (n=277)					
	Disease-specific survival			Disease-free survival			Disease-specific survival			Disease-free survival		
	Relative risk	Hazard ratio (95% CI)	p-value	Relative risk	Hazard ratio (95% CI)	p-value	Relative risk	Hazard ratio (95% CI)	p-value	Relative risk	Hazard ratio (95% CI)	p-value
HLA-I expression	0.472	0.216–1.030	.059	-	-	-	0.407	0.177–0.936	.034	-	-	-
Lymphovascular invasion	0.999	0.371–2.688	.998	0.760	0.386–1.495	.426	-	-	-	-	-	-
Perineural invasion	1.518	0.622–3.704	.359	1.345	0.663–2.729	.412	1.682	0.664–4.266	.273	1.572	0.751–3.288	.230
Distant metastasis (M1)	3.847	1.123–13.179	.032	5.027	1.928–13.103	.001	3.884	1.177–12.822	.026	4.586	1.784–11.786	.002
T category (reference 1)			.067			.003			.163			.045
2	1.591	0.667–3.794	.295	1.820	1.013–3.269	.045	0.931	0.328–2.646	.894	1.053	0.487–2.276	.896
3	2.174	0.566–8.358	.258	1.328	0.395–4.470	.646	1.303	0.310–5.471	.718	0.873	0.241–3.158	.835
4	28.399	2.330–346.135	.009	76.642	6.085–965.396	.001	15.085	1.209–188.252	.035	35.171	2.677–462.078	.007
N category (reference 0)			.056			.115			.034			.210
1	1.037	0.346–3.107	.949	1.189	0.600–2.357	.619	0.780	0.243–2.501	.677	0.700	0.340–1.439	.331
2	3.262	1.081–9.848	.036	2.391	1.037–5.513	.041	2.628	0.924–7.476	.070	1.417	0.638–3.148	.392
3	5.531	1.276–23.974	.022	3.098	0.968–9.917	.057	4.331	1.262–14.867	.020	2.139	0.776–5.892	.141
Histologic grade (grade 1 vs 2, 3)	-	-	-	2.753	1.219–6.218	.015	-	-	-	-	-	-

Values of $p < .05$ in the univariate analysis were included in a multivariate analysis. CI, confidence interval; HLA-I, human leukocyte antigen class I.

HLA-I expression and lower number of Tregs, HLA-I-negative tumors may have a lower density of tumor-infiltrating lymphocytes than HLA-I-positive tumors, because they are usually low-grade, luminal A tumors. Our finding on the correlation between HLA-I expression and Tregs is in agreement with results of previous studies in breast cancer¹² and gastric cancer.¹⁴ Further study is needed to reveal the underlying mechanism of the Treg and HLA-I interaction in cancers.

Total loss of HLA-I expression was less frequent in the metastatic tumors than in the primary tumors in our study (18.1% vs 11%). Although this difference was not statistically significant, it may contradict our hypothesis that metastatic tumors would lose HLA-I expression during cancer progression. Limited studies have been conducted on the sequential development of metastases over time. In addition, it is not clear how HLA-I loss variants are generated in primary tumors and how they correlate with metastatic capacity. Previous studies on breast cancer²⁰ and osteosarcoma²¹ suggested that metastases may not selectively originate from a subclone of tumor cells that acquired HLA loss in the primary site (“acquired” phenotype), but rather that tumors with inherent defects in HLA expression may have an advantage in metastasizing (“inherent” phenotype), which ultimately leads to poor survival. Our data also support the inherent phenotype hypothesis, but the small number of metastatic tumors and heterogeneous nature of cancer should be considered when interpreting this data. Further prospective investigations are needed to examine this hypothesis.

Some evidence has indicated that the presence of Tregs in the tumor microenvironment is an adverse prognostic marker in cancer.^{14,16} Considering the immunological nature of the interaction between HLA-I expression and Treg status, we hypothesized that the combination of these two markers would more accurately stratify prognostic groups. Our data, however, showed that Treg status had no independent prognostic value in the total group and subgroup analyses. A better understanding of the biological characteristics of Tregs in different tumor microenvironments is required to maximize their potential utility in tumor immunotherapy and to not oversimplify their role.

Recently, deleterious mutations in the gene encoding β -2-microglobulin were found in melanoma and lung cancer tissues with acquired resistance to programmed death-ligand 1 inhibitors. Based on these findings, defects in the antigen presentation pathway were suggested as a mechanism of resistance to immune checkpoint inhibitors.^{22,23} This suggests the possibility that the expression and functional integrity of HLA antigens and related molecules in breast cancer could be a critical measure by which to choose candidate patients for immune checkpoint inhibitors in the future. Furthermore, restoring HLA expression could possibly prevent resistance to immunotherapy.²⁴ Continuing research on this matter may be beneficial to advanced cancer patients.

This study has several limitations. Although we analyzed a large cohort, our study has the potential for selection bias because it is a retrospective study. Moreover, heterogeneity of HLA-I expression within each tumor may reduce the reliability of assess-

ment results. Additional studies with whole tissue sections and a prospective design will be helpful in verifying the prognostic role of HLA-I in breast cancer.

In conclusion, we showed that the status of HLA-I expression is closely related to Treg infiltration and affects breast cancer patient survival, especially in patients with advanced disease. In the era of immunotherapy, HLA-I may be a promising prognostic marker and enable the application of more effective and precise immunotherapies for patients with advanced breast cancer.

ORCID

Hong Sik Park: <https://orcid.org/0000-0003-0888-0711>
 Uiju Cho: <https://orcid.org/0000-0002-6229-8418>
 So Young Im: <https://orcid.org/0000-0002-5712-9003>
 Chang Young Yoo: <https://orcid.org/0000-0001-7225-9896>
 Ji Han Jung: <https://orcid.org/0000-0003-4191-4055>
 Young Jin Suh: <https://orcid.org/0000-0001-8281-198X>
 Hyun Joo Choi: <https://orcid.org/0000-0003-2292-424X>

Author Contributions

Conceptualization: HJC.
 Data curation: HSP, UC, HJC.
 Formal analysis: HSP, UC, HJC.
 Funding acquisition: HJC.
 Investigation: HSP, UC, HJC.
 Methodology: HSP, UC, SYI, CYI, JHJ, HJC.
 Project administration: HJC.
 Resources: HJC.
 Supervision: HJC.
 Validation: SYI, CYI, JHJ, YJS, HJC.
 Visualization: HSP, UC, HJC.
 Writing—original draft: HSP, UC, HJC.
 Writing—review & editing: HSP, UC, HJC.

Conflicts of Interest

The authors declare that they have no potential conflicts of interest.

Acknowledgments

This study was funded by the St. Vincent's Hospital Research Institute of Medical Science Foundation (SVHR-2016-13).

REFERENCES

1. Hanahan D, Weinberg RA. Hallmarks of cancer: the next generation.

Cell 2011; 144: 646-74.

2. Aptsiauri N, Cabrera T, Garcia-Lora A, Lopez-Nevot MA, Ruiz-Cabello F, Garrido F. MHC class I antigens and immune surveillance in transformed cells. *Int Rev Cytol* 2007; 256: 139-89.
3. Hicklin DJ, Marincola FM, Ferrone S. HLA class I antigen down-regulation in human cancers: T-cell immunotherapy revives an old story. *Mol Med Today* 1999; 5: 178-86.
4. Garrido F, Ruiz-Cabello F, Cabrera T, et al. Implications for immunosurveillance of altered HLA class I phenotypes in human tumours. *Immunol Today* 1997; 18: 89-95.
5. Madjd Z, Spendlove I, Pinder SE, Ellis IO, Durrant LG. Total loss of MHC class I is an independent indicator of good prognosis in breast cancer. *Int J Cancer* 2005; 117: 248-55.
6. Torigoe T, Asanuma H, Nakazawa E, et al. Establishment of a monoclonal anti-pan HLA class I antibody suitable for immunostaining of formalin-fixed tissue: unusually high frequency of down-regulation in breast cancer tissues. *Pathol Int* 2012; 62: 303-8.
7. Chang CC, Campoli M, Restifo NP, Wang X, Ferrone S. Immune selection of hot-spot beta 2-microglobulin gene mutations, HLA-A2 allospecificity loss, and antigen-processing machinery component down-regulation in melanoma cells derived from recurrent metastases following immunotherapy. *J Immunol* 2005; 174: 1462-71.
8. de Kruijf EM, van Nes JG, Sajet A, et al. The predictive value of HLA class I tumor cell expression and presence of intratumoral Tregs for chemotherapy in patients with early breast cancer. *Clin Cancer Res* 2010; 16: 1272-80.
9. Lee HJ, Song IH, Park IA, et al. Differential expression of major histocompatibility complex class I in subtypes of breast cancer is associated with estrogen receptor and interferon signaling. *Oncotarget* 2016; 7: 30119-32.
10. Kaneko K, Ishigami S, Kijima Y, et al. Clinical implication of HLA class I expression in breast cancer. *BMC Cancer* 2011; 11: 454.
11. Lee HJ, Kim JY, Park IA, et al. Prognostic significance of tumor-infiltrating lymphocytes and the tertiary lymphoid structures in HER2-positive breast cancer treated with adjuvant trastuzumab. *Am J Clin Pathol* 2015; 144: 278-88.
12. Chung YR, Kim HJ, Jang MH, Park SY. Prognostic value of tumor infiltrating lymphocyte subsets in breast cancer depends on hormone receptor status. *Breast Cancer Res Treat* 2017; 161: 409-20.
13. Vinay DS, Ryan EP, Pawelec G, et al. Immune evasion in cancer: mechanistic basis and therapeutic strategies. *Semin Cancer Biol* 2015; 35 Suppl: S185-98.
14. Ishigami S, Arigami T, Uenosono Y, et al. Cancerous HLA class I expression and regulatory T cell infiltration in gastric cancer. *Cancer Immunol Immunother* 2012; 61: 1663-9.
15. Curiel TJ, Coukos G, Zou L, et al. Specific recruitment of regulatory

- T cells in ovarian carcinoma fosters immune privilege and predicts reduced survival. *Nat Med* 2004; 10: 942-9.
16. deLeeuw RJ, Kost SE, Kakal JA, Nelson BH. The prognostic value of FoxP3+ tumor-infiltrating lymphocytes in cancer: a critical review of the literature. *Clin Cancer Res* 2012; 18: 3022-9.
 17. Bates GJ, Fox SB, Han C, et al. Quantification of regulatory T cells enables the identification of high-risk breast cancer patients and those at risk of late relapse. *J Clin Oncol* 2006; 24: 5373-80.
 18. Edge SB, Byrd DR, Compton CC, Fritz AG, Greene FL, Trotti A. *AJCC cancer staging manual*. 7th ed. New York: Springer, 2010.
 19. Allred DC, Harvey JM, Berardo M, Clark GM. Prognostic and predictive factors in breast cancer by immunohistochemical analysis. *Mod Pathol* 1998; 11: 155-68.
 20. Liu Y, Komohara Y, Domenick N, et al. Expression of antigen processing and presenting molecules in brain metastasis of breast cancer. *Cancer Immunol Immunother* 2012; 61: 789-801.
 21. Tsukahara T, Kawaguchi S, Torigoe T, et al. Prognostic significance of HLA class I expression in osteosarcoma defined by anti-pan HLA class I monoclonal antibody, EMR8-5. *Cancer Sci* 2006; 97: 1374-80.
 22. Gettinger S, Choi J, Hastings K, et al. Impaired HLA class I antigen processing and presentation as a mechanism of acquired resistance to immune checkpoint inhibitors in lung cancer. *Cancer Discov* 2017; 7: 1420-35.
 23. Zaretsky JM, Garcia-Diaz A, Shin DS, et al. Mutations associated with acquired resistance to PD-1 blockade in melanoma. *N Engl J Med* 2016; 375: 819-29.
 24. Del Campo AB, Carretero J, Muñoz JA, et al. Adenovirus expressing beta2-microglobulin recovers HLA class I expression and antitumor immunity by increasing T-cell recognition. *Cancer Gene Ther* 2014; 21: 317-32.

Human Leukocyte Antigen Class I and Programmed Death-Ligand 1 Coexpression Is an Independent Poor Prognostic Factor in Adenocarcinoma of the Lung

Yeon Bi Han¹ · Hyun Jung Kwon¹
Soo Young Park¹ · Eun-Sun Kim¹
Hyojin Kim¹ · Jin-Haeng Chung^{1,2}

¹Department of Pathology, Seoul National University Bundang Hospital, Seongnam;

²Department of Pathology, Seoul National University College of Medicine, Seoul, Korea

Received: July 20, 2018

Revised: December 1, 2018

Accepted: December 26, 2018

Corresponding Author

Jin-Haeng Chung, MD, PhD
Department of Pathology, Seoul National University Bundang Hospital, 82 Gumi-ro 173beon-gil, Bundang-gu, Seongnam 13620, Korea
Tel: +82-31-787-7713
Fax: +82-31-787-4012
E-mail: chungjh@snu.ac.kr

Background: Both human leukocyte antigen (HLA) class I and programmed death-ligand 1 (PD-L1) molecules are known to play important roles in cancer immunity. In this study, we evaluated HLA class I expression in resected adenocarcinoma of the lung, and investigated its prognostic impact in correlation with PD-L1 expression. **Methods:** HLA class I and PD-L1 expression was evaluated by immunohistochemistry in a total of 403 resected lung adenocarcinomas using tissue microarray. Correlations between the expression of HLA class I/PD-L1 and clinicopathologic features and prognostic significance were analyzed. **Results:** HLA class I expression was reduced in 91.6% of adenocarcinoma, and more frequently reduced in patients with younger age, absence of vascular invasion, and low pathologic stage ($p = .033$, $p = .007$, and $p = .012$, respectively). Positive PD-L1 expression in tumor cells was 16.1% (1% cut-off), and associated with poor differentiation, presence of vascular invasion and nodal metastasis ($p < .001$, $p = .002$, and $p = .032$, respectively). On survival analysis, HLA class I or PD-L1 expression alone did not show any statistical significance. On the integrated analysis, HLA class I (+)/PD-L1 (+) subgroup showed a significantly shorter overall survival than other groups ($p = .001$). Multivariate analysis revealed that coexpression of HLA class I and PD-L1 was an independent poor prognostic factor of lung adenocarcinoma. ($p < .001$; hazard ratio, 6.106; 95% confidence interval, 2.260 to 16.501). **Conclusions:** Lung adenocarcinoma with coexpression of HLA class I and PD-L1 was associated with poor prognosis. This subgroup may evade immune attack by expressing PD-L1 protein despite HLA expression.

Key Words: Human leukocyte antigen class I; Programmed cell death-ligand 1; Carcinoma, non-small cell lung; Immunohistochemistry

Lung cancer is a leading cause of cancer-related deaths worldwide. Despite many advances in targeted therapy based on molecular testing,¹ the 5-year overall survival (OS) for advanced lung cancer still remains dismal.² Recently, there has been a remarkable progress in immunotherapies for the treatment of non-small cell lung cancer (NSCLC). Immunotherapy with antibodies blocking immune checkpoints, including anti-programmed death ligand-1 (PD-L1), showed durable tumor regression in advanced NSCLCs.³ Although PD-L1 expression has emerged as a useful biomarker capable of predicting which patients are more likely to respond to anti-programmed death-1 (PD-1)/PD-L1 therapy, PD-L1 expression is not an absolute predictive marker of clinical response. These findings have intrigued researchers to characterize the host's immune response against tumor, as well as tumor's ability to escape the immune attack.

In lung cancer, cytotoxic lymphocytes (CTLs) that play a main role in the anticancer response are actively suppressed in

tumor environment.⁴ Two major mechanisms, which affect the target cells and the effector phase of the immune response, play a crucial role in the immune editing process. One is represented by the down-regulation of tumor antigen processing and presentation caused by abnormalities in the human leukocyte antigen (HLA) class I antigen processing machinery (APM).⁵ The other is represented by the anergy of effector immune cell infiltrates in the tumor microenvironment caused by aberrant inhibitory signals such as immune checkpoint receptor ligands, PD-L1.⁵ These two mechanisms, the expression of PD-L1 and the down-regulation of HLA class I by tumor cells, are also crucial factors for the tumor development process.

Although defects in HLA class I APM components are known to be associated with a reduced OS in various types of cancer,⁶ the prognostic value of HLA class I expression in NSCLC is still controversial.⁷⁻⁹ Only limited data are available on the correlation between the expression of PD-L1 and HLA-I in NSCLC.⁷

To better understand the importance of the PD-L1 and HLA class I expression in lung adenocarcinoma (ADC), we investigated their expression in lung ADC by immunohistochemistry (IHC) and correlated with clinicopathologic features including progression-free survival (PFS) and OS.

MATERIALS AND METHODS

Patients and samples

Our cohort consisted of 403 patients with lung ADC who underwent curatively intended surgical resection between May 2003 and December 2012 at Seoul National University Bundang Hospital. None received preoperative chemotherapy or radiation therapy. Clinico-pathological information was obtained from electronic medical records and pathology reports. The pathologic staging was based on the seventh edition of the American Joint Committee on Cancer staging manual.¹⁰ The study protocol was approved by the Institutional Review Board of Seoul National University Bundang Hospital (B-1704/393-303). Informed consent was waived.

Construction of tissue microarray

Hematoxylin and eosin (H&E)-stained slides were reviewed in each case to confirm the original diagnosis and classify the histologic subtype according to 2015 World Health Organization

criteria.¹¹ The slides were independently reviewed by two pathologists (H. Kim and J.H. Chung) to select the most representative sections. The most representative tumor area was carefully marked on the H&E-stained slide of each sample tissue. A tissue microarray (TMA) was constructed using 2-mm diameter cores derived from the representative tumor areas selected at random of the formalin-fixed paraffin-embedded tissue blocks from each case by SuperBioChips Laboratories (Seoul, Korea).

Immunohistochemical analysis

TMA sections were sectioned at a thickness of 4- μ m and stained using an anti-HLA class I ABC antibody (EMR8-5, ab70328, Abcam, Cambridge, MA, USA). Briefly, the slides were stained with an anti-HLA class I ABC (EMR8-5) mouse monoclonal antibody with Ventana BenchMark XT Staining systems (Tucson, AZ, USA). Expressions of HLA class I were assessed by two pathologists (Y.B. Han and J.H. Chung). The expression level of HLA class I on tumor cells was defined as strongly positive (“retained” expression) when tumor cells for which the membrane was strongly and homogeneously stained at the same level as stromal lymphocytes or endothelial cells comprised $\geq 75\%$ of tumor cells (Fig. 1A), weakly positive for 25%–74%, or tumor cells with the membrane stained more weakly than stromal lymphocytes or endothelial cells comprising $\geq 25\%$ (Fig. 1B), and negative when stained cells comprised $< 25\%$ (Fig. 1C). Cases with negative or

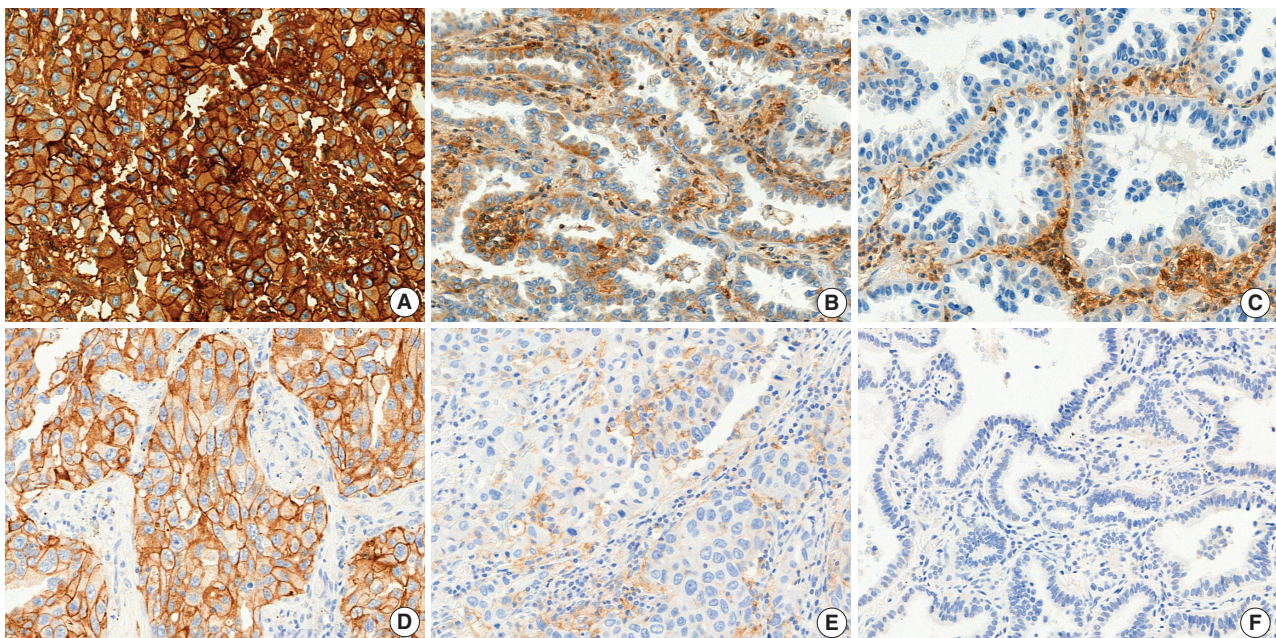


Fig. 1. Human leukocyte antigen (HLA) class I (A–C) and programmed death-ligand 1 (PD-L1) (D–E) expression in lung adenocarcinoma. (A) Strongly positive (“retained”) staining of HLA class I in tumor cells. (B) Weakly positive staining of HLA class I. (C) Negative staining of HLA class I. (D) $\geq 50\%$ positive staining of PD-L1 in tumor cells. (E) 1%–49% positive staining of PD-L1. (F) $< 1\%$ staining of PD-L1.

weakly positive staining were judged as representing “reduced” expression.

PD-L1 expression had been evaluated in a previous study with IHC using anti-PD-L1 22C3 mouse monoclonal primary antibody with the EnVision FLEX visualization system on a Dako Autostainer Link 48 system (Carpinteria, CA, USA).¹² Each tumor cell was judged as positive staining for PD-L1 when the membrane was stained at any intensity. Each patient was classified into “negative” or “positive” according to the percentage of PD-L1 positive tumor cells; two different cut-off values (1% and 50%) used on the basis of the published association of this cutoff with anti-PD-1 therapeutic response (Fig. 1D–F).¹³

Statistical analysis

The chi-square test (or Fisher exact test when appropriate) was used to assess the significance of the association of HLA class I and PD-L1 expression with clinicopathological parameters. A Kaplan-Meier analysis was performed to construct survival curves and statistical significance was assessed using the log-rank test. A multivariate analysis was performed by Cox proportional hazards regression modeling. All statistical tests were two sided and statistical significance was accepted for p-values of < .05. All statistical analysis was carried out using Statistical Package for the Social Sciences ver. 21 (IBM Corp., Armonk, NY, USA).

RESULTS

Clinicopathologic characteristics

The clinicopathological features and IHC results of the patients are summarized in Table 1. There was a female predominance in this cohort (52.6%). The mean age of patients was 65 years (range, 23 to 82 years) with 242 never smokers (60%), 89 ex-smokers (22.1%), and 72 current smokers (17.9%). Regarding pathologic stage, 234 patients were stage I (58.1%), 83 were stage II (20.6%), and 86 were (21.3%) stage III.

HLA class I and PD-L1 expression

HLA class I expression was observed in the normal bronchial epithelium, type II pneumocytes and other non-neoplastic cells with membranous staining. In the tumor cells, 34 specimens (8.4%) showed strongly positive membranous expression of HLA class I antigen, 120 specimens (29.8%) with weakly positive expression, and 249 specimens (61.8%) with negative expression. Therefore, HLA class I expression was reduced in 369 patients (91.6%) and retained in 34 patients (8.4%). Reduced HLA-class I expression was more frequently seen in younger age, absence of

Table 1. Clinicopathologic characteristics

Characteristic	No. (%)
Age (yr)	
Median (range)	65 (23–82)
Sex	
Male	191 (47.4)
Female	212 (52.6)
Smoking status ^a	
Never	242 (60.0)
Ex-smoker	89 (22.1)
Current	72 (17.9)
Differentiation ^b	
Well differentiated	34 (8.4)
Moderately differentiated	315 (78.2)
Poorly differentiated	54 (13.4)
Genetic status ^c	
EGFR mutant	192 (69.1)
ALK mutant	20 (7.2)
KRAS mutant	16 (5.8)
EGFR(-)/ALK(-)/KRAS(-)	50 (18.0)
Tumor size (cm)	
Mean (range)	31.7 (0.8–16.0)
Pleural invasion	
Absent	235 (58.3)
Present	168 (41.7)
Venous invasion	
Absent	302 (74.9)
Present	101 (25.1)
Lymphatic invasion	
Absent	213 (52.9)
Present	190 (47.1)
Perineural invasion	
Absent	380 (94.3)
Present	23 (5.7)
Pathologic stage	
IA	127 (31.5)
IB	107 (26.6)
IIA	64 (15.9)
IIB	19 (4.7)
IIIA	77 (19.1)
IIIB	9 (2.2)
HLA class I IHC (%)	
<25	249 (61.8)
25–74	120 (29.8)
≥75	34 (8.4)
PD-L1 IHC (%)	
<1	338 (83.9)
1–49	42 (10.4)
≥50	23 (5.7)
Total	403 (100)

EGFR, epidermal growth factor receptor; ALK, anaplastic lymphoma kinase; HLA, human leukocyte antigen; IHC, immunohistochemistry; PD-L1, programmed death-ligand 1.

^aSmoking status was defined as follows: never smoker (< 100 cigarettes per lifetime); ex-smoker (≥ 100 cigarettes per lifetime and quit > 1 year prior to the diagnosis); current smoker (≥ 100 cigarettes per lifetime and smoked at the time of lung cancer diagnosis or quit ≤ 1 year prior to the diagnosis);

^bDifferentiation was defined as follows: well differentiated (lepidic predominant); moderately differentiated (acinar or papillary predominant); poorly differentiated (micropapillary or solid predominant); ^cGenetic status was evaluable for 278 patients.

vascular invasion, and low pathologic stage ($p = .033$, $p = .007$, and $p = .012$, respectively). PD-L1 expression was normally expressed in membranes of the alveolar macrophages and some lympho-

cytes. In the tumor cells, 65 patients (16.1%) with cutoff value of 1% and 23 patients (5.7%) with cutoff value of 50% showed positive PD-L1 expression. Positive PD-L1 expression (1% cutoff)

Table 2. HLA class I, PD-L1 expression and clinicopathologic characteristics

Clinicopathologic feature	HLA class I expression			PD-L1 expression (1% cut-off)			PD-L1 expression (50% cut-off)		
	Retained (normal)	Reduced (loss)	p-value	Negative (<1%)	Positive (≥1%)	p-value	Negative (<50%)	Positive (≥50%)	p-value
Total	34 (8.4)	369 (91.6)		338 (83.9)	65 (16.1)		380 (94.3)	23 (5.7)	
Age (yr)									
< 65	11 (5.5)	190 (94.5)	.033	174 (86.6)	27 (13.4)	.142	191 (95.0)	10 (5.0)	.527
≥ 65	23 (11.4)	179 (88.6)		164 (81.2)	38 (18.8)		189 (93.6)	13 (6.4)	
Sex									
Male	16 (8.4)	175 (91.6)	.967	155 (81.2)	36 (18.8)	.159	176 (92.1)	15 (7.9)	.078
Female	18 (8.5)	194 (91.5)		183 (86.3)	29 (13.7)		204 (96.2)	8 (3.8)	
Smoking status									
Never	19 (7.9)	223 (92.1)	.604	206 (85.1)	36 (14.9)	.402	231 (95.5)	11 (4.5)	.218
Ex or current	15 (9.3)	146 (90.7)		132 (82.0)	29 (18.0)		149 (92.5)	12 (7.5)	
Differentiation									
WD	2 (5.9)	32 (94.1)	.422 ^a	34 (100.0)	0	<.001	34 (100)	0	.008 ^a
MD	25 (7.9)	290 (92.1)		270 (85.7)	45 (14.3)		300 (95.2)	15 (4.8)	
PD	7 (13.0)	47 (87.0)		34 (63.0)	20 (37.0)		46 (85.2)	8 (14.8)	
Genetic status ^b									
EGFR mutant	17 (8.9)	175 (91.1)	.860 ^a	175 (91.1)	17 (8.9)	.003	190 (99.0)	2 (1.0)	<.001 ^a
ALK mutant	1 (5.0)	19 (95.0)		17 (85.0)	3 (15.0)		18 (90.0)	2 (10.0)	
KRAS mutant	2 (12.5)	14 (87.5)		10 (62.5)	6 (37.5)		12 (75.0)	4 (25.0)	
EGFR(-)/ALK(-)/KRAS(-)	5 (10.0)	45 (90.0)		39 (78.0)	11 (22.0)		45 (90.0)	5 (10.0)	
Pleural invasion									
Negative	19 (8.1)	216 (91.9)	.764	199 (84.7)	36 (15.3)	.601	224 (95.3)	11 (4.7)	.294
Positive	15 (8.9)	153 (91.1)		139 (82.7)	29 (17.3)		156 (92.9)	12 (7.1)	
Vascular invasion									
Negative	19 (6.3)	283 (93.7)	.007	263 (87.1)	39 (12.9)	.002	289 (95.7)	13 (4.3)	.036
Positive	15 (14.9)	86 (85.1)		75 (74.3)	26 (25.7)		91 (90.1)	10 (9.9)	
Lymphatic invasion									
Negative	19 (8.9)	194 (91.1)	.712	184 (86.4)	29 (13.6)	.146	206 (96.7)	7 (3.3)	.027
Positive	15 (7.9)	175 (92.1)		154 (81.1)	36 (18.9)		174 (91.6)	16 (8.4)	
Perineural invasion									
Negative	30 (7.9)	350 (92.1)	.118 ^a	321 (84.5)	59 (15.5)	.236 ^a	360 (94.7)	20 (5.3)	.136 ^a
Positive	4 (17.4)	19 (82.6)		17 (73.9)	6 (26.1)		20 (87.0)	3 (13.0)	
Tumor size (cm)									
≤3	13 (5.4)	229 (94.6)	.007	208 (86.0)	34 (14.0)	.164	233 (96.3)	9 (3.7)	.035
>3	21 (13.0)	140 (87.0)		130 (80.7)	31 (19.3)		147 (91.3)	14 (8.7)	
N stage									
N0	19 (6.9)	256 (93.1)	.106	238 (86.5)	37 (13.5)	.032	261 (94.9)	14 (5.1)	.434
≥N1	15 (11.7)	113 (88.3)		100 (78.1)	28 (21.9)		119 (93.0)	9 (7.0)	
Stage									
I	14 (6.0)	220 (94.0)	.012	204 (87.2)	30 (12.8)	.079	222 (94.9)	12 (5.1)	.484 ^a
II	6 (7.2)	77 (92.8)		64 (77.1)	19 (22.9)		76 (91.6)	7 (8.4)	
III	14 (16.3)	72 (83.7)		70 (81.4)	16 (18.6)		82 (95.3)	4 (4.7)	
Stage I and others									
I	14 (6.0)	220 (94.0)	.037	204 (87.2)	30 (12.8)	.034	222 (94.9)	12 (5.1)	.555
≥IIa	20 (11.8)	149 (88.2)		134 (79.3)	35 (20.7)		158 (93.5)	11 (6.5)	
PD-L1 status (1% cutoff)									
Negative	24 (7.1)	314 (92.9)	.028						
Positive	10 (15.4)	55 (84.6)							

^ap-value was obtained by Fisher exact test; ^bGenetic status was evaluable for 278 patients.

was associated with poor differentiation, presence of vascular invasion and nodal metastasis ($p < .001$, $p = .002$, and $p = .032$, respectively). In addition, positive PD-L1 expression (1% cutoff) was correlated with epidermal growth factor receptor (EGFR) wild type tumors ($p = .003$) (Table 2).

Survival analysis

At the time of analysis, the median PFS was 36.0 months and the median OS was 65.0 months. During this time, 164 patients (40.7%) suffered tumor recurrence and 90 patients (22.3%) died due to cancer. Survival analysis using Kaplan-Meier and Cox proportional hazards analyses were performed to evaluate the

prognostic impact of HLA class I and PD-L1 protein expression. There was no significant difference in OS according to HLA class I status (5-year survival, 81.4% in “reduced” patients vs. 69.3% in “retained” patients; $p = .115$) (Fig. 2A).

There was no significant difference in OS according to PD-L1 expression status, either. (Fig. 2B). The 5-year OS of PD-L1–positive and PD-L1–negative patients using each cutoff value was 75.4% and 81.3% (cutoff, 1%; $p = .423$), 78.7% and 80.5% (cutoff, 50%; $p = .534$), respectively. However, when both markers were analyzed simultaneously, coexpression of HLA class I and PD-L1 (1% cutoff) group ($n = 10$) had a significantly shorter OS than other groups (5-year survival, 42.0%; $p = .009$) (Fig. 2C).

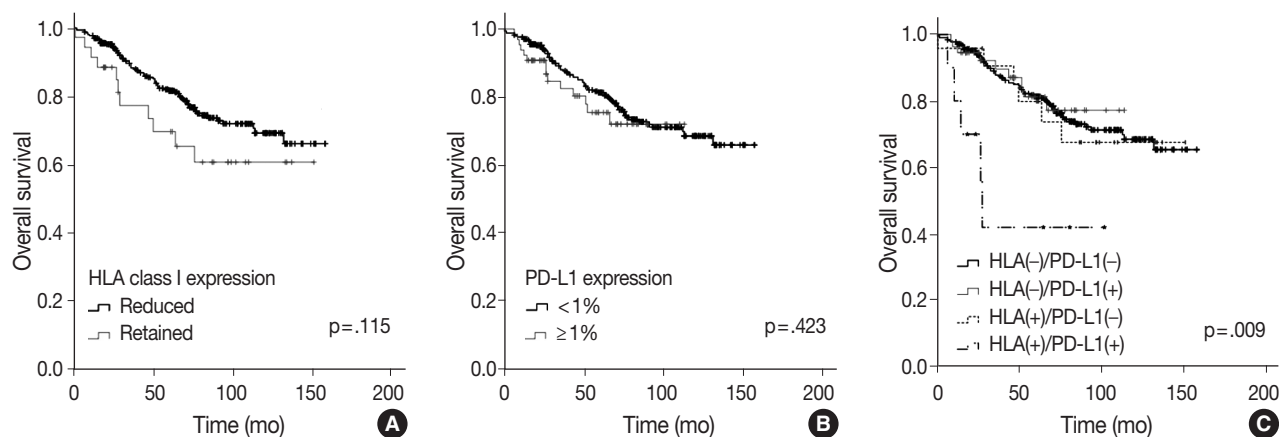


Fig. 2. Association of human leukocyte antigen (HLA) class I antigen and programmed death-ligand 1 (PD-L1) expression in lung adenocarcinoma (ADC) lesions with overall survival in patients. (A) Overall survival curves of patients with lung ADC according to their HLA class I expression. (B) Overall survival curves according to PD-L1 expression status classified by the percentage of tumor cells expressing PD-L1 at the cutoff value of 1%. (C) Overall survival in patients classified by expression of HLA class I and PD-L1. Patients were divided into four groups: HLA class I (-)/PD-L1 (-), HLA class I (-)/PD-L1 (+), HLA class I (+)/PD-L1 (-), HLA class I (+)/PD-L1 (+).

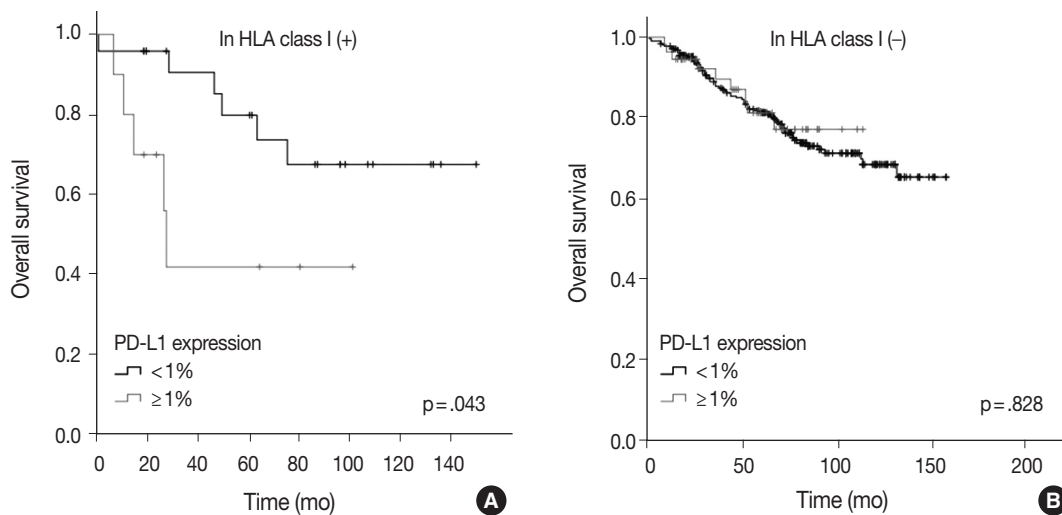


Fig. 3. Overall survival according to programmed death-ligand 1 (PD-L1) expression after stratification by human leukocyte antigen (HLA) class I expression status. (A) Overall survival curves according to PD-L1 expression status (1% cutoff) among “retained” HLA class I cases. (B) Overall survival curves according to PD-L1 expression status (1% cutoff) among “reduced” HLA class I cases.

When analyzed by PD-L1 expression with stratification by HLA class I status, a significantly poor prognosis in PD-L1-positive patients (1% cutoff) was documented only when HLA class I expression was “retained” ($n = 34$, $p = .043$) (Fig. 3A). Among patients with “reduced” HLA class I expression, PD-L1 expression status provided no prognostic impact ($p = .828$) (Fig. 3B).

In addition, there was no significant difference in PFS according to HLA class I status and PD-L1 status. Multivariate analysis using Cox’s proportional hazards model revealed coexpression of HLA class I and PD-L1 as an independent factor associated with poor prognosis ($p < .001$; hazard ratio, 6.106; 95% confidence

interval, 2.260 to 16.501) (Table 3).

DISCUSSION

In this study, we evaluated the expression of HLA class I and PD-L1 protein in 403 lung ADCs and investigated the relationship between HLA class I/PD-L1 protein expression and various clinicopathologic factors and molecular characteristics. Our study showed that HLA class I expression was reduced in 91.6%, and positive PD-L1 expression was 16.1% (1% cutoff) in surgically resected lung ADC. On survival analysis, HLA class I or PD-L1 expression alone did not show any statistical significance. On the integrated analysis, HLA class I (+)/PD-L1 (+) subgroup showed a significant shorter OS than other groups ($p = .009$). Multivariate analysis revealed that coexpression of HLA class I and PD-L1 was an independent poor prognostic factor of lung ADC ($p < .001$; hazard ratio, 6.106; 95% confidence interval, 2.260 to 16.501).

The frequency of HLA class I antigen reduction in this cohort seemed to be high compared to other studies for NSCLC (43% to 93.6%).^{7-9,14} Hirai et al.⁷ reported that reduced HLA class I expression was observed in 43% of the stage I lung ADC, and they used 20% and 80% cutoff. Ramnath et al.⁹ reported that reduced HLA class I expression was observed in 93.6% of the NSCLC patients, and they used 25% and 75% cutoff. CTLs can recognize tumor-specific antigens presented on various types of HLA class I molecules on the tumor.^{15,16} As the prerequisite of anti-tumor activity of CTLs is the recognition of immunogenic epitopes presented on HLA class I molecules on the tumor cells, reduced expression of HLA class I molecule in lung ADC is not surprising. However, the prognostic impact of HLA class I molecule expression is highly controversial.

High HLA class I expression had been reported to be associated with a better survival in esophageal cancer, hepatocellular carcinoma and pancreatic cancer,¹⁷⁻¹⁹ or poor prognosis in gastric cancer and colorectal cancer.^{16,20,21} These contradictory results might be explained by multilateral function of HLA class I molecules. As HLA-B/C molecule has been known to act as an inhibitory receptor against natural killer (NK) cells, cancer cells with loss of HLA class I molecule could be attacked by NK cells.^{15,16} The prognostic impact of HLA class I molecule expression could be variable depending on the mechanism of activation of the immune system in each organ. In the present study, there was no significant correlation between HLA class I expression status and survival, which may reflect HLA class I antigen’s diverse roles in immune system.

Table 3. Univariate and multivariate analyses of clinicopathologic factors and overall survival in lung ADC patients

Clinicopathologic variable	Univariate		Multivariate	
	p-value	p-value	HR (95% CI)	
Age				
< 65 yr vs ≥ 65 yr	< .001	< .001	2.871 (1.715–4.804)	
Sex				
Male vs female	< .001			
Smoking Hx				
Never vs ever or current	.025	.026	1.774 (1.073–2.935)	
Differentiation				
WD vs MD vs PD	.077	-	-	
Genetic status				
<i>EGFR</i> mutant vs <i>ALK</i> mutant vs <i>KRAS</i> mutant vs wild type ^a	.179	-	-	
Pleural invasion				
Negative vs positive	< .001	-	-	
Vascular invasion				
Negative vs positive	.002	-	-	
Lymphatic invasion				
Negative vs positive	< .001	-	-	
Perineural invasion				
Negative vs positive	< .001	-	-	
Tumor size				
≤ 3 cm vs > 3 cm	< .001	-	-	
N category				
N0 vs ≥ N1	< .001	.122	2.143 (0.815–5.632)	
Stage				
I vs II vs III	< .001	.039		
I vs II		.294	1.732 (0.621–4.827)	
I vs III		.027	3.295 (1.142–9.508)	
HLA expression				
< 75% vs ≥ 75%	.115	-	-	
PD-L1 expression				
< 1% vs ≥ 1%	.423	-	-	
HLA(+)/PD-L1(+)				
Others vs double positive	.001	< .001	6.106 (2.260–16.501)	

ADC, adenocarcinoma; HR, hazard ratio; CI, confidence interval; Hx, history; WD, well differentiated; MD, moderately differentiated; PD, poorly differentiated; *EGFR*, epidermal growth factor receptor; *ALK*, anaplastic lymphoma kinase; HLA, human leukocyte antigen; PD-L1, programmed death-ligand 1. ^aWild type defined as *EGFR*(-)/*ALK*(-)/*KRAS*(-).

In this cohort, positive PD-L1 expression was associated with poor differentiation, wild type *EGFR*, presence of vascular invasion and nodal metastasis, which is consistent with previous reports.^{7,12,22} However, there was no significant difference between PD-L1 expressions and survival. Even though neither HLA class I nor PD-L1 alone was associated with the clinical outcome of the patients, integrated analysis of revealed that coexpression of HLA class I and PD-L1 was significantly associated with poor OS. While the patients with PD-L1 (+)/HLA class 1 (+) showed worse prognosis, PD-L1 (+)/HLA class 1 (-) group had no significant prognostic impact.

These results might be explained as below.

(1) The tumor cells with retained HLA class I expression can inhibit NK cells and evade immune system by expressing PD-L1. The immunosurveillance of CD8 T cells may be more critical for patients with high HLA class I expression than for patients who express it at a low level. (2) The tumor cells with reduced HLA class I expression may evade immune attack regardless of PD-L1 expression on tumor cells, which may account for the lack of prognostic impact of PD-L1 status. Nevertheless, tumor cells with HLA class I expression can be recognized by CTLs and may evade immune attack by expressing PD-L1, which also may account for the result that PD-L1 positivity was associated with a poor prognosis in tumors with normal HLA class I expression. The exact role of immune mechanism of the HLA class 1 molecule on the pulmonary ADC needs further functional studies. However, we assessed HLA class I status by only anti-HLA class I ABC antibody and the lack of available data concerning clinical response to anti-PD-1/PD-L1 therapy represents a major limitation of our study.

In conclusion, coexpression of HLA class I and PD-L1 was associated with poor prognosis in lung ADC. Because coexpression of HLA class I and PD-L1 was an independent prognostic factor for an extremely poor outcome, postoperative patients with HLA class 1 (+)/PD-L1 (+) should be recommended for short interval follow-up and observation.

ORCID

Yeon Bi Han: <https://orcid.org/0000-0002-3657-5012>

Hyun Jung Kwon: <https://orcid.org/0000-0001-8822-7899>

Soo Young Park: <https://orcid.org/0000-0002-1469-2787>

Eun-Sun Kim: <https://orcid.org/0000-0003-3394-2646>

Hyojin Kim: <https://orcid.org/0000-0001-9201-8328>

Jin-Haeng Chung: <https://orcid.org/0000-0002-6527-3814>

Author Contributions

Conceptualization: JHC.

Data curation: YBH.

Formal analysis: HK, JHC.

Funding acquisition: JHC.

Investigation: YBH.

Methodology: YBH, SYP, ESK, HJK, HK, JHC.

Project administration: JHC.

Resources: JHC.

Supervision: JHC.

Validation: YBH, JHC.

Visualization: YBH, JHC.

Writing—original draft: YBH, JHC.

Writing—review & editing: YBH, SYP, HJK, HK, JHC.

Conflicts of Interest

The authors declare that they have no potential conflicts of interest.

Acknowledgments

This study was supported by Research Grants from Seoul National University Bundang Hospital (SNUBH 14-2018-018), NRF Grant funded by the Korean Government (MSIT) (No.2017R1A5A1015626) and the Korea Healthcare Technology R&D Project, Ministry of Health & Welfare, Republic of Korea (HI17C1290).

REFERENCES

1. Shim HS, Choi YL, Kim L, et al. Molecular testing of lung cancers. *J Pathol Transl Med* 2017; 51: 242-54.
2. Torre LA, Sauer AM, Chen MS Jr, Kagawa-Singer M, Jemal A, Siegel RL. Cancer statistics for Asian Americans, Native Hawaiians, and Pacific Islanders, 2016: converging incidence in males and females. *CA Cancer J Clin* 2016; 66: 182-202.
3. Somasundaram A, Burns TF. The next generation of immunotherapy: keeping lung cancer in check. *J Hematol Oncol* 2017; 10: 87.
4. Domagala-Kulawik J. The role of the immune system in non-small cell lung carcinoma and potential for therapeutic intervention. *Transl Lung Cancer Res* 2015; 4: 177-90.
5. Concha-Benavente F, Srivastava R, Ferrone S, Ferris RL. Immunological and clinical significance of HLA class I antigen processing machinery component defects in malignant cells. *Oral Oncol* 2016; 58: 52-8.
6. Campoli M, Ferrone S. HLA antigen changes in malignant cells: epigenetic mechanisms and biologic significance. *Oncogene* 2008;

- 27: 5869-85.
7. Hirai A, Yoneda K, Shimajiri S, et al. Prognostic impact of programmed death-ligand 1 expression in correlation with human leukocyte antigen class I expression status in stage I adenocarcinoma of the lung. *J Thorac Cardiovasc Surg* 2018; 155: 382-92.e1.
 8. Kikuchi E, Yamazaki K, Torigoe T, et al. HLA class I antigen expression is associated with a favorable prognosis in early stage non-small cell lung cancer. *Cancer Sci* 2007; 98: 1424-30.
 9. Ramnath N, Tan D, Li Q, et al. Is downregulation of MHC class I antigen expression in human non-small cell lung cancer associated with prolonged survival? *Cancer Immunol Immunother* 2006; 55: 891-9.
 10. Edge SB, Byrd DR, Compton CC, Fritz AG, Greene FL, Trotti A. *AJCC cancer staging manual*. 7th ed. New York: Springer, 2010.
 11. Travis WD, Brambilla E, Nicholson AG, et al. The 2015 World Health Organization classification of lung tumors: impact of genetic, clinical and radiologic advances since the 2004 classification. *J Thorac Oncol* 2015; 10: 1243-60.
 12. Kim H, Kwon HJ, Park SY, Park Y, Park E, Chung JH. Clinicopathological analysis and prognostic significance of programmed cell death-ligand 1 protein and mRNA expression in non-small cell lung cancer. *PLoS One* 2018; 13: e0198634.
 13. Herbst RS, Baas P, Kim DW, et al. Pembrolizumab versus docetaxel for previously treated, PD-L1-positive, advanced non-small-cell lung cancer (KEYNOTE-010): a randomised controlled trial. *Lancet* 2016; 387: 1540-50.
 14. Perea F, Sánchez-Palencia A, Gómez-Morales M, et al. HLA class I loss and PD-L1 expression in lung cancer: impact on T-cell infiltration and immune escape. *Oncotarget* 2018; 9: 4120-33.
 15. Campbell KS, Purdy AK. Structure/function of human killer cell immunoglobulin-like receptors: lessons from polymorphisms, evolution, crystal structures and mutations. *Immunology* 2011; 132: 315-25.
 16. Ljunggren HG, Kärre K. In search of the 'missing self': MHC molecules and NK cell recognition. *Immunol Today* 1990; 11: 237-44.
 17. Imai D, Yoshizumi T, Okano S, et al. The prognostic impact of programmed cell death ligand 1 and human leukocyte antigen class I in pancreatic cancer. *Cancer Med* 2017; 6: 1614-26.
 18. Mizukami Y, Kono K, Maruyama T, et al. Downregulation of HLA Class I molecules in the tumour is associated with a poor prognosis in patients with oesophageal squamous cell carcinoma. *Br J Cancer* 2008; 99: 1462-7.
 19. Umemoto Y, Okano S, Matsumoto Y, et al. Prognostic impact of programmed cell death 1 ligand 1 expression in human leukocyte antigen class I-positive hepatocellular carcinoma after curative hepatectomy. *J Gastroenterol* 2015; 50: 65-75.
 20. Menon AG, Morreau H, Tollenaar RA, et al. Down-regulation of HLA-A expression correlates with a better prognosis in colorectal cancer patients. *Lab Invest* 2002; 82: 1725-33.
 21. Ueda Y, Ishikawa K, Shiraishi N, Yokoyama S, Kitano S. Clinical significance of HLA class I heavy chain expression in patients with gastric cancer. *J Surg Oncol* 2008; 97: 451-5.
 22. Zhang M, Li G, Wang Y, et al. PD-L1 expression in lung cancer and its correlation with driver mutations: a meta-analysis. *Sci Rep* 2017; 7: 10255.

Guanabenz Acetate Induces Endoplasmic Reticulum Stress–Related Cell Death in Hepatocellular Carcinoma Cells

Hyo Jeong Kang^{1*}
Hyang Sook Seol^{2*} · Sang Eun Lee²
Young-Ah Suh² · Jihun Kim¹
Se Jin Jang^{1,2} · Eunsil Yu^{1,3}

¹Department of Pathology, ²Asan Institute for Life Science, ³Asan Liver Center, Asan Medical Center, University of Ulsan College of Medicine, Seoul, Korea

Received: January 5, 2018
Revised: December 28, 2018
Accepted: January 14, 2019

Corresponding Author

Se Jin Jang, MD, PhD
Department of Pathology, Asan Medical Center,
University of Ulsan College of Medicine,
88 Olympic-ro 43-gil, Songpa-gu, Seoul 05505,
Korea
Tel: +82-2-3010-5608
Fax: +82-2-472-7898
E-mail: jangsejin@amc.seoul.kr

Eunsil Yu, MD, PhD
Department of Pathology, Asan Medical Center,
University of Ulsan College of Medicine,
88 Olympic-ro 43-gil, Songpa-gu, Seoul 05505,
Korea
Tel: +82-2-3010-4552
Fax: +82-2-472-7898
E-mail: d890075@gmail.com

*Hyo Jeong Kang and Hyang Sook Seol contributed equally to this work.

Background: Development of chemotherapeutics for the treatment of advanced hepatocellular carcinoma (HCC) has been lagging. Screening of candidate therapeutic agents by using patient-derived preclinical models may facilitate drug discovery for HCC patients. **Methods:** Four primary cultured HCC cells from surgically resected tumor tissues and six HCC cell lines were used for high-throughput screening of 252 drugs from the Prestwick Chemical Library. The efficacy and mechanisms of action of the candidate anti-cancer drug were analyzed via cell viability, cell cycle assays, and western blotting. **Results:** Guanabenz acetate, which has been used as an antihypertensive drug, was screened as a candidate anti-cancer agent for HCC through a drug sensitivity assay by using the primary cultured HCC cells and HCC cell lines. Guanabenz acetate reduced HCC cell viability through apoptosis and autophagy. This occurred via inhibition of growth arrest and DNA damage-inducible protein 34, increased phosphorylation of eukaryotic initiation factor 2 α , increased activating transcription factor 4, and cell cycle arrest. **Conclusions:** Guanabenz acetate induces endoplasmic reticulum stress–related cell death in HCC and may be repositioned as an anti-cancer therapeutic agent for HCC patients.

Key Words: Hepatocellular carcinoma; Primary cell culture; Drug sensitivity; Drug repositioning; Guanabenz acetate

Hepatocellular carcinoma (HCC) is one of the most common malignancies worldwide, and its incidence is increasing because of the dissemination of hepatitis B and C viruses.^{1,2} HCC is the third most common cause of cancer-related deaths, with approximately 600,000 deaths per year.³⁻⁶ Although surgical resection and transplantation are effective treatments for HCC, most patients present with advanced-stage disease at the time of diagnosis and are not suitable candidates for curative surgery.⁴ Inoperable HCC patients undergo various loco-regional treatments, including transarterial chemoembolization, radiofrequency ablation, and percutaneous ethanol injection, with or without systemic chemo-

therapy using adriamycin, cisplatin, or sorafenib.⁷⁻⁹ Despite the development of various treatments for advanced HCC patients, HCC remains difficult to treat because these methods do not significantly improve mortality.¹⁰ Therefore, novel approaches to develop targeted therapeutic agents are needed.

Immortalized cancer cell lines have been typically used for high-throughput screening of chemical libraries to develop novel therapeutics in the past. Although immortalized cancer cell lines have the advantage of being robust and tractable, they have significant limitations recapitulating tumor heterogeneity of *in vivo* human tumors.¹¹⁻¹³ Primary cultured cancer cells from patient tumors

have been reported to maintain similarity with the original tumors with respect to histopathology, biomarker expression, genomic mutation profiles, and drug responsiveness.¹⁴ Therefore, primary cultured cells have been suggested as a substitute preclinical model of various tumors for screening and evaluation of anti-cancer therapeutic candidates.

The traditional approach to drug discovery involves de novo identification and validation of new molecular entities, which is a time-consuming and costly process.¹⁵ Despite huge investments in drug discovery and development, and explosive advances in biological technologies during the past decades, the number of new drugs introduced into the clinic has not increased accordingly. Alternatively, identification of new therapeutic indications for approved drugs i.e., drug repurposing has attracted particular attention for anti-cancer drug discovery.¹⁵⁻¹⁷ This strategy has several advantages over the traditional de novo drug discovery approach, including reducing development time, costs, and the risks associated with pharmacokinetics and toxicology.¹⁷⁻²⁰ For drug repurposing research, several established clinical drug libraries approved by the U.S. Food and Drug Administration (FDA), European Medicines Agency (EMA), and other agencies are available.

In the present study, we conducted drug repurposing study and could select guanabenz acetate (GA), an antihypertensive drug, as a candidate therapeutic molecule by high throughput screening on patient derived primary cultured HCC cells using the Prestwick Chemical Library which are all approved by the U.S. FDA and EMA. Mechanistically, GA inhibited growth arrest and DNA damage-inducible protein 34 (GADD34)-mediated dephosphorylation of eukaryotic initiation factor 2 α (eIF2 α), and subsequently induced apoptosis and autophagy of the HCC cells.

MATERIALS AND METHODS

Ethical approval

This study was approved by the Institutional Review Board of Asan Medical Center with a waiver of informed consent (IRB No. 2012-0112).

Patients and samples

Four patients with HCC, who were confirmed to have the disease via liver protocol dynamic computed tomography scans at Asan Medical Center, Seoul, Korea, were selected to establish primary cultured cells. A portion of the tumor tissues obtained from surgical resection were fixed in cold 2% formaldehyde for 4 hours and embedded in paraffin at 56°C. Sections from the paraffin blocks (4- μ m thick) were stained with hematoxylin and

eosin (H&E). All H&E slides were reviewed by two pathologists (E.Y. and H.J.K.) who were blinded to the clinical information.

Primary culture of HCC cells

The fresh tissues of the four cases obtained during surgery were put into a tube containing Dulbecco's modified Eagle medium: nutrient mixture F-12 (DMEM/F12; Sigma-Aldrich, St. Louis, MO, USA), with penicillin and streptomycin, and were transported to the tissue culture room. After removing normal liver tissue and connective tissue, tumor tissues were minced with scissors and subsequently digested with 0.1% type IV collagenase (Sigma-Aldrich) in a shaking incubator for 60 minutes at 37°C. After incubation, tissues were washed three to four times with DMEM/F12 containing 10% fetal bovine serum (FBS; Sigma-Aldrich). The HCC pellets obtained after centrifugation were plated on collagen type I dishes and incubated at 37°C in a 5% CO₂ atmosphere. To favor the adhesion and growth of epithelial tumor cells, hepatocyte basal media containing human epidermal growth factor, transferrin, hydrocortisone, bovine serum albumin, ascorbic acid, GA-1000 (gentamicin and amphotericin B), insulin, 10% FBS, and a Triiodothyronine-SingleQuots kit (Biocompare, South San Francisco, CA, USA) were used to culture primary HCC tumor cells. The cultured HCC cells were harvested and stored in liquid nitrogen.

MTT cell proliferation assay/drug sensitivity assay

Two hundred and fifty-two small molecules from the Prestwick Chemical Library (Prestwick Chemical, Illkirch, France) were blindly selected for screening of anti-cancer effect. The primary cultured HCC cells (10³ cells/well) were seeded in collagen type I coated 96-well plates. Following a 24-hour incubation at 37°C, the cells were treated with 252 small molecules (20 μ M each). After 72 hours, 50 mg/mL of MTT [3-(4,5-dimethylthiazol-2-yl)-2,5-diphenyltetrazolium bromide] reagent were added to each well, and the plates were incubated for 4 hours at 37°C. After the reduced formazan precipitate was dissolved in dimethyl sulfoxide, the absorbance at 540 nm was measured using a microplate reader (EL800, BioTek, Winooski, VT, USA). The concentration of candidate molecules to inhibit 50% of cell viability (IC₅₀ value) was calculated using CalcuSyn Software (Biosoft, Cambridge, UK). These results were validated in six stable HCC cell lines (i.e., SNU398, SNU423, SNU449, SNU475, Hep3B, and Huh7). Five HCC cell lines (i.e., SNU398, SNU423, SNU449, SNU475, and Huh7) and one HCC cell line (Hep3B) were respectively grown in RPMI 1640 medium (Sigma-Aldrich) and Minimum Essential Medium (Sigma-Aldrich), both supplemented

with 10% FBS, penicillin, and streptomycin.

Small interfering RNA transfection

Hep3B and Huh7 HCC cells were treated with small interfering RNA (siRNA) specific to GADD34 and non-specific siRNA (Genolution Pharmaceuticals Inc., Seoul, Korea). Targeting sequences of siRNA were as follows: siGADD34-1, 5'-GGAU-AAGGAAGAUGAUUCAUU-3'; siGADD34-2, 5'-GCCUAU-AAUUUAUUAACUAUU-3'; and as a negative control, non-specific siRNA, 5'-CCUCGUGCCGUCCAUCAGGUAGUU-3'. HCC cells were transiently transfected with GADD34 siRNA or non-specific siRNA with Lipofectamine 2000 (Invitrogen, Carlsbad, CA, USA). Six hours later, the medium was replaced with regular culture medium, and the cells were incubated. The efficiency of silencing was assessed via western blotting 48 hours after transfection.

Western blot analysis

Harvested cells were lysed in Cell Lysis Buffer (Cell Signaling Technology, Beverly, MA, USA) for 20 minutes and centrifuged at 13,500 rpm for 5 minutes. Twenty micrograms of proteins were separated by sodium dodecyl sulfate–polyacrylamide gel electrophoresis using 8%–12% gels and transferred to nitrocellulose membranes (POTRAN nitrocellulose membrane, Whatman, Kent, UK) using an iBlot dry blotting system (Invitrogen). The membranes were blocked with 5% non-fat dried milk and incubated with specific primary antibodies for (1) GADD34 (1:1,000), activating transcription factor 4 (ATF4; 1:1,000), p53 (1:1,000), and β -actin (1:2,000) from Santa Cruz Biotechnology (Dallas, TX, USA); (2) eIF2 (1:1,000), phospho-eIF2 (p-eIF2, 1:1,000),

p-p53 (Ser15, 1:2,000), p21Waf1/Cip1 (1:500), cyclin B1 (1:1,000), cyclin E2 (1:1,000), p-cdc2 (p-cdk1, 1:2,000), Bax (1:1,000), Bcl-xL (1:2,000), procaspase-9 (1:2,000), and cleaved caspase-9 (1:1,000) from Cell Signaling Technology. After incubation with appropriate horseradish peroxidase-conjugated secondary IgG antibodies, bands were detected using ECL reagent (Amersham-GE Healthcare Life Sciences, Pittsburgh, PA, USA).

Cell cycle assay

The effect of the agent on the cell cycle of HCC cell lines was analyzed by flow cytometry using propidium iodide (PI) staining. Briefly, 10^6 cells were seeded in 60-mm dishes and incubated with the agent (30 μ M) or phosphate-buffered saline (PBS) as a control for 24 hours at 37°C. After incubation, the cells were fixed with ice-cold 70% ethanol at 4°C overnight, washed twice with PBS, incubated with 10 μ g/mL RNase A, and stained with 30 μ g/mL PI. The stained cells were subsequently analyzed using flow cytometry (FACSCalibur machine, Becton Dickinson, Mountain View, CA, USA) with a 560-nm dichroic mirror and a 600-nm pass filter (bandwidth, 35 μ m). The percentages of cells in G1, S, and G2 phases were determined using Cell Quest 3.1 software (Becton Dickinson).

RESULTS

GA screened as a potential therapeutic drug for HCC

Four primary cultured HCC cells were established using surgically resected fresh tumor tissues from four HCC patients and subsequently confirmed via pathologic examination (Fig. 1A, B). The clinicopathologic features of the patients are listed in Table 1.

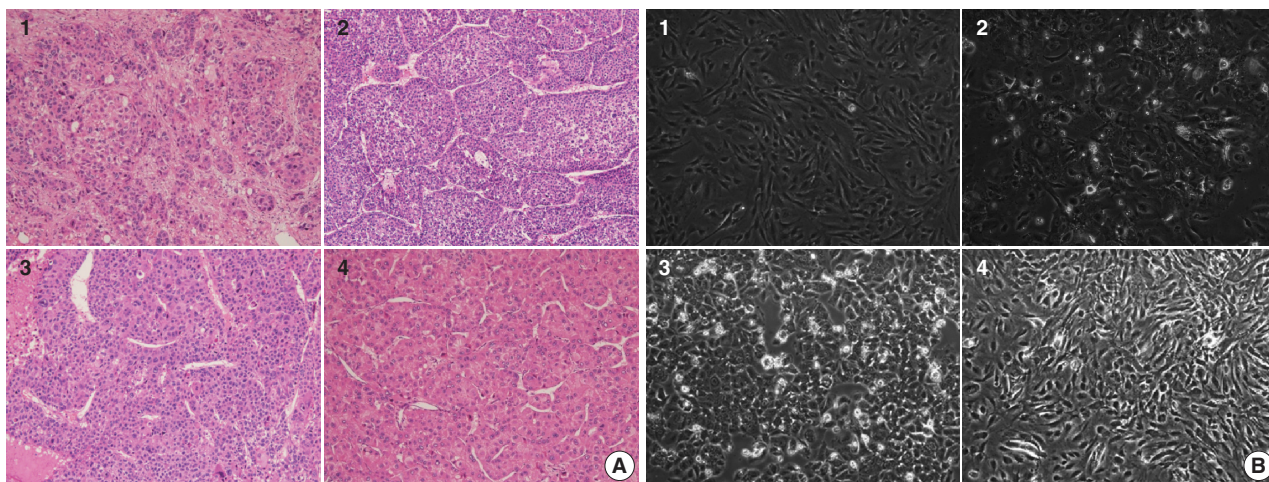


Fig. 1. (A) Histological features of surgically resected hepatocellular carcinomas, cases 1–4, respectively. (B) Cytological characteristics of primary cultured hepatocellular carcinoma cells with 3 passages, cases 1–4, respectively.

Table 1. Clinicopathologic features of four cases of hepatocellular carcinoma from which the PDX model was established

Case No.	Age (yr)	Sex	Size (cm)	Edmondson-Steiner grade	Underlying disease	Previous treatment
1	58	M	13	III	Cirrhosis/HBV	No
2	56	M	4.5	III	Periportal fibrosis/HBV	No
3	70	M	4.7	III	Cirrhosis/HBV	TACE
4	55	M	11	II	Cirrhosis/HBV	No

PDX, patient derived xenograft; HBV, hepatitis B virus; TACE, transarterial chemoembolization.

High-throughput drug screening using the Prestwick Chemical Library, which contains 1,120 FDA-approved drugs (Supplementary Table S1), was performed on the four primary cultured HCC cells. Two hundred and fifty-two of the 1,120 molecules were randomly selected and screened and identified GA as a candidate. The results were confirmed using individual *in vitro* assay. After 72-hour incubation with a concentration range of the molecules (0–50 μM), cell viability was inhibited more than 50% with 20 μM GA (i.e., compound 41) (Fig. 2A) in three out of four primary cultured HCC cells, measured using the MTT assay.

GA inhibited growth of HCC cell lines

To further validate the anti-cancer effect of GA in HCC, six HCC cell lines were treated with GA (Sigma-Aldrich) or with a control molecule, sorafenib. After 72-hour incubation with GA, growth of Hep3B ($\text{IC}_{50} = 30 \mu\text{M}$) and Huh7 ($\text{IC}_{50} = 50 \mu\text{M}$) were inhibited (Fig. 2B). The IC_{50} values of GA for SNU423, SNU449, and SNU475 cells were 100 μM , and the viability of SNU 398 cells did not drop below 50%, even at 100 μM GA (Fig. 2B). When the inhibitory effects of sorafenib on cell proliferation were compared with those of GA, the decline in viability occurred at similar or lower concentrations with sorafenib in all six HCC cell lines (Fig. 2B).

GA targets PERK signaling pathway through GADD34 inactivation

GA is an agonist of the α_2 adrenergic receptor that is used as an antihypertensive drug. GA is also known to block dephosphorylation of eIF2 α by inactivation of GADD34 in the protein kinase RNA-like ER kinase (PERK) signaling pathway, which would finally lead to expression of genes involved in apoptosis and autophagy. Therefore, the protein expression levels of genes associated with PERK signaling were evaluated by western blotting in the Hep3B and Huh7 cell lines to study the mechanisms of GA in HCC. The level of p-eIF2 α was upregulated, and ATF4 protein was increased after GA treatment of Hep3B and Huh7 cells (Fig. 3A). In addition, when HCC cells were transfected with GADD34 siRNA, levels of p-eIF2 α and ATF4 were upregulated in both Hep3B and Huh7 HCC cells compared with levels

in control HCC cells (Fig. 3A). These results reveal that GA acts as an inhibitor of dephosphorylation of eIF2 α , likely by inactivation of GADD34 in HCC.

GA induces apoptosis and autophagy-related cell death in HCC cells

ATF4, a transcription factor that induces the expression of genes, is involved in amino acid responses, metabolism, antioxidant responses, apoptosis, autophagy, and GADD34-mediated effects. To assess if GA induces HCC cell death via apoptosis and/or autophagy following ATF4 upregulation, expression levels of apoptosis-related proteins (i.e., Bax, Bcl-xL, procaspase-9, and cleaved caspase-9) and an autophagy-related protein (i.e., microtubule-associated protein light chain 3, LC3) were examined in Hep3B and Huh7 by western blotting. In the Hep3B and Huh7 cells treated with GA, Bax protein expression was higher, while Bcl-xL protein expression was lower than the expressions in control HCC cells (Fig. 3B). In addition, protein levels of procaspase-9 were decreased, while cleaved caspase-9 was increased in both Hep3B and Huh7 cells (Fig. 3C). Both LC3-I and LC3-II protein levels increased in Hep3B, but only LC3-II protein level increased in Huh7 treated with GA (Fig. 3D). These results clearly demonstrate that both mechanism of apoptosis and autophagy play a role in GA-induced cell death. Activated ATF4 in the PERK pathway is considered an essential gateway for apoptosis and autophagy in HCC cells.

Different types of cell cycle arrest in different HCC cell lines treated with GA

To examine whether GA reduces HCC cell viability by inducing cell cycle arrest, flow cytometry was performed. The expression levels of checkpoint proteins in the G1/S and G2/M transitions and cell cycle regulating factors were then examined by western blotting. The cell cycle distribution pattern was different between the two HCC cell lines. In Hep3B cells treated with GA, the percentage of G1 phase cells increased, while the percentages of S and G2 phase cells concomitantly decreased (Fig. 4A). In contrast to Hep3B, the cell cycle distribution of Huh7 treated with GA revealed an increase in the percentage of G2 phase cells, while

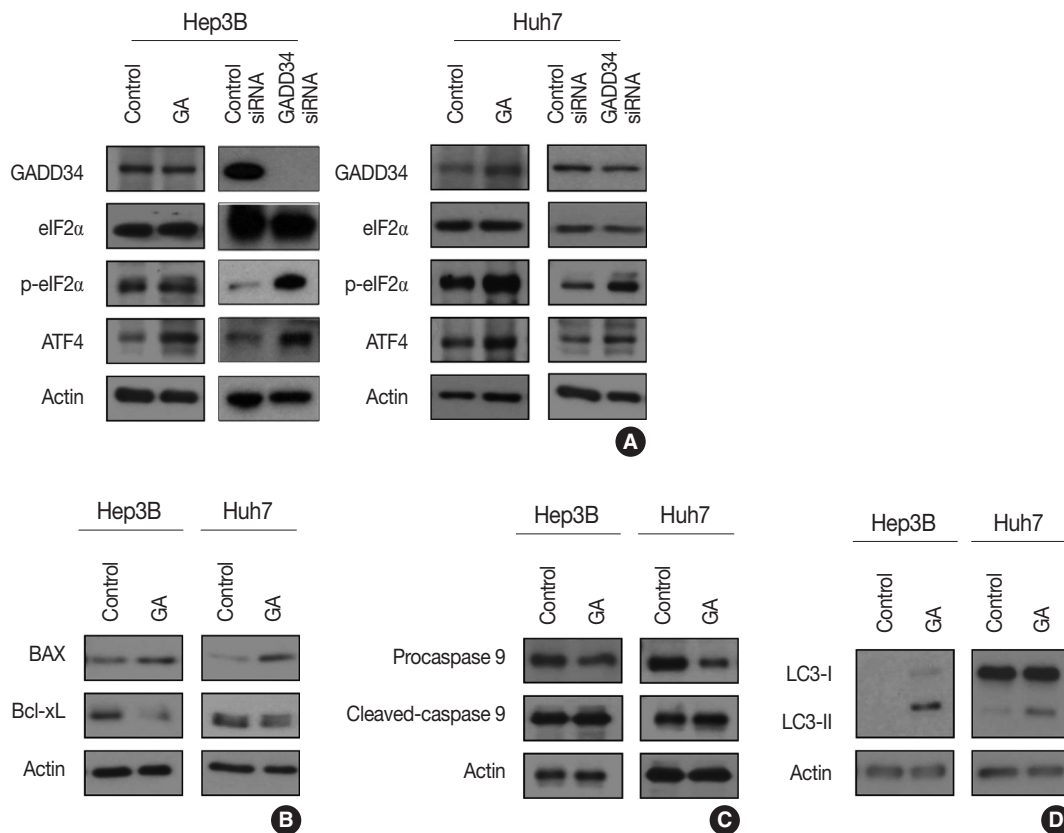


Fig. 3. (A) Western blotting showing that the effect of guanabenz acetate (GA) is associated with the protein kinase RNA-like endoplasmic reticulum kinase signaling pathway in hepatocellular carcinoma (HCC). Similar patterns of eIF2 α phosphorylation (p-eIF2 α) and activating transcription factor 4 (ATF4) protein expression are observed in HCC cells treated with GA and HCC cells transfected with growth arrest and DNA damage-inducible protein 34 (GADD34) siRNA. (B–D) Western blotting showing apoptosis- and autophagy-related protein levels after GA treatment of HCC cells. (B) The protein expression levels of BAX and Bcl-xL are increased and decreased, respectively, by GA in both Hep3B and Huh7 cells. (C) The protein expression level of procaspase-9 is decreased and that of cleaved caspase-9 is increased by GA in Hep3B and Huh7 cells. (D) The levels of autophagy-related proteins, LC3-I and LC3-II, are upregulated in GA-treated Hep3B cells, and LC3-II is upregulated in GA-treated Huh 7 cells.

producing a concomitant decrease in the percentage of G1 phase cells (Fig. 4B). Among cell cycle-related proteins, the total protein level of p21 increased remarkably after GA treatment in Hep3B and Huh7 cells. The protein level of cyclin B1 slightly decreased, p-cdc2 remained unchanged, and cyclin E2 decreased in Hep3B cells. In Huh7 cells, however, the protein level of cyclin B1 increased, p-cdc2 remarkably decreased, and cyclin E2 slightly decreased (Fig. 4C). These results suggest that the reduced viability of HCC cells by GA treatment is regulated by cell cycle arrest. Moreover, the patterns of cell cycle arrest by GA treatment can vary among different HCC cell lines.

DISCUSSION

In this study, we discovered that GA can be repurposed as a potential anti-cancer drug for HCC patients via preclinical drug

efficacy screening by using primary cultured HCC cells that we established using the surgically resected HCCs and stable HCC cell lines.

A new functional mechanism of GA was recently reported. In this mechanism, PERK activity, which is one of three pathways of the unfolded protein response (UPR) in the endoplasmic reticulum (ER), is increased by selective inactivation of GADD34-mediated dephosphorylation of eIF2 α , subsequently inducing apoptosis and autophagy (summarized in Fig. 5).^{21–24} UPR acts as a protective mechanism to alleviate ER stress by increasing protein-folding capacity, inhibiting general protein translation, and promoting degradation of unfolded or misfolded proteins. Interestingly, the aggregation of unfolded or misfolded proteins resulting in ER stress is associated with progression of various diseases, such as cancer, metabolic diseases, diabetes, inflammation, liver dysfunction, neurodegenerative disorders, and brain

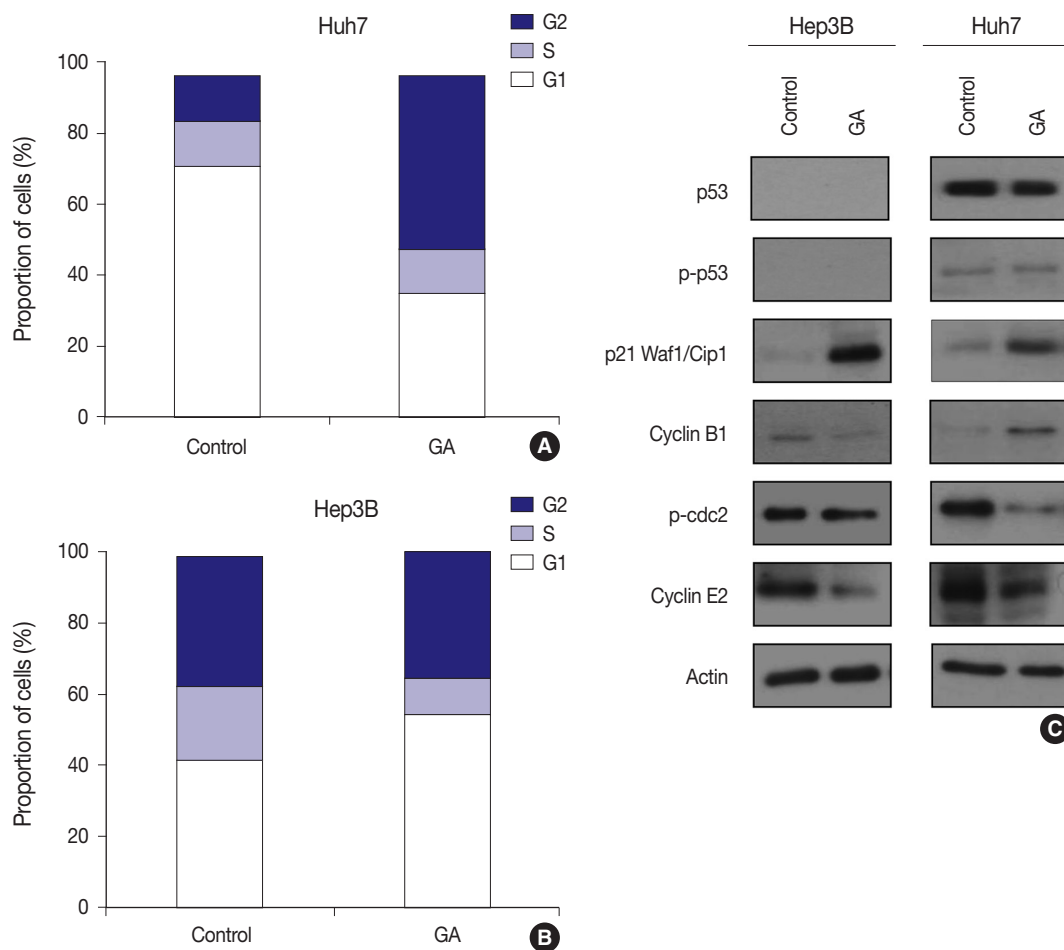


Fig. 4. Flow cytometry and western blotting showing that the type of cell cycle arrest induced by guanabenz acetate (GA) varies between hepatocellular carcinoma cell lines. (A) Flow cytometry shows increased percentage of G1 phase cells in GA-treated Hep3B cells. (B) Flow cytometry shows increased percentage of G2 phase cells in GA-treated Huh7 cells. (C) Western blotting shows the effect of GA treatment on expression levels of checkpoint proteins in the G1/S and G2/M transition and cell cycle regulating factors in Hep3B and Huh7 cells.

and heart ischemia.²²⁻²⁵ Moreover, when ER stress is persistent and cannot be resolved, apoptotic signaling is initiated, which eventually leads to cell death.²³ Thus, the UPR signaling pathway can be an attractive target for drug discovery in diverse diseases. Recent studies have demonstrated that GA acts as a novel therapeutic agent by inhibition of dephosphorylation of eIF2 α in the UPR pathway for several disorders, including progressive neurodegenerative disease (especially amyotrophic lateral sclerosis), toxoplasmosis, and breast cancer.^{21,26-28}

In the cases of HCC that were responsive to GA, the mechanisms of action were consistent with the known mechanism. First, we confirmed that GA acts on the PERK signaling pathway possibly by inactivation of GADD34 in HCC. The HCC cells treated with GA showed an increase in the phosphorylation of eIF2 α and expression of ATF4. Moreover, both GA-treated HCC cells and GADD34 siRNA-transfected HCC cells showed

the same patterns of p-eIF2 α and ATF4, supporting that GA inhibits GADD34. Second, we also identified that GA reduced cell viability by both mechanisms of apoptosis and autophagy in HCC cells. In GA-treated HCC cells, apoptosis and autophagy reactions were confirmed by decreased expression of procaspase-9 and the increased levels of cleaved caspase-9 and LC3. We also discovered that GA independently affects the cell cycle. GA-treated HCC cells showed arrest in the G1 or G2 phase of the cell cycle, the pattern of which was different between the two HCC cell lines. Additional studies are needed to elucidate the reason why the phase of cell cycle arrest is different among HCC cell lines, and the mechanisms of these differences. In addition, the markedly upregulated p21Waf1/Cip1 protein levels in both Hep3B and Huh7 cells indicate that a p53-dependent pathway could be involved in the cell cycle arrest by GA.

The present study is the first to perform a drug repurposing

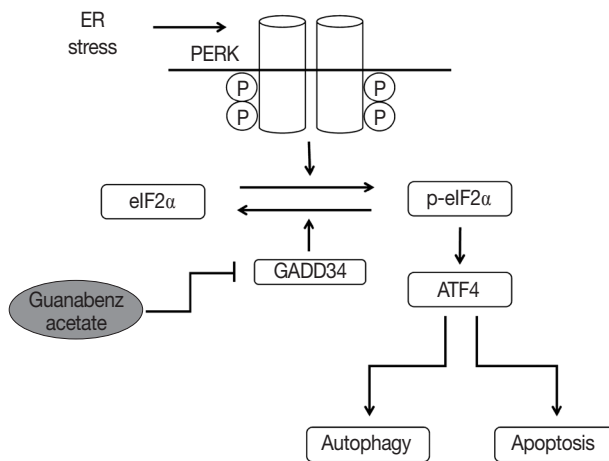


Fig. 5. Mechanisms of guanabenz acetate stimulation of the protein kinase RNA-like endoplasmic reticulum (ER) kinase (PERK) signaling pathway. Guanabenz acetate selectively inhibits growth arrest and DNA damage-inducible protein 34 (GADD34) and increases phosphorylation of eukaryotic initiation factor 2 α (eIF2 α). Phosphorylation of eIF2 α leads to increased activating transcription factor 4 (ATF4), which triggers cell apoptosis and autophagy.

study using primary cultured cells that we established from HCC patients with a high-throughput screening approach to discover novel therapeutics. The drug discovery process was developed based on genome-based drug discovery, high-throughput screening, and combinatorial chemistry.¹⁷ Contrary to expectations, novel agents identified through traditional methods have gradually declined because of high costs, time-consuming processes, and unexpected adverse reactions in clinical trials. This has led to a process called drug repositioning or repurposing.^{29,30} Drug repositioning is a new approach for drug discovery and is believed to offer great benefits over the traditional method of searching for new active substances, since the safety and pharmacokinetics have already been established.^{17,18,31,32} A representative new indication, introduced by drug repositioning, is thalidomide, a sedative hypnotic agent, which demonstrated significant clinical activity against multiple myeloma and leprosy.^{33,34} Moreover, the combination therapy of drugs found by drug repositioning and conventional anticancer drugs may increase efficacy and reduce adverse reactions.¹⁷ Thus, drug repositioning may become a key approach for treating variable malignancies, including HCC, in novel drug discovery.

The commercially available libraries of marketed drugs and natural compounds have been widely used in drug screening tests for a broad spectrum of diseases, including cancers, viral or fungal infections, neurodegenerative disorders, and neuromuscular disorders, but never have been used for drug efficacy tests of HCC.³⁵ Although the unexpected effects of GA on the reduction of HCC

cell viability were discovered from randomly selected drugs, the effects of GA on malignant cells have already been reported in breast cancer. A previous study revealed that combined treatment of GA and salubrinal can attenuate the malignant phenotype and tumor growth of triple negative breast cancer cells through the eIF2 α -mediated Rac1 pathway.²⁸ As mentioned previously, GA acts as an inhibitor of dephosphorylation of eIF2 α and can be used potentially as an anti-cancer drug for other malignancies, especially those originating from ER-rich organs.

This study has a few limitations. It was performed *in vitro* and the GA IC₅₀ value is high for a clinically achievable dose. Therefore, additional *in vitro* and *in vivo* studies are needed to conclusively determine whether GA can be a novel anti-cancer agent for inoperable HCC patients at a clinically achievable dose. In addition, molecular and immunohistochemical studies are needed to determine the predictive marker(s) for the therapeutic effects of GA in HCC patients. Finally, the effect of GA as an anti-cancer agent could be evaluated in other malignancies of ER-rich organs.

In conclusion, GA, which was screened in primary cultured HCC cells, reduces HCC cell viability via the combined effects of apoptosis, autophagy, and cell cycle arrest. Therefore, GA may be repositioned as an anti-cancer therapeutic agent for HCC patients.

Electronic Supplementary Material

Supplementary materials are available at Journal of Pathology and Translational Medicine (<http://jpatholm.org>).

ORCID

Hyo Jeong Kang: <https://orcid.org/0000-0002-5285-8282>

Young-Ah Suh: <https://orcid.org/0000-0002-4694-714X>

Jihun Kim: <https://orcid.org/0000-0002-8694-4365>

Se Jin Jang: <https://orcid.org/0000-0001-8239-4362>

Eunsil Yu: <https://orcid.org/0000-0001-5474-9744>

Author Contributions

Conceptualization: HJK, HSS.

Data curation: HJK, HSS.

Formal analysis: HJK, HSS, SEL, YAS.

Methodology: HJK, HSS, SEL, YAS.

Supervision: EY, SJJ.

Visualization: HJK, HSS, YAS.

Writing—original draft: HJK.

Writing—review & editing: EY, SJJ, JK.

Conflicts of Interest

The authors declare that they have no potential conflicts of interest.

REFERENCES

- Bosch FX, Ribes J, Cléries R, Díaz M. Epidemiology of hepatocellular carcinoma. *Clin Liver Dis* 2005; 9: 191-211.
- Shaw JJ, Shah SA. Rising incidence and demographics of hepatocellular carcinoma in the USA: what does it mean? *Expert Rev Gastroenterol Hepatol* 2011; 5: 365-70.
- Llovet JM, Burroughs A, Bruix J. Hepatocellular carcinoma. *Lancet* 2003; 362: 1907-17.
- Karaman B, Battal B, Sari S, Verim S. Hepatocellular carcinoma review: current treatment, and evidence-based medicine. *World J Gastroenterol* 2014; 20: 18059-60.
- Forner A, Llovet JM, Bruix J. Hepatocellular carcinoma. *Lancet* 2012; 379: 1245-55.
- Venook AP, Papandreou C, Furuse J, de Guevara LL. The incidence and epidemiology of hepatocellular carcinoma: a global and regional perspective. *Oncologist* 2010; 15 Suppl 4: 5-13.
- Crissien AM, Frenette C. Current management of hepatocellular carcinoma. *Gastroenterol Hepatol (N Y)* 2014; 10: 153-61.
- Keating GM, Santoro A. Sorafenib: a review of its use in advanced hepatocellular carcinoma. *Drugs* 2009; 69: 223-40.
- Patel A, Sun W. Molecular targeted therapy in hepatocellular carcinoma: from biology to clinical practice and future. *Curr Treat Options Oncol* 2014; 15: 380-94.
- Berk V, Kaplan MA, Tonyali O, et al. Efficiency and side effects of sorafenib therapy for advanced hepatocellular carcinoma: a retrospective study by the anatolian society of medical oncology. *Asian Pac J Cancer Prev* 2013; 14: 7367-9.
- De Witt Hamer PC, Van Tilborg AA, Eijk PP, et al. The genomic profile of human malignant glioma is altered early in primary cell culture and preserved in spheroids. *Oncogene* 2008; 27: 2091-6.
- Seol HS, Suh YA, Ryu YJ, et al. A patient-derived xenograft mouse model generated from primary cultured cells recapitulates patient tumors phenotypically and genetically. *J Cancer Res Clin Oncol* 2013; 139: 1471-80.
- Seol HS, Kang HJ, Lee SI, et al. Development and characterization of a colon PDX model that reproduces drug responsiveness and the mutation profiles of its original tumor. *Cancer Lett* 2014; 345: 56-64.
- Mitra A, Mishra L, Li S. Technologies for deriving primary tumor cells for use in personalized cancer therapy. *Trends Biotechnol* 2013; 31: 347-54.
- Shim JS, Liu JO. Recent advances in drug repositioning for the discovery of new anticancer drugs. *Int J Biol Sci* 2014; 10: 654-63.
- Würth R, Thellung S, Bajetto A, Mazzanti M, Florio T, Barbieri F. Drug-repositioning opportunities for cancer therapy: novel molecular targets for known compounds. *Drug Discov Today* 2016; 21: 190-9.
- Banno K, Iida M, Yanokura M, et al. Drug repositioning for gynecologic tumors: a new therapeutic strategy for cancer. *ScientificWorldJournal* 2015; 2015: 341362.
- Langedijk J, Mantel-Teeuwisse AK, Slijkerman DS, Schutjens MH. Drug repositioning and repurposing: terminology and definitions in literature. *Drug Discov Today* 2015; 20: 1027-34.
- Saxena A, Becker D, Preeshagul I, Lee K, Katz E, Levy B. Therapeutic effects of repurposed therapies in non-small cell lung cancer: what is old is new again. *Oncologist* 2015; 20: 934-45.
- Oprea TI, Overington JP. Computational and practical aspects of drug repositioning. *Assay Drug Dev Technol* 2015; 13: 299-306.
- Wang L, Popko B, Tixier E, Roos RP. Guanabenz, which enhances the unfolded protein response, ameliorates mutant SOD1-induced amyotrophic lateral sclerosis. *Neurobiol Dis* 2014; 71: 317-24.
- Rozpedek W, Markiewicz L, Diehl JA, Pytel D, Majsterek I. Unfolded protein response and PERK kinase as a new therapeutic target in the pathogenesis of Alzheimer's disease. *Curr Med Chem* 2015; 22: 3169-84.
- Shah SZ, Zhao D, Khan SH, Yang L. Unfolded protein response pathways in neurodegenerative diseases. *J Mol Neurosci* 2015; 57: 529-37.
- Stone S, Lin W. The unfolded protein response in multiple sclerosis. *Front Neurosci* 2015; 9: 264.
- Harada M, Nose E, Takahashi N, et al. Evidence of the activation of unfolded protein response in granulosa and cumulus cells during follicular growth and maturation. *Gynecol Endocrinol* 2015; 31: 783-7.
- Vieira FG, Ping Q, Moreno AJ, et al. Guanabenz treatment accelerates disease in a mutant SOD1 mouse model of ALS. *PLoS One* 2015; 10: e0135570.
- Benmerzouga I, Checkley LA, Ferdig MT, Arrizabalaga G, Wek RC, Sullivan WJ Jr. Guanabenz repurposed as an antiparasitic with activity against acute and latent toxoplasmosis. *Antimicrob Agents Chemother* 2015; 59: 6939-45.
- Hamamura K, Minami K, Tanjung N, et al. Attenuation of malignant phenotypes of breast cancer cells through eIF2alpha-mediated downregulation of Rac1 signaling. *Int J Oncol* 2014; 44: 1980-8.
- Jadamba E, Shin M. A systematic framework for drug repositioning from integrated omics and drug phenotype profiles using pathway-drug network. *Biomed Res Int* 2016; 2016: 7147039.

30. Ashburn TT, Thor KB. Drug repositioning: identifying and developing new uses for existing drugs. *Nat Rev Drug Discov* 2004; 3: 673-83.
31. Temesi G, Bolgár B, Arany A, Szalai C, Antal P, Mátyus P. Early repositioning through compound set enrichment analysis: a knowledge-recycling strategy. *Future Med Chem* 2014; 6: 563-75.
32. Mizushima T. Identification of a molecular mechanism for actions of existing medicines and its application for drug development. *Yakugaku Zasshi* 2012; 132: 713-20.
33. Schwab C, Jagannath S. The role of thalidomide in multiple myeloma. *Clin Lymphoma Myeloma* 2006; 7: 26-9.
34. Walker SL, Waters MF, Lockwood DN. The role of thalidomide in the management of erythema nodosum leprosum. *Lepr Rev* 2007; 78: 197-215.
35. Choulier L, Nomine Y, Zeder-Lutz G, et al. Chemical library screening using a SPR-based inhibition in solution assay: simulations and experimental validation. *Anal Chem* 2013; 85: 8787-95.

Intraoperative Frozen Cytology of Central Nervous System Neoplasms: An Ancillary Tool for Frozen Diagnosis

Myunghee Kang* · Dong Hae Chung*
Na Rae Kim · Hyun Yee Cho
Seung Yeon Ha · Sangho Lee
Jungsuk An · Jae Yeon Seok
Gie-Taek Yie¹ · Chan Jong Yoo¹
Sang Gu Lee¹ · Eun Young Kim¹
Woo Kyung Kim¹ · Seong Son¹
Sun Jin Sym² · Dong Bok Shin²
Hee Young Hwang³ · Eung Yeop Kim³
Kyu Chan Lee⁴

Departments of Pathology and ¹Neurosurgery,
²Division of Medical Oncology, Department of
Internal Medicine, Departments of ³Radiology
and ⁴Radiation Oncology, Gil Medical Center,
Gachon University College of Medicine, Incheon,
Korea

Received: October 1, 2018
Revised: November 7, 2018
Accepted: November 10, 2018

Corresponding Author

Na Rae Kim, MD
Department of Pathology, Gil Medical Center,
Gachon University College of Medicine,
21 Namdong-daero 774 beon-gil, Namdong-gu,
Incheon 21565, Korea
Tel: +82-32-460-3073
Fax: +82-32-460-2394
E-mail: clara_nrk@gilhospital.com

*Myunghee Kang and Dong Hae Chung contributed
equally to this work.

Background: Pathologic diagnosis of central nervous system (CNS) neoplasms is made by comparing light microscopic, immunohistochemical, and molecular cytogenetic findings with clinico-radiologic observations. Intraoperative frozen cytology smears can improve the diagnostic accuracy for CNS neoplasms. Here, we evaluate the diagnostic value of cytology in frozen diagnoses of CNS neoplasms. **Methods:** Cases were selected from patients undergoing both frozen cytology and frozen sections. Diagnostic accuracy was evaluated. **Results:** Four hundred and fifty-four cases were included in this retrospective single-center review study covering a span of 10 years. Five discrepant cases (1.1%) were found after excluding 53 deferred cases (31 cases of tentative diagnosis, 22 cases of inadequate frozen sampling). A total of 346 cases of complete concordance and 50 cases of partial concordance were classified as not discordant cases in the present study. Diagnostic accuracy of intraoperative frozen diagnosis was 87.2%, and the accuracy was 98.8% after excluding deferred cases. Discrepancies between frozen and permanent diagnoses (n=5, 1.1%) were found in cases of nonrepresentative sampling (n=2) and misinterpretation (n=3). High concordance was observed more frequently in meningeal tumors (97/98, 99%), metastatic brain tumors (51/52, 98.1%), pituitary adenomas (86/89, 96.6%), schwannomas (45/47, 95.8%), high-grade astrocytic tumors (47/58, 81%), low grade astrocytic tumors (10/13, 76.9%), non-neoplastic lesions (23/36, 63.9%), in decreasing frequency. **Conclusions:** Using intraoperative cytology and frozen sections of CNS tumors is a highly accurate diagnostic ancillary method, providing subtyping of CNS neoplasms, especially in frequently encountered entities.

Key Words: Crush cytology; Central nervous system; Neoplasm; Frozen sections

Intraoperative diagnosis of central nervous system (CNS) neoplasms is limited by marked artifacts due to ice crystals during freezing and the difficulty of observing nuclear details of the tumor cells.¹ Since the first study of intraoperative cytological smears of CNS lesions in 1930 by Eisenhardt and Cushing,² the use of smear cytology has increased in the diagnosis of CNS neoplasms. Recently, diagnosing CNS neoplasms has shown a rapid transition to molecular incorporation for layered diagnoses. However, cytology continues to provide important clues in frozen diagnoses of CNS neoplasms.³ Few studies exist relating to cytomorpho-

logic significance, especially on frozen diagnoses, and inadequate experience and resultant poor interpretations hinder conclusive diagnoses.

Herein, we evaluate the diagnostic accuracy of intraoperative combined cytology and frozen sections in the diagnosis of CNS neoplasms.

MATERIALS AND METHODS

We retrieved 454 cases that underwent both intraoperative

frozen cytologic smears and frozen section slides of brain and cord from the archives of the Department of Pathology at a tertiary referral hospital from 2006 to 2015. In cases where only small specimens were submitted, only frozen cytology was examined. The frozen cytology was prepared by squash or touch smears, which were immediately immersed in 95% ethanol for two minutes and stained with hematoxylin and eosin (H&E). The remaining specimens were frozen sectioned; the tissue was processed in a cryostat at -15°C . Thin sections (5- μm thickness) were made and then stained using H&E.⁴ The frozen diagnoses were compared to permanent diagnoses. Disease entities were classified according to the 2007 World Health Organization (WHO) classification of CNS tumors with the combined application of new concepts from the 2016 revised edition, e.g., solitary fibrous tumors/hemangiopericytoma.^{5,6} To determine discordance, we categorized cases as complete concordance, partial concordance, discordance, and deferred cases including inadequate samples. Cases were considered complete concordance when specified frozen entities were the same as final ones, and as partial concordance when entities were not conclusive, but suggestive upon frozen diagnosis. Cases were considered deferred when, for example, glioblastoma was reported as suspicious for glioblastoma. We arbitrarily defined major and minor entities when the incidence was more than 10% or less than 10%, respectively. Comparison between diagnostic accuracy was assessed using chi-square tests in SPSS ver. 17 (SPSS Inc., Chicago, IL, USA), and $p < .05$ was considered significant. All procedures were in accordance with the Helsinki Declaration of 1964 and later versions. This study is approved by Gil Medical Center's Institutional Review Board (GBIRB2016-323), and informed consent from patients was waived.

RESULTS

Diseases diagnosed through smear cytological examination

The most commonly encountered diseases were meningiomas, followed by (in order of decreasing frequency) pituitary adenomas, low- and high-grade astrocytic gliomas, and metastatic tumors. The cytologic features are shown in Fig. 1. The results are shown in Table 1.

Concordance rate by disease entities

The accuracy of cytology was 87.2% (396/454), and reached 98.8% (396/401) after excluding deferred cases ($n = 53$). Five cases were categorized as discordant (Table 2, Fig. 2). Minor disease entities showed low complete concordance (less than 50%),

compared with major disease entities showing high concordance (range, 69% to 95.5%). When excluding metastatic brain tumors, disease entities comprising more than 10% of the total showed statistically significant diagnostic accuracy by frozen cytology, compared to less common tumors (meningioma including atypical ones, pituitary adenoma, high-grade glioma and schwannoma) ($p < .001$).

Deferred cases

Tentative diagnoses in the present study were 6.8% ($n = 31$) and were categorized as deferred diagnoses, except in the case of inadequate samples. These results are shown in Table 3. The rates of deferred cases between major disease entities (i.e., more than 10% of incidence) and non-major disease entities were significantly different ($p < .001$).

DISCUSSION

The present study retrospectively assessed the use of both cytology and frozen sections, so direct comparison of the frozen cytology and frozen sections is limited. The use of intraoperative frozen sections of CNS neoplasms has long been an important diagnostic tool, but agreement varies among histopathological entities and shows low sensitivity in diagnosing low-grade tumors and edematous lesions, compared to intraoperative frozen cytology. Various limitations in frozen diagnoses of CNS neoplasms exist in both frozen cytologic smears and frozen sections. Due to their soft, friable, and watery nature, frozen sections frequently have marked freezing artifacts and ice crystals, resulting in obscured nuclear details. These limitations may be resolved by frozen cytology, except for CNS lesions with a firm consistency such as schwannomas, metastatic carcinomas, or non-neoplastic inflammatory lesions. In the latter lesions, only frozen sections can maintain architectural morphology and subsequently yield high diagnostic accuracy. Here, we retrospectively assessed diagnostic utility using both frozen cytology and frozen sections; discrepancies between frozen diagnosis and final diagnosis may be ascribed to sampling error and incorrect evaluation of histologic typing or grading.⁷ Except for grading, previous studies showed the most sensitive yield was achieved in tumors including astrocytoma, meningioma, oligodendroglioma, metastatic tumor, glioblastoma, and ependymoma in descending order.^{3,8} Glial tumors show heterogeneous distribution,⁹ high grade, i.e., grades III and IV astrocytic tumors may be diagnosed as low-grade tumors in frozen diagnosis.¹⁰ These errors can be avoided by taking samples from multiple portions of the tumors.¹¹ In frozen cytology and sections

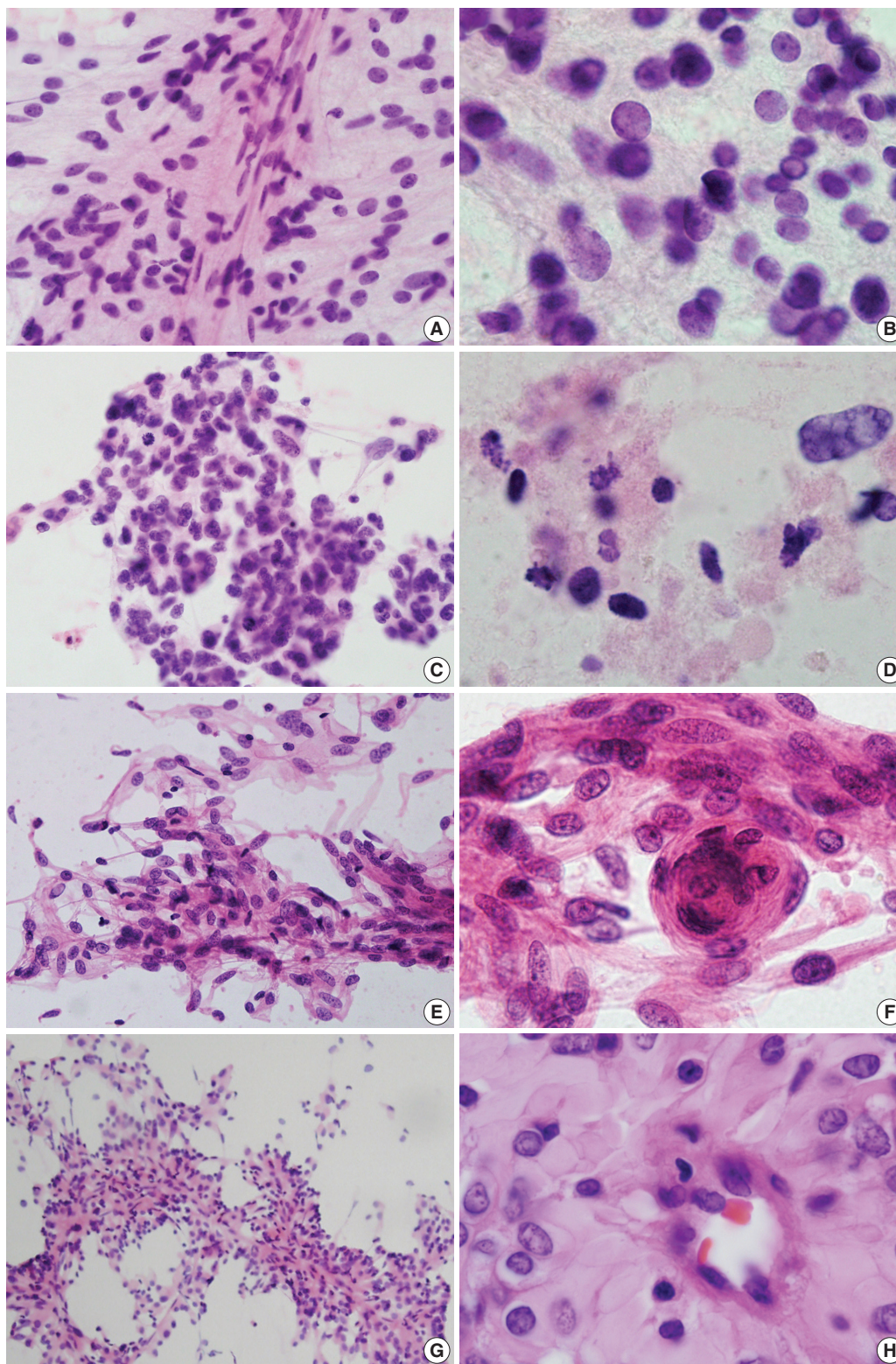


Fig. 1. (A, B) Ependymoma. Spindle-shaped tumor cells around thin capillaries. Note fibrillary cytoplasm and occasional nuclear inclusion. (C, D) Glioblastoma. Clusters show ovoid to slightly elongated hyperchromatic nuclei with occasional mitosis. Note necrosis in the extracellular area. (E, F) Fibrous meningioma. Ovoid to spindle cells have round to elongated nuclei with fine chromatin. Note nuclear pseudoinclusion and meningeal whorls. (G, H) Rhabdoid and papillary meningioma. Papillae have thick collagenous cytoplasm rather than fibrillary features that are commonly found in ependymoma.

Table 1. Diagnostic comparison between frozen cytological diagnoses and permanent histologic diagnoses

Disease entities	Completely concordant cases	Partially concordant cases	Sum of concordant cases	Discordant cases	Deferred cases including inadequate samples
Meningioma (n=98)	91 (92.9)	6 (6.1)	97 (99.0)	1 (1)	0
Pituitary adenoma (n=89)	85 (95.5)	1 (1.1)	86 (96.6)	0	3 (3.4)
Glial tumor					
Astrocytic tumor, high grade (n=58)	40 (69.0)	7 (12.1)	47 (81.1)	2 (3.4)	9 (15.5)
Astrocytic tumor, low grade (n=13)	4 (30.8)	6 (46.2)	10 (76.9)	1 (7.7)	2 (15.4)
Ependymoma (n=10)	3 (30.0)	1 (10.0)	4 (40.0)	0	6 (60.0)
Oligodendroglioma (n=3)	2 (66.7)	1 (33.3)	3 (100)	0	0
Anaplastic oligodendroglioma (n=3)	3 (100)	0	3 (100)	0	0
Neurogenic tumor					
Schwannoma (n=47)	38 (80.9)	7 (14.9)	45 (95.7)	0	2 (4.3)
Neurofibroma (n=2)	0	2 (100)	2 (100)	0	0
Dysembryoplastic neuroepithelial tumor (n=2)	1 (50)	1 (50)	2 (100)	0	0
Germ cell tumor (n=3)	1 (33.3)	0	1 (33.3)	1 (33.3)	1 (33.3)
Malignant SFT/HP (n=3)	1 (33.3)	0	1 (33.3)	0	2 (66.7)
Hematologic malignancy (n=9)	3 (33.3)	5 (55.6)	8 (88.9)	0	1 (11.1)
Metastatic tumor (n=52)	46 (88.5)	5 (9.6)	51 (98.1)	0	1 (1.9)
Other malignant tumors (n=6)	1 (16.7)	2 (33.3)	3 (50)	0	3 (50)
Other benign tumors (n=20)	8 (40.0)	2 (10.0)	10 (50)	0	10 (50.0)
Non-neoplastic lesions (n=36)	19 (52.8)	4 (11.1)	23 (63.9)	0	13 (36.1)
Total cases (n=454)	346 (76.2)	50 (11.0)	396 (87.2)	5 (1.1)	53 (11.7)

Values are presented as number (%).

SFT/HP, solitary fibrous tumor/hemangiopericytoma.

Table 2. Comparison between frozen and permanent diagnoses and analysis of reason for diagnostic error of discordant cases

Case No.	Frozen cytology and section diagnosis	Permanent diagnosis	Reason for error
1	Atypical glial cell proliferation with necrotic debris, favor reactive change	Diffuse astrocytoma	Misinterpretation
2	Consistent with benign glial tumor	Glioblastoma	Misinterpretation
3	Histiocytic lesion	Glioblastoma	Nonrepresentative sample
4	Ependymoma	Papillary and rhabdoid meningioma	Misinterpretation
5	Squamous epithelium, suggestive of craniopharyngioma	Immature teratoma	Nonrepresentative sample

of glial lesions, discrimination between normal brain reactive gliosis versus low-grade gliomas (WHO grades I and II) is difficult; evaluation of true cellularity is limited in both frozen cytology and frozen sections. Increased gliosis is insufficient to diagnose glioma. Features showing unevenly distributed astrocytes with mild nuclear irregularities, no discernible cytoplasm, high nuclear to cytoplasmic ratios, and hyperchromatic chromatin favor low-grade glioma. Low cellular smears composed of spindle cells, especially the peripheral areas of high-grade gliomas, are difficult to interpret. Radiation injury may mimic glioblastoma by cytological findings such as bizarre nuclear features.¹² Necrosis and vascular endothelial proliferation are reliable cytologic findings of high-grade glioma.^{10,13,14} Because they share clinicoradiologic findings, glioblastoma should be distinguished from metastasis and lymphoma. Glioblastoma is characterized by highly malignant cells and endothelial proliferation, i.e., a bulbous collection of

overlapped and haphazardly oriented nuclei attached to vessels on frozen cytology.¹⁵ On the other hand, lymphoma cytology lacks endothelial proliferation, shows no tumor cells within the walls of blood vessels, exhibits a spread of atypical, round nuclei with vesicular, open chromatin and distinct nucleoli, and displays abundant lymphoglandular bodies with tingible body macrophages in the background. Pleomorphic xanthoastrocytoma belongs to astrocytic tumors showing marked nuclear pleomorphism with no mitotic activity in frozen cytology.¹⁶

Among CNS neoplasms showing spindle cell morphology, frozen cytology samples of meningeal neoplasms are notorious for having diverse cytologic findings. Most conventional, low-grade meningiomas show nuclear inclusion or vesicular nuclear clearing and thick collagenous cytoplasm as well as syncytial whorls.¹⁷ Compared to low-grade meningiomas, high-grade meningiomas such as rhabdoid or papillary types (WHO grade III)

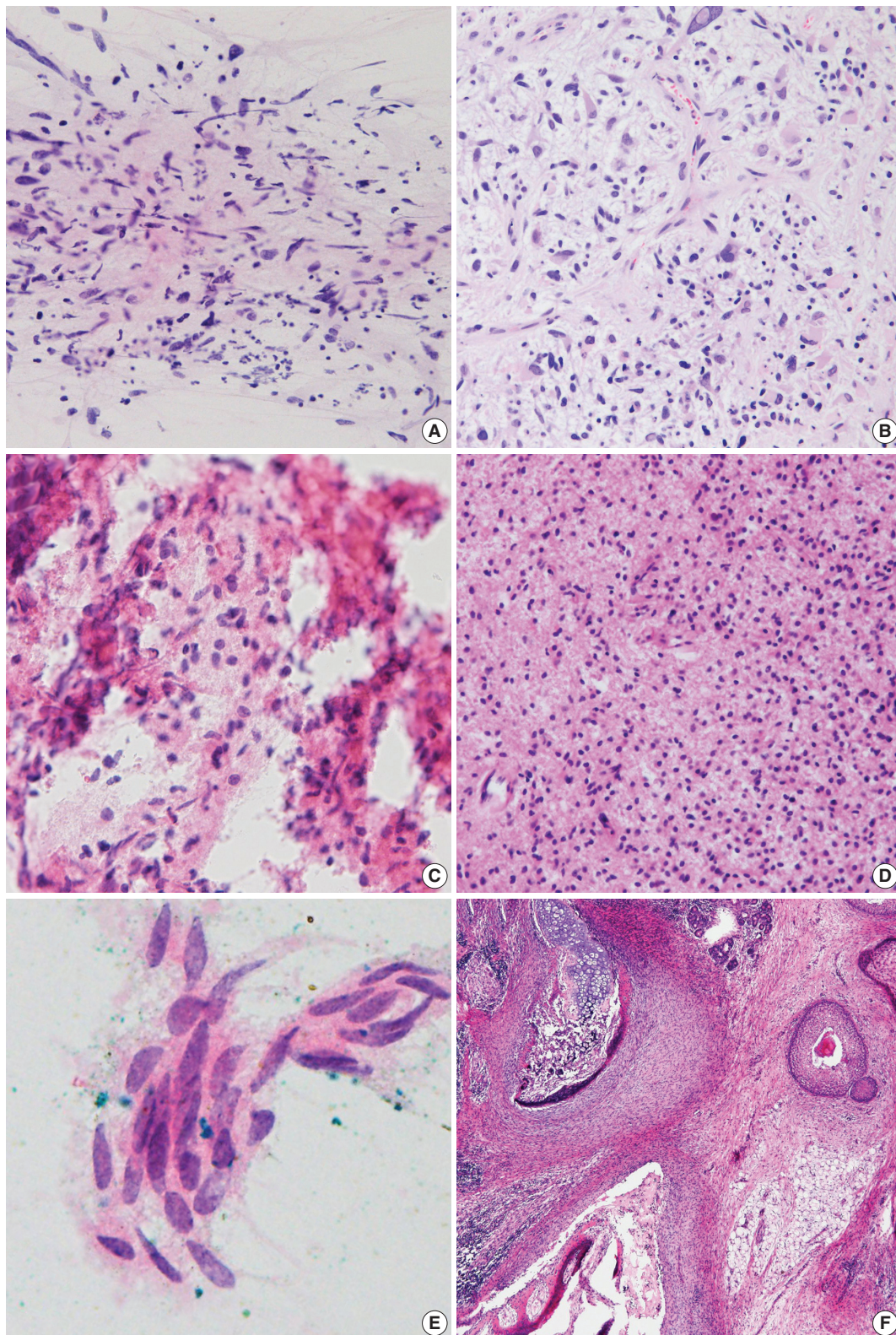


Fig. 2. Discordant cases. (A, B) Spindle cells with occasional atypical cells are mixed with karyorrhectic debris (A), and glioblastoma is diagnosed in the permanent section (B). (C, D) A tiny focus of round cells shows eosinophilic fibrillary cytoplasm in a bloody background (C), and diffuse astrocytoma is diagnosed in the permanent section (D). (E) Only one cluster of squamoid epithelium is seen in frozen smears. (F) Immature teratoma with neuroepithelium is finally diagnosed in permanent section.

Table 3. Deferred cases excluding inadequate specimens in the frozen diagnoses

Disease entities	No.
Pituitary adenoma	3
Astrocytic tumor, low grade	2
Gliomatosis cerebri	1
Piloxyoid astrocytoma	1
Astrocytic tumor, high grade	8
Glioblastoma	5
Anaplastic astrocytoma	3
Ependymoma	6
Ependymoma	3
Cellular ependymoma	1
Myxopapillary ependymoma	2
Schwannoma	1
Germ cell tumor	1
Mature teratoma	1
Malignant solitary fibrous tumor/hemangiopericytoma	2
Hematologic malignancy	1
Plasmacytoma	1
Metastatic tumor	1
Metastatic adenocarcinoma	1
Other malignant tumor	2
Hemangioblastoma	2
Other benign tumors	4
Vascular malformation	1
Hemangioma	2
Rathke's cleft cyst	1
Non-neoplastic lesions	1
No diagnostic abnormality	1

may share cytological findings of ependymoma because meningiomas of rhabdoid or papillary types show few meningeal whorls and predominant perivascular rosette-like arrangements that were misdiagnosed as ependymoma.¹⁸ Nuclear inclusions on cytologic smears may be shared by these two disease entities.^{15,18} Eosinophilic hyalinized cytoplasm and hyaline globules of rhabdoid meningioma should be distinguished from atypical teratoid/rhabdoid tumors, germinoma, or embryonal carcinomas.¹⁹ Even anaplastic meningioma shows pleomorphic cells, mimicking carcinoma or sarcoma. Schwannomas lack whorls and have elongated, wavy cytoplasm.^{15,20} Distinguishing meningioma and schwannoma is not difficult in most cases. However, uncommon locations such as intracerebral or sellar schwannoma require careful intraoperative diagnoses.²¹

Round cell lesions such as oligodendroglioma containing abundant thin capillary structures may easily exclude astrocytic lesions due to a perinuclear halo artifact that is typically seen in permanent formalin-fixed processing of oligodendrogliomas.^{14,22} Cytological smears of oligodendroglioma-mimicking round cell tumors such as central neurocytoma, hemangioblastoma, metastatic clear

cell renal cell carcinoma, and dysembryoplastic neuroepithelial tumor should be differentiated from oligodendroglioma and small cell glioblastoma.^{23,24} Central neurocytoma, an oligodendroglioma-mimicker, is a well-differentiated tumor showing features of neuronal differentiation that may mimic the frozen histology of oligodendroglioma, clear cell ependymoma, or even necrotic glioblastoma due to eosinophilic acellular fibrillary areas masquerading as necrotic portions under frozen histologic sections, despite the small round cells having fine, granular nuclear chromatin and cytoplasm.^{20,25} When pathologists observe cytological findings such as arborizing thin-walled vasculature, calcification, or mucoid foci, these shared features should be distinguished from clear cell ependymoma, central neurocytoma, or oligodendroglioma. Nuclear features that include a salt-pepper appearance are features of neurocytoma, but cellular areas with alternating acellular fibrillary neuropil-rich areas may mimic or be easily misinterpreted as ependymal rosettes.²⁴ Nuclear details of ependymomas are distinguished from those of neurocytomas by the presence of nuclear grooves and nuclear inclusions.²⁵ On observing nuclear features, round to oval nuclei with stippled chromatin, as well as nuclear grooves and intracytoplasmic lumina, are seen in ependymomas.¹⁸ Clear cell ependymoma, one of the oligodendroglioma-mimickers, may pose a significant diagnostic challenge because cytological findings of a few cells with a clear cytoplasm and eccentric nucleus are unconventional for ependymoma;²⁰ conventional type ependymomas show a distinct cytomorphology, but less-epithelial variants of ependymomas, such as tancytic variants, may resemble astrocytic tumors even in cytological smears.²⁶ Ependymomas having acellular perivascular fibrillary pseudorosettes are composed of round-shaped, monotonous, cohesive tumor cells.²⁵ However, cytological findings such as loosely arranged monotonous round-shaped tumor cells with small nuclei and stippled chromatin have provided diagnostic distinguishing points in cases with acellular fibrillary areas scattered in the cytology smears.¹ The WHO classification of CNS neoplasms classifies ependymomas into three grades, considering parameters of cellularity, pleomorphism, mitosis, necrosis, and microvascular proliferation.⁶ Cellular pleomorphism and microvascular proliferation were the most reliable indicators of WHO grade III ependymomas compared to mitosis or necrosis patterns.²⁷ Intraoperative cytological characteristics of ependymomas are well described, but cytologic characteristics by grading are rarely documented.

Intraoperative frozen sections provide an important tool, but agreement varies among histopathological entities and is lower in low-grade tumors than in high-grade tumors, compared to intraoperative cytology.²⁸ For example, frozen diagnosis of menin-

gliomas is not different from intraoperative cytology. Because the present study retrospectively assessed the use of both cytology and frozen sections, direct comparison of the two is limited. The cytologic characteristics described here with frozen sections revealed that diagnostic accuracy of intraoperative frozen diagnosis was 87.2% (396/454), and the accuracy was elevated up to 98.8% after excluding deferred cases. Two out of five discordant cases were ascribed to sampling error taken from nonrepresentative tissue portions. The remaining three cases were misinterpreted as reactive gliosis or low-grade tumors in bloody backgrounds. Bloody backgrounds may contribute to false negative diagnoses, so clinical confirmation is always desirable in unusual smears. With respect to correct grading of glial tumors, concordance of glial tumors was low. Distinguishing between reactive gliosis and low-grade gliomas is limited and difficult, by both frozen cytology and frozen section.³ Non-neoplastic CNS lesions mimicking glial tumors include demyelinating diseases and tissue-destructive lesions such as infarctions, abscesses, radio-necrosis, and areas with resolving hemorrhage.^{22,29}

These cytomorphologic features in conjunction with the clinical history and radiologic findings provided an accurate diagnosis in 87.2% of the cases in the present study, similar to previous studies reporting a diagnostic accuracy varying from 86% to 97.3%.^{1,30} Relatively high concordance rates of major disease entities in the present study are related with frequent exposure and experience with those CNS neoplasms. This diagnostic accuracy can be improved through knowledge of clinical and neuroimaging correlation as well as experienced pathologists.

Given the clinical significance of intraoperative tentative diagnoses of CNS lesions, it is important to examine cytological smears and frozen sections combined with clinicoradiologic findings to increase diagnostic accuracy. Intraoperative frozen diagnoses using combined cytology and frozen sections encompass limitations in layered diagnosis according to revised upcoming WHO classifications and inevitable deferral of grading, and awareness of these pitfalls is important for neuropathologists and neurosurgeons. Despite the limitations of retrospective studies, this study describes the 10-year retrospective experience of prompt and accurate intraoperative frozen section diagnoses in CNS lesions with the combined use of smear cytology and highlights its diagnostic value as a reliable method.

ORCID

Myunghee Kang: <https://orcid.org/0000-0003-4083-888X>

Dong Hae Chung: <https://orcid.org/0000-0002-4538-0989>

Na Rae Kim: <https://orcid.org/0000-0003-2793-6856>

Hyun Yee Cho: <https://orcid.org/0000-0003-3603-5750>

Seung Yeon Ha: <https://orcid.org/0000-0001-7071-1623>

Sangho Lee: <https://orcid.org/0000-0003-4636-7521>

Jungsuk An: <https://orcid.org/0000-0003-0312-2460>

Jae Yeon Seok: <https://orcid.org/0000-0002-9567-6796>

Gie-Taek Yie: <https://orcid.org/0000-0002-8706-7253>

Chan Jong Yoo: <https://orcid.org/0000-0002-2680-7692>

Sang Gu Lee: <https://orcid.org/0000-0001-9943-4906>

Eun Young Kim: <https://orcid.org/0000-0002-4942-8425>

Woo Kyung Kim: <https://orcid.org/0000-0002-0974-903X>

Seong Son: <https://orcid.org/0000-0002-2815-9908>

Sun Jin Sym: <https://orcid.org/0000-0002-1340-6291>

Dong Bok Shin: <https://orcid.org/0000-0002-6872-4043>

Hee Young Hwang: <https://orcid.org/0000-0002-1152-5684>

Eung Yeop Kim: <https://orcid.org/0000-0002-9579-4098>

Kyu Chan Lee: <https://orcid.org/0000-0002-6295-3996>

Author Contributions

Conceptualization: NRK.

Data curation: KCL.

Formal analysis: MK, DHC.

Investigation: SJS, DBS.

Project administration: NRK.

Resources: SGL, EYK (Eun Young Kim), CJY, GTY, WKK, SS.

Supervision: NRK, HYC, SYH.

Validation: JA, SL, JYS.

Visualization: SGL, EYK (Eung Yeop Kim), HYH.

Writing—original draft: NRK, MK, DHC.

Writing—review & editing: NRK, MK, DHC.

Conflicts of Interest

The authors declare that they have no potential conflicts of interest.

REFERENCES

1. Marshall LF, Adams H, Doyle D, Graham DI. The histological accuracy of the smear technique for neurosurgical biopsies. *J Neurosurg* 1973; 39: 82-8.
2. Eisenhardt L, Cushing H. Diagnosis of intracranial tumors by supravital technique. *Am J Pathol* 1930; 6: 541-52.
3. Gal AA, Cagle PT. The 100-year anniversary of the description of the frozen section procedure. *JAMA* 2005; 294: 3135-7.
4. Cahill EM, Hidvegi DF. Crush preparations of lesions of the central nervous system: a useful adjunct to the frozen section. *Acta Cytol*

- 1985; 29: 279-85.
5. Louis DN, Ohgaki H, Wiestler OD, Cavenee WK. WHO classification of tumours of the central nervous system. 4th ed. Lyon: IARC Press, 2016.
 6. Louis DN, Ohgaki H, Wiestler OD, Cavenee WK. WHO classification of tumours of the central nervous system. Lyon: IARC Press, 2007.
 7. Folkerth RD. Smears and frozen sections in the intraoperative diagnosis of central nervous system lesions. *Neurosurg Clin N Am* 1994; 5: 1-18.
 8. Rushing EJ, Wesseling P. Towards an integrated morphological and molecular WHO diagnosis of central nervous system tumors: a paradigm shift. *Curr Opin Neurol* 2015; 28: 628-32.
 9. Inagawa H, Ishizawa K, Hirose T. Qualitative and quantitative analysis of cytologic assessment of astrocytoma, oligodendroglioma and oligoastrocytoma. *Acta Cytol* 2007; 51: 900-6.
 10. Kang M, Kim NR, Chung DH, Yoo CJ. Crush cytologic findings of a cerebral granular cell astrocytoma. *Acta Cytol* 2012; 56: 571-5.
 11. Shioyama T, Muragaki Y, Maruyama T, Komori T, Iseki H. Intraoperative flow cytometry analysis of glioma tissue for rapid determination of tumor presence and its histopathological grade: clinical article. *J Neurosurg* 2013; 118: 1232-8.
 12. Lampert PW, Davis RL. Delayed effects of radiation on the human central nervous system: "early" and "late" delayed reactions. *Neurology* 1964; 14: 912-7.
 13. Lee S, Kim NR, Chung DH, Yee GT, Cho HY. Squash cytology of a dural-based high-grade chondrosarcoma may mimic that of glioblastoma in the central nervous system. *Acta Cytol* 2015; 59: 219-24.
 14. Plesec TP, Prayson RA. Frozen section discrepancy in the evaluation of central nervous system tumors. *Arch Pathol Lab Med* 2007; 131: 1532-40.
 15. Lee HS, Tihan T. The basics of intraoperative diagnosis in neuropathology. *Surg Pathol Clin* 2015; 8: 27-47.
 16. Yamada SM, Murakami H, Tomita Y, et al. Glioblastoma multiforme versus pleomorphic xanthoastrocytoma with anaplastic features in the pathological diagnosis: a case report. *Diagn Pathol* 2016; 11: 65.
 17. Seok JY, Kim NR, Cho HY, Chung DH, Yee GT, Kim EY. Crush cytology of microcystic meningioma with extensive sclerosis. *Korean J Pathol* 2014; 48: 77-80.
 18. Jeong J, Kim NR, Lee SG. Crush cytology of a primary intraspinal rhabdoid papillary meningioma: a case report. *Acta Cytol* 2013; 57: 528-33.
 19. Raisanen J, Hatanpaa KJ, Mickey BE, White CL 3rd. Atypical teratoid/rhabdoid tumor: cytology and differential diagnosis in adults. *Diagn Cytopathol* 2004; 31: 60-3.
 20. Kobayashi S. Meningioma, neurilemmoma and astrocytoma specimens obtained with the squash method for cytodiagnosis: a cytologic and immunochemical study. *Acta Cytol* 1993; 37: 913-22.
 21. Kim NR, Suh YL. Primary intrasellar schwannoma: a case report. *Korean J Pathol* 2002; 36: 274-7.
 22. Plesec TP, Prayson RA. Frozen section discrepancy in the evaluation of nonneoplastic central nervous system samples. *Ann Diagn Pathol* 2009; 13: 359-66.
 23. Can B, Akpolat I, Meydan D, Üner A, Kandemir B, Söylemezoğlu F. Fine-needle aspiration cytology of metastatic oligodendroglioma: case report and literature review. *Acta Cytol* 2012; 56: 97-103.
 24. Hernández-Martínez SJ, De Leija-Portilla JO, Medellín-Sánchez R. Cytologic features during intraoperative assessment of central neurocytoma: a report of three cases and review of the literature. *Acta Cytol* 2013; 57: 400-5.
 25. Deb P, Manu V, Pradeep H, Bhatoe HS. Intraparenchymal clear cell ependymoma. *J Cytol* 2011; 28: 73-6.
 26. Chaudhuri PM, Chaudhuri S, Chakrabarty D, et al. Squash cytology of tancytic ependymoma: a report of two cases. *Diagn Cytopathol* 2017; 45: 270-3.
 27. Wang M, He X, Chang Y, Sun G, Thabane L. A sensitivity and specificity comparison of fine needle aspiration cytology and core needle biopsy in evaluation of suspicious breast lesions: a systematic review and meta-analysis. *Breast* 2017; 31: 157-66.
 28. Mahe E, Ara S, Bishara M, et al. Intraoperative pathology consultation: error, cause and impact. *Can J Surg* 2013; 56: E13-8.
 29. Monabati A, Kumar PV, Kamkarpour A. Intraoperative cytodagnosis of metastatic brain tumors confused clinically with brain abscess: a report of three cases. *Acta Cytol* 2000; 44: 437-41.
 30. Chand P, Amit S, Gupta R, Agarwal A. Errors, limitations, and pitfalls in the diagnosis of central and peripheral nervous system lesions in intraoperative cytology and frozen sections. *J Cytol* 2016; 33: 93-7.

Squamous Cell Carcinoma of the Extrahepatic Common Hepatic Duct

Myunghye Kang · Na Rae Kim
Dong Hae Chung · Hyun Yee Cho
Yeon Ho Park¹

Departments of Pathology and ¹Surgery,
Gil Medical Center, Gachon University College of
Medicine, Incheon, Korea

Received: July 9, 2018
Revised: August 22, 2018
Accepted: September 3, 2018

Corresponding Author

Na Rae Kim, MD, PD
Department of Pathology, Gil Medical Center,
Gachon University College of Medicine, 21
Namdong-daero 774beon-gil, Namdong-gu,
Incheon 21565, Korea
Tel: +82-32-460-3073
Fax: +82-32-460-2394
E-mail: clara_nrk@gilhospital.com

We report a rare case of hilar squamous cell carcinoma. A 62-year-old Korean woman complaining of nausea was referred to our hospital. Her biliary computed tomography revealed a 28 mm-sized protruding solid mass in the proximal common bile duct. The patient underwent left hemihepatectomy with S1 segmentectomy and segmental excision of the common bile duct. Microscopically, the tumor was a moderately differentiated squamous cell carcinoma of the extrahepatic bile duct, without any component of adenocarcinoma or metaplastic portion in the biliary epithelium. Immunohistochemically, the tumor was positive for cytokeratin (CK) 5/6, CK19, p40, and p63. Squamous cell carcinoma of the extrahepatic bile duct is rare. To date, only 24 cases of biliary squamous cell carcinomas have been reported. Here, we provide a clinicopathologic review of previously reported extrahepatic bile duct squamous cell carcinomas.

Key Words: Carcinoma, squamous cell; Klatskin tumor; Hepatic duct, common; Hilum; Chemotherapy

Cholangiocarcinoma is a malignant tumor arising from the biliary tree at any portion of the bile duct: from the bile ductules of the intrahepatic area to the ampulla of Vater. Most of the tumors are adenocarcinomas, and squamous cell carcinoma (SCC) of the extrahepatic bile duct is rare. Since the first reported case by Cabot and Painter,¹ about 24 cases of bile duct SCC have been reported in the literature.²⁻¹⁸

Here, we review the clinicopathologic characteristics of the reported cases of biliary SCC.

CASE REPORT

Clinical summary

A 62-year-old Korean woman complained of continuous nausea and abdominal discomfort for two months. Except for the diagnosis of thyroid papillary carcinoma 13 years prior to presentation, she had no history of other malignancies or cholelithiasis. Abdominal computed tomography (CT) performed at a local clinic revealed a dilated bile duct (Fig. 1A). Magnetic resonance cholangiopancreatography revealed luminal narrowing in the distal bile duct with proximal dilation (Fig. 1B). Perihilar proximal biliary cholangiocarcinoma was suspected. Liver magnetic

resonance images (MRI) showed a 1 cm-sized, non-enhancing, T2 high signal intensity lesion in the left lobe, suggesting hepatic cyst or abscess. Metastasis to the common hepatic artery, portocaval lymph node, and hepatic duct ligament was also suspected. Preoperatively, an endoscopic retrograde cholangiopancreatography-assisted biopsy was performed, and a diagnosis of carcinoma with squamous differentiation was rendered. Subsequently, left hemihepatectomy with S1 segmentectomy and segmental excision of the common bile duct were performed. After surgical resection, abdominal CT revealed an enlarged common hepatic arterial lymph node, resulting in suspicion of metastasis. The patient developed ascites and a pleural effusion. In addition, a thrombus developed in the superior vena cava. Heparin was used for treatment of thrombus; however, heparin-induced thrombocytopenia was followed. The patient received 5-fluorouracil (5-FU) and cisplatin, but chemotherapy had to be stopped after the first cycle due to pancytopenia, aggravating thrombocytopenia, and persistent fever. The patient refused additional chemoradiotherapy. During the postoperative 15 months, liver MRI showed metastasis with increased size in the hepatic duct lymph nodes, portocaval, and paraduodenal areas, and the largest size increased from 1.8 to 3.1 cm in short diameter. The patient was alive

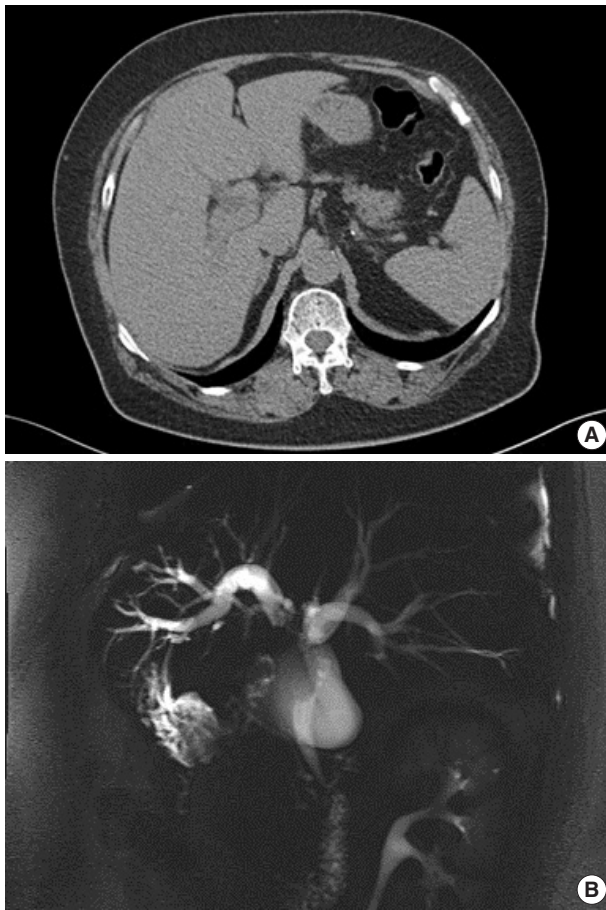


Fig. 1. (A) Computed tomography reveals perihilar cholangiocarcinoma with metastatic lymph nodes. (B) Magnetic resonance cholangiopancreatography shows strictures of the left intrahepatic duct to common hepatic duct.

over the 15-month follow-up period.

Pathological findings

Left hemihepatectomy with S1 segmentectomy and segmental excision of the common bile duct were performed. Serial sections revealed a firm grayish-white mass measuring 2.8 cm at the proximal common hepatic duct near the hilar region (Fig. 2A). The mass did not involve the cystic duct or the right and left hepatic ducts. Microscopically, the papillary-protruded mass was composed entirely of squamous cells with eosinophilic keratin pearls (Fig. 2B). The surface of the mass was denuded and inflamed due to preoperative stent insertion. No mucin production or duct formation was detected. There were no metaplastic or biliary intraepithelial neoplastic lesions. An abrupt transition to neoplastic squamous epithelium from the cuboidal biliary epithelium was noted (Fig. 2C). Mitosis was frequently found. The tumor extended to the pericholedochal fibroconnective tis-

sue. Lymphovascular and perineural invasion were noted. The tumor cells were positive for cytokeratin (CK) 5/6 (CK5/6; 1:100, D5/16 B4, Dako, Glostrup, Denmark), CK19 (prediluted, B/70, Novocastra, Newcastle upon Tyne, UK), p63 (prediluted, DAK-P63, Dako), p40 (prediluted, BC28, Dako), and Ki-67 (1:100, MIB-1, Dako). However, the tumor cells were negative for CK7 (1:100, OV-TL 12/30, Dako), CK20 (1:100, KS 20.8, Dako), periodic acid Schiff, and polyclonal carcinoembryonic antigen (prediluted, polyclonal, Dako). The tumor cells were focally non-block positive for p16 (1:200, JC8, Santa Cruz Biotechnology, Santa Cruz, CA, USA). Entirely embedded sections of tumor and bile duct revealed no adenocarcinoma component. The tumor was diagnosed as a pure SCC with moderate differentiation. Ultrastructurally, polygonal to elongated tumor cells were filled with dilated rough endoplasmic reticulum, intermediate filaments, and primary and secondary lysosomes with prominent golgi apparatus (Fig. 3). Well-formed desmosomes were found. The gallbladder was separately submitted and showed only inflammation without any stones. A 1 cm-sized abscess with periductal inflammation was noted in the background liver parenchyma. Aspiration cytology of the enlarged common hepatic arterial lymph node showed metastatic SCC (pT2aN1M0, stage IIIc according to American Joint Committee on Cancer). Human papillomavirus was not detected using the HPV 9G DNA kit (BMT, Chuncheon, Korea) in accordance with the manufacturer's protocol.

Approval was obtained from our Institutional Review Board (No. GCIRB2018-066) for this case report with a waiver of informed consent.

DISCUSSION

Histologically, the biliary mucosa is composed of a single-layered cuboidal epithelium without squamous epithelial cells. Adenocarcinoma is the most common histologic type of biliary tract malignancies, and biliary SCC is rare. By definition, the diagnosis of adenosquamous carcinoma of the gallbladder and extrahepatic bile ducts can be made when SCC comprises more than 25% of the tumor component, but the current classification system by the World Health Organization requires that no glandular component is present for a diagnosis of biliary SCC.

The pathogenesis of this rare biliary SCC has not been elucidated to date. It is presumed that the normal columnar epithelium undergoes squamous metaplasia by continuous irritation due to an inflammatory stimulus, which then may result in carcinomatous changes through dysplasia.¹ Predisposing conditions

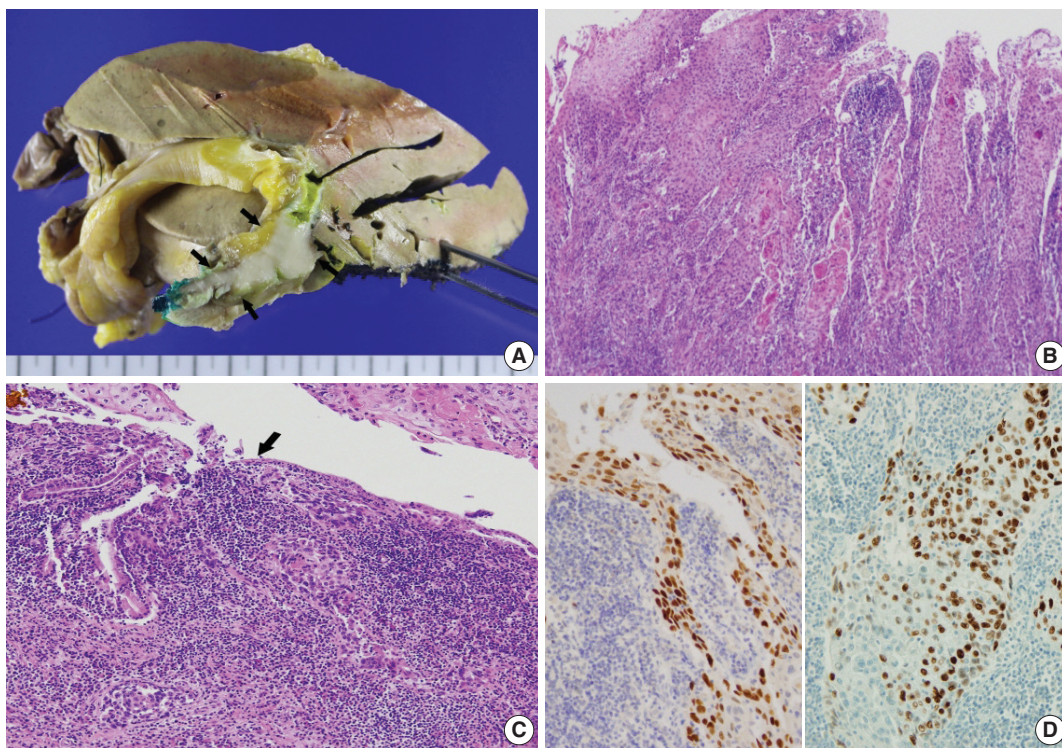


Fig. 2. (A) The gross specimen revealed a protruded mass (arrows) accounting for all layers of the hepatic duct wall. (B) Histologically, thickened papillary squamous epithelium shows moderately differentiated dyskeratotic squamous cells with keratin pearls with stromal invasion. (C) Surface epithelium shows a transition from unilayered cuboidal to squamous epithelium (arrow). (D) Immunohistochemically, the tumor cells are positive for p63 (left) and p40 (right).

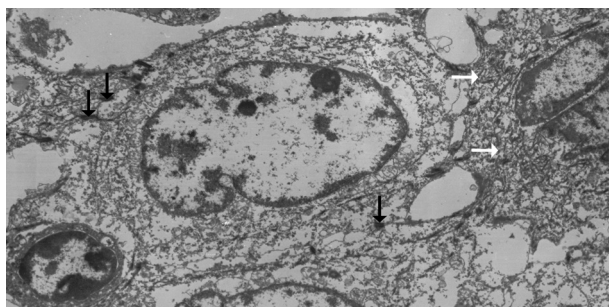


Fig. 3. Ultrastructurally, ovoid-shaped tumor cells have cytoplasmic tonofilaments (white arrows) and are connected with well-formed desmosomes (black arrows, $\times 2,500$).

that can lead to squamous metaplasia of the biliary epithelium and biliary SCC include hepatolithiasis, recurrent pyogenic cholangitis, and clonorchiasis.¹ Secondly, pluripotent bile duct stem cells are known to undergo malignant transformation. Other possible theories include heterotopic squamous epithelium or squamous metaplasia of preexisting adenocarcinoma.^{9,13} The second and third theories might explain biliary SCC cases that lack preexisting normal squamous epithelium, like the present case. Our patient’s histology revealed pure SCC, and there was no hepato-

lithiasis or choledochal cysts on imaging studies. There was no underlying squamous epithelium, but there was an abrupt transition to dysplastic squamous epithelium from the biliary mucosa. On the other hand, a previous case reported by Abbas et al.¹⁰ showed biliary SCC associated with high-grade squamous dysplasia, similar to cervical carcinogenesis. Their finding supports the metaplasia-dysplasia-carcinoma sequence theory. However, the direct causality of inflammation-metaplasia-dysplasia should be questioned. Whether gallstones predispose to cholangiocarcinoma remain unclear, and most reported cases have not been accompanied by a metaplasia-dysplasia lesion. Another possible theory may be that SCCs are derived from undifferentiated basal cells. Immunoreactivity for CK7, CK8, CK14, CK18, and/or CK5/6 suggests the origin of the cancer cells to be the basal cells of keratinized squamous epithelium. Moreover, positive staining for biliary CK19 would confirm the bile ductular ontogeny of the neoplastic cells.¹⁹

The incidence of cholangiocarcinoma increases with age, and most reported cases occur in the fifth to seventh decades. Due to its rare incidence and strict diagnostic criteria, biliary SCC is rarely reported, and there are few reports to be retrieved for review.

Table 1. Clinicopathologic summary of reported cases of squamous cell carcinoma of the extrahepatic bile duct

No.	Age (yr)/Sex	Site	Clinical summary including tumor markers	Remarkable pathologic findings	Distant metastasis	TNM/AJCC at the diagnosis	Treatment	Outcome (follow-up)
1	58/M	Proximal CBD (upper 1/4)	Jaundice, knife-like abdominal pain	No	Liver, retroperitoneal lymph node	Stage IVB ^a	No surgery	Died (23 days)
2	24/F	Junction of proximal CBD and cystic duct	Jaundice, RUQ pain, elevated CEA	SCC, MD without lymphovascular, perineural invasion	Liver	T2aN0M1 Stage IVB ^a	Pancreaticoduodenectomy, CTx (cyclophosphamide, MTX, doxorubicin, procarbazine)	Died (8 mo)
3	68/M	Mid CBD	Secondary biliary cirrhosis, portal hypertension, hepatic failure	SCC, WD	No	TxN0M0 in autopsy Stage I	Cholecystectomy with T tube and wedge biopsy of liver	Died (6 mo)
4	56/M	Hilar	Jaundice	SCC, PD	Liver	Stage IVB ^a	Cholecystectomy with T tube, RT	Died (3 mo)
5	68/M	Mid CBD	Jaundice, elevated CA19-9, elastase I	SCC, WD with direct invasion of pancreas head	No	TxN0M0 Stage III	Pancreaticoduodenectomy, CTx (cisplatin, 5-FU), immunotherapy (OK-432)	Alive (3 mo)
6	68/M	Distal CBD	Jaundice, elevated CA19-9	1.8 cm, direct invasion of pancreas	No	T3N0M0 Stage IIIA ^a	Pancreaticoduodenectomy	Alive (27 mo)
7	50/M	Hilar	Elevated CA19-9, AFP, CEA, PIVKA II	4 cm	Liver (S2, 1 cm)	TxNxM1 Stage IVB ^a	Extended left hepatic lobectomy, T tube	Died (10 mo)
8	75/M	Distal CBD	Jaundice, elevated CA19-9	1.5 cm CEA+ CA19-9+	No	TxN1M0 Stage III ^a	Pancreaticoduodenectomy	Alive (6 mo)
9	57/F	Distal CBD and ampulla of Vater	Jaundice	Invasion to pancreas and duodenum, CEA- PAS- 1.5 cm invasion to pancreas and duodenum	No	T3bN0M0 Stage IIIA ^a	Pylorus-preserving pancreaticoduodenectomy	Not described
10	63/M	Distal CBD	Jaundice, elevated CA19-9	1.5 cm invasion to pancreas and duodenum	No	T2N1M0 Stage II	Pancreaticoduodenectomy	Alive (6 mo)
11	86/F	Junction of CBD and cystic duct	Jaundice, RUQ pain	PanCK	Not described	Not described	CTx, external beam radiation, and high-dose radiation endoluminal brachytherapy (1,800 cGy)	Died (18 mo)
12	61/F	Mid CBD	Jaundice, WNL of CA19-9, CA125, AFP History of cholecystectomy	3 cm, CK(MNF116)+ CK10/13+	Peritoneal carcinomatosis	T3N0M1 Stage IIIA ^a	Simple resection and hepatojejunial anastomosis	Died (16 mo)
13	60/M	Distal CBD	Recurrent episodes of cholangitis and obstructive jaundice	SCC, WD, 2 cm with metaplasia, dysplasia	No	T2N0M0 Stage II ^a	Pancreaticoduodenectomy	Not described
14	28/F	Hilar	Jaundice, RUQ pain	SCC, MD with high-grade squamous dysplasia	Not described	Not described	Extended left hepatic lobectomy, RT	Alive (18 mo)
15	41/F	Hilar	Jaundice, elevated CA19-9, choledochal cyst	Direct invasion to portal vein and duodenum	Not described	T4NxMx, Stage IV ^a	Endoscopic biliary stent, palliative CTx, RT	Not described

(Continued on the next page)

Table 1. Continued

No.	Age (yr)/Sex	Site	Clinical summary including tumor markers	Remarkable pathologic findings	Distant metastasis	TNM/AJCC at the diagnosis	Treatment	Outcome (follow-up)
16	64/M	Distal CBD	Abdominal discomfort, jaundice	3 cm, CK19+	No	T3N2M0, Stage IIIB ^a	Pancreaticoduodenectomy, CTx (CPT-11, PPD)	Hepatic metastasis (30 days) and died (5 mo)
17	66/M	Hilar	Jaundice, elevated CA19-9, SPan-1, DUPAN-2	SCC, WD, 3 cm, invasion of portal vein and liver, CK+ CAM5.2-	T4 (Stage IV)	T4N1M0 Stage IVA ^a	Extended right hepatic lobectomy, CTx (cisplatin+5-FU, gemcitabine+S-1)	Hepatic metastasis (6 mo) and died (12 mo)
18	67/M	CHD	Icteric sclera, elevated CA19-9	Synchronous double adenocarcinoma Metastatic adenocarcinoma in one regional lymph node	No	T1N1M0 Stage IIIB ^a	Pylorus-preserving pancreaticoduodenectomy	Multiple hepatic metastasis (3 mo) and died (8 mo)
19	77/F	Mid CBD	Jaundice, WNL of CA19-9, CEA, DUPAN-2	SCC, PD, 1.7 cm, invasion to right hepatic artery CK5/6+ p53+ PAS-	No	T4N0M0, Stage IVA ^a	Pylorus-preserving pancreaticoduodenectomy, CTx (gemcitabine)	Local recurrence (20 mo) and died (32 mo)
20	78/M	Distal CBD	Jaundice, brown urine, WNL of CEA, CA19-9, DUPAN-2	SCC, MD, 3 cm	No	T1N1M0 Stage IIIB ^a	Subtotal stomach-preserving pancreaticoduodenectomy, CTx (S-1, cisplatin)	Paraaortic lymph node metastasis (6 mo), alive (10 mo), Died (5 mo)
21	62/M	CHD	Jaundice, RUQ pain, elevated CA19-9	1.5 cm, perineural invasion PanCK+ CAM5.2+ CK5/6+ p63+ p40+ PAS-	Not described	T1N0M0 Stage I ^a	Curative resection and cholechojejunostomy, CTx (oral fluoropyrimidine S-1)	Died (32 mo)
22	77/M	CHD	Elevated CA19-9, choledochal cyst	Not described	Not described	Not described	Curative resection and cholechojejunostomy	Died (47 mo) Alive (45 mo)
23	67/F	CHD	Elevated CA19-9	Not described	Not described	Not described	Pancreaticoduodenectomy	Alive (9 mo)
24	73/M	Mid CBD	WNL of CA19-9 and CEA	4 cm, CK5/6+ p63+	No	Not described	Left hepatic lobe and caudate lobe resection, subtotal preserving pancreaticoduodenectomy	Alive (9 mo)
25 (present case)	62/F	Hilar	Nausea, abdominal discomfort, elevated CA19-9	2.8 cm, CEA- p40+ p63+ CK5/6+ CK7-	No	T2N1M0, Stage IIIC	Cholecystectomy, left hemihepatectomy, S1 segmentectomy, CTx (5-FU, cisplatin)	Alive (9 mo)

AJCC, American Joint Committee on Cancer; M, male; F, female; CBD, common bile duct; RUQ, right upper quadrant; CEA, carcinoembryonic antigen; SCC, squamous cell carcinoma; MD, moderately differentiated; CTx, chemotherapy; MTX, methotrexate; WD, well differentiated; PD, poorly differentiated; RT, radiation therapy; CA 19-9, carbohydrate antigen 19-9; WNL, within normal limit; AFP, α -fetoprotein; CEA, carcinoembryonic antigen; +, positive; -, negative; CK, cytokeratin; S-1, tegafur/gimeracil/oteradi; CHD, common hepatic duct.
^aThe stage was modified as the AJCC 8th edition.

From the literature, we found 34 cases of biliary SCCs in the extrahepatic bile duct. Among the 34 reported cases of SCC of the extrahepatic duct, only 24 provided well-described clinicopathologic data.²⁻¹⁸ Only one case associated with a choledochal cyst demonstrated predisposing precursors. A review of the cases revealed that age ranged from 24 to 86 years (mean, 62 years). The male-to-female ratio was 16:9. The site of occurrence of biliary SCC was the common hepatic duct region in four cases, hilar region in seven cases, proximal common bile duct region in two cases, mid portion in five cases, and distal common bile duct in seven cases.

A review of the previously reported cases demonstrated that the prognosis of biliary SCCs is extremely grave. Cholangiocarcinoma containing a component of SCC showed the following trends: rapid progression to advanced stage, short survival time, large tumor size, aggressive intrahepatic spreading, and frequent metastasis. Findings related to poor prognosis include elevated preoperative level carbohydrate antigen 19-9, resection margin involvement, advanced T category, and metastatic lymph node.²⁰ The mortality rate of biliary SCCs was up to 63.6% (14/22 cases of available data) during the follow-up period (mean, 14.8 months). Twenty out of 25 cases with available data (80%) underwent surgical resection with or without chemoradiotherapy. Among them, nine cases were combined with chemoradiotherapy. Two out of 25 cases (8%) received only conservative treatment. Ten cases (40%) received chemotherapy with or without radiation. The mean survival of patients without surgery was less than 12 months. Unlike head and neck SCCs, there is no supportive evidence for radiation therapy for unresectable biliary SCC. However, there are some reports of chemotherapy's important palliative value for painful localized metastasis or uncontrolled bleeding.²⁰ These results are summarized in Table 1. Patients undergoing surgery had a better prognosis than those receiving conservative, non-surgical treatments (median survival, 32 months vs 3 months, $p = .009$). However, age and stage at diagnosis and associated general medical condition were also influential factors. Cases with additional chemotherapy showed a tendency toward poorer prognosis than those with surgery only, although the difference was not statistically significant (median survival, 12 months vs 32 months; $p = .085$). Other clinical findings, including sex, age, and site of bile duct involvement, had no impact on prognosis.

Due to the extremely rare incidence of biliary SCCs, no standardized therapeutic strategies have been established. The recommended treatment for biliary SCCs is surgical resection with or without chemoradiotherapy, and the recommended chemotherapy is GEMOX (gemcitabine plus oxaliplatin) or GP (gem-

citabine plus cisplatin), as in bile duct adenocarcinomas.²⁰ Similar to the treatment for cancers of the gastrointestinal tract such as esophageal cancers, chemotherapy with docetaxel plus cisplatin plus 5-FU therapy or S-1 plus cisplatin therapy may be helpful. With such a regimen (S-1 plus cisplatin), one patient with biliary SCC was successfully treated.¹⁶ Combined targeted therapy, such as epidermal growth factor receptor-targeted therapy, has shown certain benefits in other cancer types, and its effects are being investigated.

Here, we reported a case of SCC of the hilar bile duct and reviewed previous reports regarding biliary SCCs. The poor prognosis observed in SCC patients may be attributed to its rarity, initial advanced stage, and lack of accumulated clinical data.

ORCID

Myunghee Kang: <https://orcid.org/0000-0003-4083-888X>

Na Rae Kim: <https://orcid.org/0000-0003-2793-6856>

Dong Hae Chung: <https://orcid.org/0000-0002-4538-0989>

Hyun Yee Cho: <https://orcid.org/0000-0003-3603-5750>

Yeon Ho Park: <https://orcid.org/0000-0003-1623-2167>

Author Contributions

Investigation: YHP.

Supervision: DHC, HYC.

Writing—original draft: MK, NRK.

Writing—review & editing: MK, NRK.

Conflicts of Interest

The authors declare that they have no potential conflicts of interest.

REFERENCES

1. Cabot RC, Painter FM. Case records of the Massachusetts General Hospital: Case 16261: four months' jaundice and rectal pain. *N Engl J Med* 1930; 202: 1260-2.
2. Burger RE, Meeker WR, Luckett PM. Squamous cell carcinoma of the common bile duct. *South Med J* 1978; 71: 216-9.
3. Gulsrud PO, Feinberg M, Koretz RL. Rapid development of cirrhosis secondary to squamous cell carcinoma of the common bile duct. *Dig Dis Sci* 1979; 24: 166-9.
4. Aranha GV, Reyes CV, Greenlee HB, Field T, Brosnan J. Squamous cell carcinoma of the proximal bile duct: a case report. *J Surg Oncol* 1980; 15: 29-35.
5. Kim KS, Park HB, Yeo HS, et al. A case of squamous cell carcinoma

- of the common bile duct. *Korean J Gastrointest Endosc* 1999; 19: 486-90.
6. Cho T, Nakamura J, Tomita H, et al. A case of squamous cell carcinoma of the distal extrahepatic bile duct. *J Jpn Sug Assoc* 2000; 61: 1853-6.
 7. Gatof D, Chen YK, Shah RJ. Primary squamous cell carcinoma of the bile duct diagnosed by transpapillary cholangioscopy: case report and review. *Gastrointest Endosc* 2004; 60: 300-4.
 8. La Greca G, Conti P, Urrico GS, et al. Biliary squamous cell carcinoma. *Chir Ital* 2004; 56: 289-95.
 9. Sewkani A, Kapoor S, Sharma S, et al. Squamous cell carcinoma of the distal common bile duct. *JOP* 2005; 6: 162-5.
 10. Abbas R, Willis J, Kinsella T, Siegel C, Sanabria J. Primary squamous cell carcinoma of the main hepatic bile duct. *Can J Surg* 2008; 51: E85-6.
 11. Price L, Kozarek R, Agoff N. Squamous cell carcinoma arising within a choledochal cyst. *Dig Dis Sci* 2008; 53: 2822-5.
 12. Kim GM, Choi GH, Kim DH, Kang CM, Lee WJ. A case of squamous cell carcinoma of the distal common bile duct. *Korean J Hepatobiliary Pancreat Surg* 2008; 12: 210-3.
 13. Yamana I, Kawamoto S, Nagao S, Yoshida T, Yamashita Y. Squamous cell carcinoma of the hilar bile duct. *Case Rep Gastroenterol* 2011; 5: 463-70.
 14. Yoo Y, Mun S. Synchronous double primary squamous cell carcinoma and adenocarcinoma of the extrahepatic bile duct: a case report. *J Med Case Rep* 2015; 9: 116.
 15. Goto T, Sasajima J, Koizumi K, et al. Primary poorly differentiated squamous cell carcinoma of the extrahepatic bile duct. *Intern Med* 2016; 55: 1581-4.
 16. Nishiguchi R, Kim DH, Honda M, Sakamoto T. Squamous cell carcinoma of the extrahepatic bile duct with metachronous para-aortic lymph node metastasis successfully treated with S-1 plus cisplatin. *BMJ Case Rep* 2016; 2016: bcr2016218177.
 17. Yang G, Li J, Meng D. Primary squamous cell cholangiocarcinoma: a case report. *Int J Clin Exp Pathol* 2016; 9: 5772-6.
 18. Mori H, Kaneoka Y, Maeda A, Takayama Y, Fukami Y, Onoe S. A perihilar bile duct squamous cell carcinoma treated by left hepatic lobe and caudate lobe resection, subtotal stomach preserving pancreaticoduodenectomy, and portal vein resection. *Jpn J Gastroenterol Surg* 2017; 50: 26-32.
 19. Pastuszak M, Groszewski K, Pastuszak M, Dyrła P, Wojtuń S, Gil J. Cytokeratins in gastroenterology: systematic review. *Prz Gastroenterol* 2015; 10: 61-70.
 20. Khan SA, Davidson BR, Goldin RD, et al. Guidelines for the diagnosis and treatment of cholangiocarcinoma: an update. *Gut* 2012; 61: 1657-69.

Primary Malignant Melanoma of the Breast

Jiwon Koh¹ · Jihyeon Lee²
So Youn Jung³ · Han Sung Kang³
Tak Yun⁴ · Youngmee Kwon^{2,3}

¹Department of Pathology, Seoul National University College of Medicine, Seoul; ²Department of Pathology, National Cancer Center, Goyang; ³Center for Breast Cancer, National Cancer Center, Goyang; ⁴Center for Specific Organs Center, National Cancer Center, Goyang, Korea

Received: September 26, 2018

Revised: October 13, 2018

Accepted: October 18, 2018

Corresponding Author

Youngmee Kwon, MD, PhD
Department of Pathology, National Cancer Center,
323 Ilsan-ro, Ilsandong-gu, Goyang 10408, Korea
Tel: +82-31-920-1742
Fax: +82-31-920-1369
E-mail: ymk@ncc.re.kr

Primary malignant melanoma of the breast (PMMB) is a rare tumor with only a few case reports available in the literature. We report two cases of PMMB, one derived from the breast parenchyma and the other from the breast skin. The first case consisted of atypical epithelioid cells without overt melanocytic differentiation like melanin pigments. The tumor cells showed diffuse positivity for S100 protein, tyrosinase, and *BRAF* V600E. However, the tumor cells were negative for cytokeratin, epithelial membrane antigen, and HMB-45. The second case showed atypical melanocytic proliferation with heavy melanin pigmentation. The tumor cells were positive for S100 protein, HMB-45, tyrosinase, and *BRAF* V600E. These two cases represent two distinct presentations of PMMB in terms of skin involvement, melanin pigmentation, and HMB-45 positivity. Although PMMB is very rare, the possibility of this entity should be considered in malignant epithelioid neoplasms in the breast parenchyma.

Key Words: Breast; Malignant melanoma; *BRAF*

Malignant melanoma is the malignant neoplasm of melanocytes which occurs predominantly in the skin, and about 4%–5% of primary melanomas arise from noncutaneous sites including mucous membranes, gastrointestinal tract, and leptomeninges.^{1,2} Primary malignant melanoma of the breast (PMMB) is particularly rare, accounting for less than 0.5% of breast cancers and 3%–5% of malignant melanoma of all tissue types.^{3,4} Only six cases of PMMB derived from the breast parenchyma without skin involvement have been reported in the literature,⁵ whereas less than 190 cases have been reported from the skin overlying the breast.⁴

PMMB can present as either (1) parenchymal melanoma without skin involvement⁵ or (2) cutaneous melanoma involving the skin overlying the breast.⁶ Here, we describe two cases of PMMB, one of each type. This case study was approved by the Institutional Review Board of National Cancer Center with a waiver of informed consent (IRB No. NCC 2018-0183).

CASE REPORT

Case 1 was a 70-year-old female who presented with her right palpable breast mass. There were no abnormal findings on the overlying skin, and magnetic resonance imaging (MRI) of the breast revealed a 2.1 cm single enhancing mass on the deep portion of the right upper inner quadrant (Fig. 1A). No hypermetabolic lesion suggesting distant metastasis was noted on positron emission tomography (PET) (Fig. 1B). The differential diagnosis of malignant epithelioid neoplasms such as sarcomatoid carcinoma, sarcoma with epithelioid features or malignant melanoma was considered by core needle biopsy. The patient underwent right breast-conserving surgery and sentinel lymph node biopsy uneventfully. Gross examination showed a 2.1 cm solid gray-white mass with an expanding border within the breast parenchyma (Fig. 1C). No discernable lesion was noted on the overlying skin. On microscopic examination, the tumor showed a solid growth pattern with partial peripheral rimming of lymphoid cells (Fig. 1D). It also contained some scattered lymphoid cells in the central portion with focal tumor necrosis (Fig. 1E). The

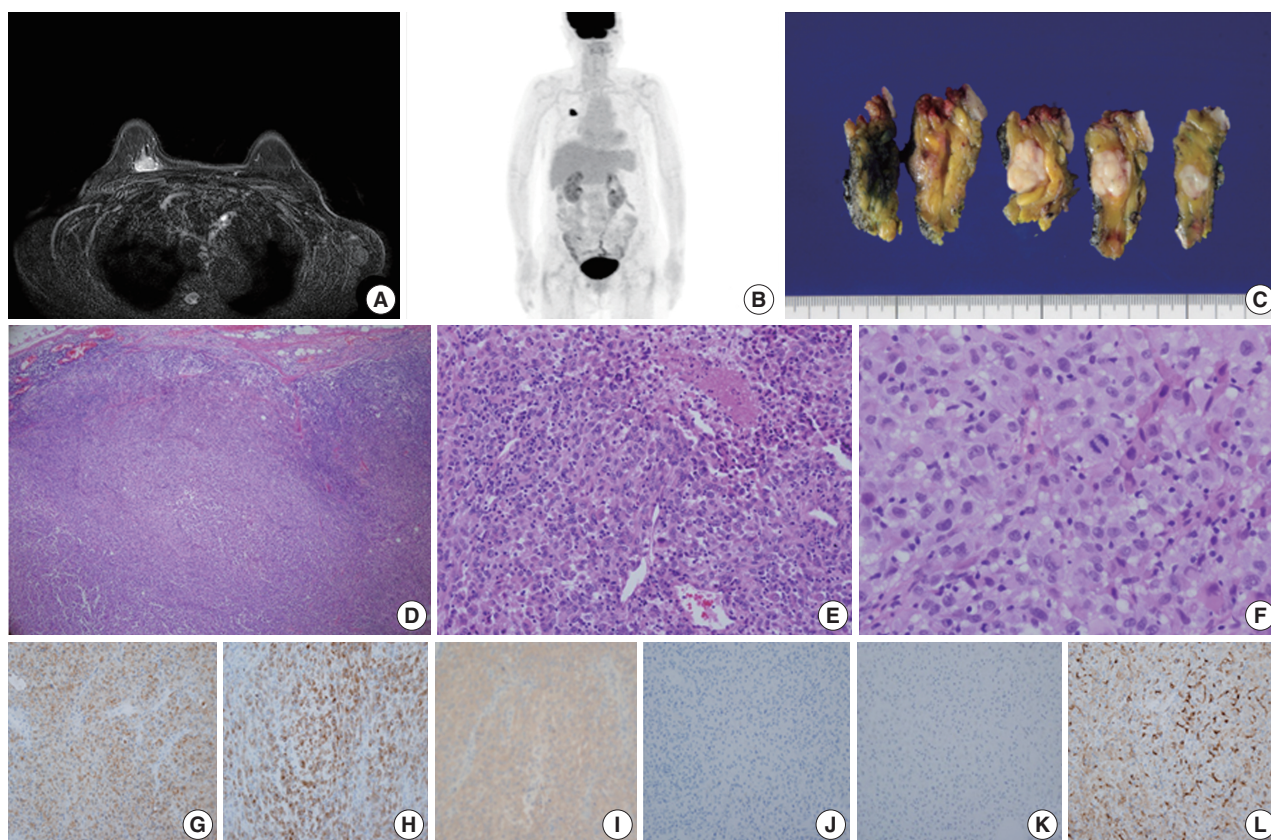


Fig. 1. (A, B) Breast magnetic resonance imaging (A) and positron emission tomography scan (B) show a solitary breast mass without regional or distant metastasis. (C) Gross examination reveals a grayish white solid mass within the breast parenchyma without skin involvement. (D–F) Microscopically, the tumor shows solid growth pattern (D) and focal tumor necrosis (E), consisting of atypical epithelioid cells. (G–L) The tumor cells are diffusely positive for S100 protein (G) and tyrosinase (H) and weakly positive for *BRAF* V600E (I), while they are negative for HMB-45 (J) and cytokeratin (K) with nonspecific weak staining for CD68 (L).

tumor consisted of polygonal epithelioid cells with abundant eosinophilic cytoplasm and oval eccentric nuclei (Fig. 1F). The tumor cells exhibited significant nuclear pleomorphism and occasional mitoses (up to 10/10 high-power field). No overt features of melanocytic differentiation such as melanin pigments were noted. By immunohistochemistry (IHC), the tumor cells showed diffuse positivity for S100 protein, tyrosinase, and *BRAF* V600E, despite HMB-45 negativity (Fig. 1G–J). The tumor cells were negative for epithelial markers such as cytokeratin (CK) (Fig. 1K), low molecular weight CK, high molecular weight CK, and epithelial membrane antigen. Furthermore, *BRAF* V600E mutation was confirmed by real-time polymerase chain reaction using a peptide nucleic acid clamping method (Supplementary Fig. S1). Therefore, the final diagnosis was primary noncutaneous malignant melanoma of the breast (PNCMB). Four sentinel lymph nodes were negative for metastasis. After a follow-up of 23 months, multiple metastases involving the left neck, left adrenal gland, left thigh muscle, and peritoneum were noted on PET

scan. Since the discovery of metastases, the patient has received immune checkpoint inhibitor therapy for three months.

Case 2 was a 30-year-old female who had a wart-like lesion on her left breast skin since childhood that recently rapidly increased to 3.0 cm in size. Breast MRI showed only mild thickening and enhancement of the left breast skin (Fig. 2A). No abnormal lesion other than that of the breast skin was observed during systemic workup studies including PET scan (Fig. 2B). Left breast-conserving surgery and axillary lymph node dissection were performed. On gross examination, the dark brown-colored skin lesion measured 4.5 cm in its greatest dimension, and no abnormal lesion within the breast parenchyma was noted on serial sections (Fig. 2C). On microscopic examination, atypical melanocytic proliferation with heavy pigmentation was observed (Fig. 2D). The lesion displayed an invasive front extending to the reticular dermis (Clark level IV), measuring 0.2 cm in thickness. The tumor cells stained positive for S100 protein, tyrosinase, HMB-45, and *BRAF* V600E but negative for CK by IHC (Fig. 2E–I). Thus,

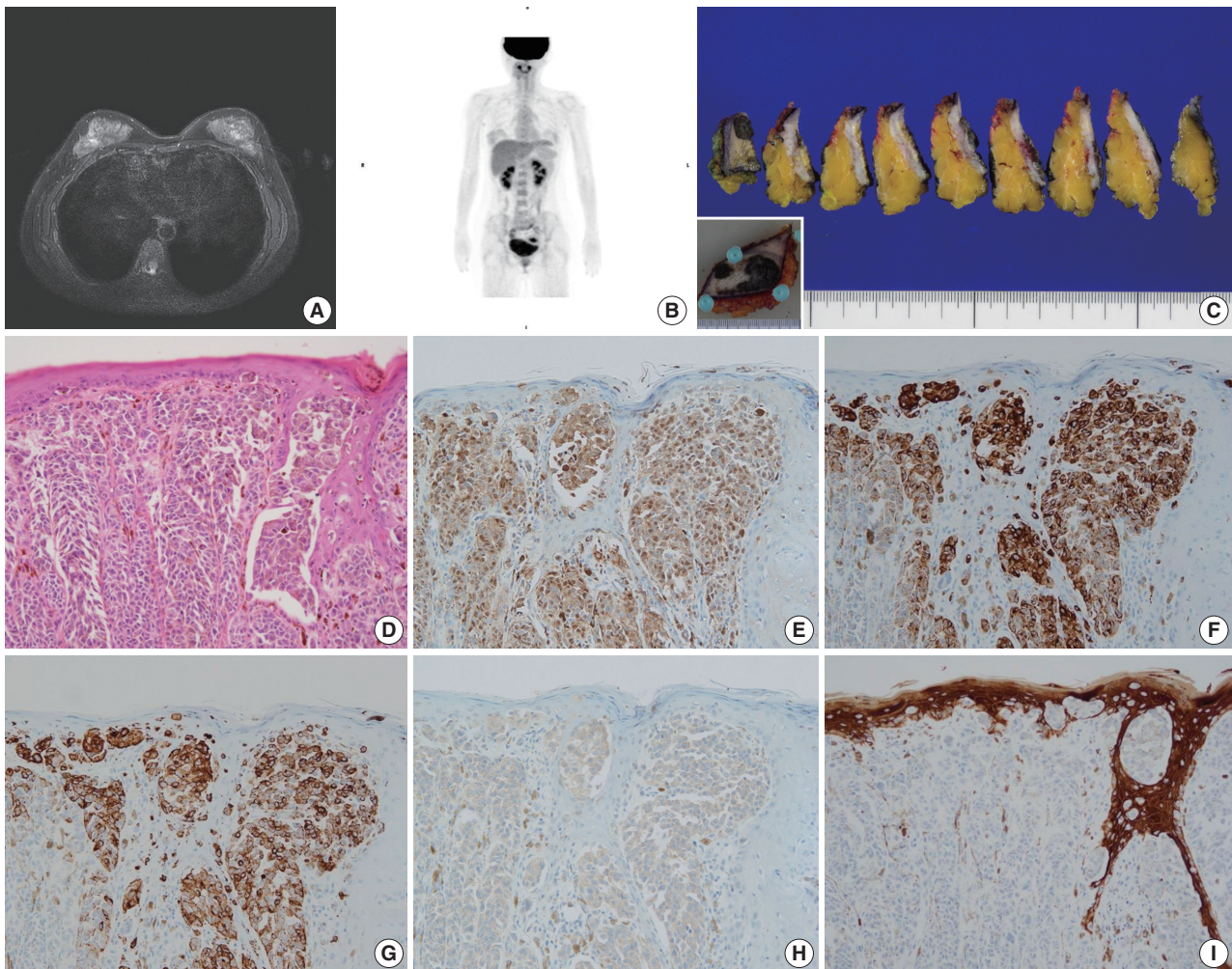


Fig. 2. (A, B) No remarkable findings other than mild thickening of the left breast skin are seen on breast magnetic resonance imaging (A) or positron emission tomography scan (B). (C) Gross examination reveals a relatively demarcated dark brown lesion. (D) Microscopically, the tumor is composed of atypical melanocytic proliferation with melanin pigmentation. (E–I) The tumor cells are strongly positive for S100 protein (E), tyrosinase (F), and HMB-45 (G); weakly positive for *BRAF* V600E (H); but negative for cytokeratin (I).

the diagnosis was primary cutaneous malignant melanoma of the breast (PCMB). Lymph node metastasis was identified in one of 19 axillary lymph nodes. At 8-month follow-up appointment, lung and bone metastases were detected with computed tomography and bone scans. Immune checkpoint inhibitor therapy was recommended, but the patient refused the treatment and was lost to follow-up.

DISCUSSION

Malignant melanomas occurring in the breast can be classified into three categories: (1) primary noncutaneous melanomas of the breast parenchyma, (2) primary cutaneous melanomas of the skin overlying the breast, and (3) metastatic melanomas to the breast

from other cutaneous locations.⁵ PMMB involving the breast skin or parenchyma is rare across the globe, but metastatic melanomas to the breast are observed with varying frequencies. For example, metastatic melanoma to the breast from other skin locations is the most common metastatic tumor to the breast in the United States⁷ but not in Korea.⁸ Fewer than 190 cases of PCMB have been reported, while only a few cases of PNCMB have been reported in the literature.⁵ We present two cases of PMMB with distinct presentation in terms of skin involvement, melanin pigmentation, and HMB-45 positivity. Their clinicopathologic characteristics are summarized in Table 1.

While it is known to be rare, the exact incidence of PMMB is unknown.⁴ PNCMB is exceedingly rare. Rassouli and Voutsadakis⁵ have reported that there are only six cases of PNCMB in

Table 1. Clinicopathologic features of two cases of primary malignant melanoma of the breast

	Case 1	Case 2
Age (yr)	70	30
Sex	Female	Female
Location of tumor	Right breast parenchyme Upper inner quadrant	Left breast skin
Key histologic features	Atypical epithelioid cells No pigmentation (amelanotic)	Atypical melanocytes Heavy pigmentation
Size of tumor (cm)	2.1	4.5
Depth of invasion (mm)	NA	2
Sentinel lymph node status	Negative	Positive
IHC		
CK	Negative	Negative
EMA	Negative	NA
Vimentin	Positive	Positive
S100 protein	Positive	Positive
HMB-45	Negative	Positive
Tyrosinase	Positive	Positive
<i>BRAF</i> V600E	Positive	Positive
Pathologic diagnosis	PNCMB	PCMB

NA, not applicable; IHC, immunohistochemistry; CK, cytokeratin; EMA, epithelial membrane antigen; HMB-45, human melanoma black-45; *BRAF*, rapidly accelerated fibrosarcoma (*RAF*) kinase-related oncogene homolog B; PNCMB, primary noncutaneous melanoma of the breast; PCMB, primary cutaneous melanoma of the breast.

the English literature. Due to the rarity of PNCMB, its clinicopathology is largely unknown, leading to diagnostic difficulty. Differential diagnoses include sarcomatoid carcinoma and sarcoma with epithelioid features such as clear cell sarcoma and histiocytic sarcoma.

Considering its low incidence, poorly differentiated invasive breast carcinoma is the first to be ruled out during diagnosis. Some authors have reported rare cases of metaplastic carcinoma with melanocytic differentiation, characterized by a melanocytic portion that lacks keratin staining but is positive for S100 protein and HMB-45, in the midst of a CK-positive metaplastic carcinoma area.⁹ However, the first case in our report exhibits no evidence of epithelial differentiation, further supported by total IHC negativity for CK, low molecular weight CK, and high molecular weight CK, which is in contrast with previous reports about metaplastic carcinoma with melanocytic differentiation.

One difficulty in the differential diagnosis of our first case was the interpretation of S100 protein positivity with HMB-45 negativity by IHC. There have been reports of S100 protein positivity in some metaplastic carcinoma and basal-type breast cancers.¹⁰ Additionally, many studies focused on the immunohistochemical features of melanoma have demonstrated that HMB-45 has the lowest sensitivity (albeit with high specificity) among the ma-

yor melanocytic markers such as S100 protein, HMB-45, Melan-A, and tyrosinase.¹¹ In addition, previous studies have suggested that HMB-45 is less sensitive in amelanotic melanomas.¹² Therefore, when PMMB is suspected, use of multiple melanocytic markers would be useful for enhancing the diagnostic yield.

Clear cell sarcoma is well-known for its histology, which is almost identical to that of malignant melanoma. There have been efforts to find the ideal biomarker for differentiating these two entities, and some recent studies have suggested that the presence of *BRAF* mutation favors the diagnosis of melanoma over clear cell sarcoma.¹³ Case 1 in this study showed positivity for *BRAF* V600E by IHC, implying *BRAF* mutation¹⁴ and supporting the diagnosis of malignant melanoma.

Histiocytic sarcoma is also included in differential diagnoses of PNCMB due to the histologic features such as a polygonal nucleus and abundant eosinophilic cytoplasm with indistinct cell borders. However, the positivity of melanocytic markers is an important finding for the diagnosis of PNCMB, despite nonspecific weak CD68 staining, as in our case (Fig. 1L).

The most notable features of the second case presented here compared to the first case are skin involvement and overt melanocytic differentiation with heavy pigmentation. These characteristic findings clearly support the diagnosis of PCMB; however, it is also recommended that IHC be performed to rule out the possibility of its mimicker, pigmented mammary Paget disease. Pigmented Paget disease accounts for a minute portion of mammary Paget disease. Pagetoid spread of malignant epithelial cells with pigmentation can indicate cutaneous melanoma or pigmented mammary Paget disease.¹⁵ However, IHC for melanocytic markers and epithelial markers can distinguish malignant melanoma from pigmented mammary Paget disease.

It is interesting to see that both our PNCMB and PCMB cases were positive for *BRAF* V600E by IHC. Furthermore, the *BRAF* V600E mutation was also confirmed in case 1 by real-time polymerase chain reaction using the peptide nucleic acid clamping method. To date, only two other cases of PNCMB have been tested for *BRAF* mutation, and one case reported by Rassouli and Voutsadakis⁵ had a *BRAF* V600E mutation.⁴ Our first case is the second reported case of PNCMB with *BRAF* mutation. The clinicopathologic features of PNCMB reported in the English literature are summarized in Table 2 and are compared to the case reported here.^{5,16-19} Case 1 presented here and the previously reported *BRAF* mutant PMMB case have some additional features in common: both are solitary amelanotic tumors confined to the breast parenchyma, show positivity for S100 protein by IHC, have no evidence of primary melanoma except the breast on systemic workup stud-

Table 2. Summary of clinicopathologic features of PNCMB reported in the English literature by comparison with our case

Case No.	Study	Age (yr)	Size (cm)	Histology	IHC		BRAF mutations	LN status
					Positive	Negative		
1	Bernardo et al. ¹⁶	76	2.5	Meshwork of spindle cells with heavy granular pigmentation	NA	NA	NA	No
2	Roy et al. ¹⁷	40	3.0	Large pleomorphic cells with vesicular nucleus and single prominent nucleolus, moderate eosinophilic cytoplasm	S100 protein HMB-45 Vimentin	CK EMA CHR SYN SMA ER, PR, HER2	NA	No
3	Biswas et al. ¹⁸	32	4.0	Abundant clear cytoplasm and large vesicular nucleus with prominent nucleolus, no pigment	S100 protein HMB-45	CK EMA Vimentin SMA	NA	No
4	He et al. ¹⁹	26	3.0	Round or oval cells with large nuclei and abundant cytoplasm, no significant pigmentation	S100 protein HMB-45 Melan A	CK EMA Vimentin SMA ER, PR, HER2	NA	Yes
5	Drueppel et al. ⁴	54	10.0	Undifferentiated histology	S100 protein Melan A Vimentin	HMB-45 Desmin Actin CD34	Negative	No
6	Rassouli and Voutsadakis ⁵	50	1.2	Irregular cells with abundant amelanotic cytoplasm and prominent nucleoli	S100 protein HMB-45 Melan A	ER PR p63	Positive	No
Present case		70	2.1	Polygonal epithelioid cells with eosinophilic cytoplasm and oval eccentric nucleus, no significant pigmentation	S100 protein Tyrosinase Vimentin	CK EMA HMB-45	Positive	No

PNCMB, primary noncutaneous melanoma of the breast; IHC, immunohistochemistry; BRAF, rapidly accelerated fibrosarcoma (RAF) kinase-related oncogene homolog B; LN, lymph node; NA, not applicable; HMB-45, human melanoma black-45; CK, cytokeratin; EMA, epithelial membrane antigen; CHR, chromogranin; SMA, smooth muscle actin; ER, estrogen receptor; PR, progesterone receptor; HER2, human epidermal growth factor receptor 2.

ies, and were diagnosed at an early stage without nodal involvement. The presence of *BRAF* mutation in PMMB cases suggests that PMMB may have similar pathogenesis with typical malignant melanoma, and that PMMB may also be eligible for targeted therapy such as BRAF inhibitors.

Pathogenesis of PNCMB is not yet well-defined. Some authors have suggested that it may be a metastatic tumor from an unknown primary or a primary tumor that has completely regressed.¹⁷ Others have proposed that it may be a true primary tumor arising from ectopic melanocytes in the breast epithelium. Metaplastic transformation of a normal mammary duct precursor could be another alternative pathogenic pathway.⁵

In summary, we report two cases of PMMB with distinct clinical manifestations. Since PMMB is a very rare tumor in the breast, it can be a diagnostic challenge for pathologists. PNCMB can present as an amelanotic neoplasm without skin involvement, so it should be included in the differential diagnosis of poorly differentiated neoplasms within the breast parenchyma. The cocktail IHC of multiple melanocytic markers is a crucial ancillary test for the diagnosis of PMMB, and *BRAF* V600E IHC may

also be helpful for both diagnosis and therapy.

Electronic Supplementary Material

Supplementary materials are available at Journal of Pathology and Translational Medicine (<http://jpatholm.org>).

ORCID

Jiwon Koh: <https://orcid.org/0000-0002-7687-6477>

Tak Yun: <https://orcid.org/0000-0001-9540-0397>

Youngmee Kwon: <https://orcid.org/0000-0002-1370-2496>

Author Contributions

Conceptualization: YK.

Data curation: JK, YK.

Formal analysis: JK, YK.

Investigation: JK, JL, SYJ, HSK, TY, YK.

Writing—original draft: JK, YK.

Writing—review & editing: JK, JL, SYJ, HSK, TY, YK.

Conflicts of Interest

The authors declare that they have no potential conflicts of interest.

REFERENCES

1. Hussein MR. Extracutaneous malignant melanomas. *Cancer Invest* 2008; 26: 516-34.
2. McLaughlin CC, Wu XC, Jemal A, Martin HJ, Roche LM, Chen VW. Incidence of noncutaneous melanomas in the U.S. *Cancer* 2005; 103: 1000-7.
3. Kurul S, Tas F, Buyukbabani N, Mudun A, Baykal C, Camlica H. Different manifestations of malignant melanoma in the breast: a report of 12 cases and a review of the literature. *Jpn J Clin Oncol* 2005; 35: 202-6.
4. Drupeppel D, Schultheis B, Solass W, Ergonenc H, Tempfer CB. Primary malignant melanoma of the breast: case report and review of the literature. *Anticancer Res* 2015; 35: 1709-13.
5. Rassouli M, Voutsadakis IA. Primary noncutaneous malignant melanoma of the breast. *Breast J* 2016; 22: 688-91.
6. Alzaraa A, Sharma N. Primary cutaneous melanoma of the breast: a case report. *Cases J* 2008; 1: 212.
7. Williams SA, Ehlers RA 2nd, Hunt KK, et al. Metastases to the breast from nonbreast solid neoplasms: presentation and determinants of survival. *Cancer* 2007; 110: 731-7.
8. Oh YL, Ko YH. Fine needle aspiration cytology of metastatic melanoma in the breast: a case report. *Korean J Cytopathol* 1998; 9: 111-6.
9. Bendic A, Bozic M, Durdov MG. Metaplastic breast carcinoma with melanocytic differentiation. *Pathol Int* 2009; 59: 676-80.
10. Liu D, Rudland PS, Sibson DR, Platt-Higgins A, Barraclough R. Expression of calcium-binding protein S100A2 in breast lesions. *Br J Cancer* 2000; 83: 1473-9.
11. Blessing K, Sanders DS, Grant JJ. Comparison of immunohistochemical staining of the novel antibody melan-A with S100 protein and HMB-45 in malignant melanoma and melanoma variants. *Histopathology* 1998; 32: 139-46.
12. Ohsie SJ, Sarantopoulos GP, Cochran AJ, Binder SW. Immunohistochemical characteristics of melanoma. *J Cutan Pathol* 2008; 35: 433-44.
13. Yang L, Chen Y, Cui T, et al. Identification of biomarkers to distinguish clear cell sarcoma from malignant melanoma. *Hum Pathol* 2012; 43: 1463-70.
14. Long GV, Wilmott JS, Capper D, et al. Immunohistochemistry is highly sensitive and specific for the detection of V600E *BRAF* mutation in melanoma. *Am J Surg Pathol* 2013; 37: 61-5.
15. Petersson F, Ivan D, Kazakov DV, Michal M, Prieto VG. Pigmented Paget disease: a diagnostic pitfall mimicking melanoma. *Am J Dermatopathol* 2009; 31: 223-6.
16. Bernardo MM, Mascarenhas MJ, Lopes DP. Primary malignant melanoma of the breast. *Acta Med Port* 1980; 2: 39-43.
17. Roy S, Dhingra K, Mandal S, Khurana N. Unusual presentation of metastatic amelanotic melanoma of unknown primary origin as a solitary breast lump. *Melanoma Res* 2008; 18: 447-50.
18. Biswas A, Goyal S, Jain A, et al. Primary amelanotic melanoma of the breast: combating a rare cancer. *Breast Cancer* 2014; 21: 236-40.
19. He Y, Mou J, Luo D, Gao B, Wen Y. Primary malignant melanoma of the breast: a case report and review of the literature. *Oncol Lett* 2014; 8: 238-40.

Coexisting Mucinous Cystic Neoplasm of the Pancreas and Type 1 Autoimmune Pancreatitis

Mee-Jeong Kim · Tae Jun Song¹
Hyoung Jung Kim² · Song-Cheol Kim³
Myung-Hwan Kim¹
Seung-Mo Hong

Departments of Pathology and ¹Gastroenterology, ²Department of Radiology and Research Institute of Radiology, ³Department of Surgery, Asan Medical Center, University of Ulsan College of Medicine, Seoul, Korea

Received: October 1, 2018

Revised: October 17, 2018

Accepted: October 24, 2018

Corresponding Author

Seung-Mo Hong, MD, PhD
Department of Pathology, Asan Medical Center,
University of Ulsan College of Medicine,
88 Olympic-ro 43-gil, Songpa-gu, Seoul 05505,
Korea
Tel: +82-2-3010-4558
Fax: +82-2-472-7898
E-mail: smhong28@gmail.com

Type 1 autoimmune pancreatitis (AIP1) is an IgG4-related systemic disease that mimics tumors. We report a rare case of AIP1 accompanied by mucinous cystic neoplasm (MCN). A pancreatic lesion was incidentally detected in a woman in her 60s. After 6 years of follow-up, the lesion abruptly increased in size. Computed tomography showed a 3.5 cm unilocular cyst in the tail of the pancreas and distal pancreatectomy was performed. On microscopic examination, the cyst was lined by mucinous and non-mucinous epithelial cells with mild cytologic atypia. The surrounding stroma comprised ovarian-type spindle cells with progesterone receptor positivity. The pericyclic pancreas exhibited multifocal lymphoid follicles, lymphoplasmacytic infiltrations, obliterative phlebitis, and storiform fibrosis. IgG4-positive plasma cell infiltration (215 cells high-power field) and the IgG4/IgG ratio (57%) were increased. Cases of MCN coexisting with AIP1 are extremely rare; only two such cases have been reported in the English-language literature. This third case featured low-grade MCN with AIP1.

Key Words: Pancreas; Mucinous cystic neoplasm; Autoimmune pancreatitis

Mucinous cystic neoplasms (MCNs) of the pancreas are cyst-forming and composed of columnar mucinous epithelia with varying degrees of cytologic atypia.¹ Traditionally, MCNs have been classified as low-, intermediate-, or high-grade dysplasia according to the degree of cytological atypia.¹ Recently, however, the Baltimore consensus meeting proposed a two-tiered system for pancreatic precursor lesions, including MCNs and intraductal papillary mucinous neoplasms (IPMNs), classifying them as either low-grade (which includes the previous low- and intermediate-grade dysplasia) or high-grade.² MCNs are histologically recognizable precursor lesions of pancreatic ductal adenocarcinomas.³ They are associated with ovarian-type stroma and do not communicate with the pancreatic ductal system, which are diagnostic differential points with IPMNs.⁴ The majority of MCNs occur in women aged 40–60 years at the time of diagnosis.¹ The body and tail of the pancreas are the most common locations for MCNs; involvement of the head is rare.¹

Autoimmune pancreatitis (AIP) is a type of chronic pancre-

atitis that presents with obstructive jaundice and/or a pancreatic mass, with histologic features of dense lymphoplasmacytic infiltrations and fibrosis; it responds well to steroid treatment.⁵ AIP is classified as types 1 and 2. The diagnostic criteria for type 1 AIP (AIP1) are well established by international consensus and include clinical, serological, imaging, and pathology components.⁶ The characteristic histologic features of AIP1 are dense lymphoplasmacytic infiltration, storiform fibrosis, and obliterative phlebitis.⁷ A diagnosis of AIP1 is made based on the number of these histologic features observed and the number of IgG4-positive plasma cell infiltrations seen in high-power fields (> 50 cells for surgical resection or > 10 cells for biopsy specimens).⁷

There have been several case reports about AIP1 accompanied by other pancreatic lesions, such as a pseudocyst or IPMN.⁸⁻¹¹ However, MCN with AIP1 is extremely rare and only two cases have been reported in the English-language literature.^{12,13} Here, we report a third case, a patient with both low-grade MCN and AIP1.

CASE REPORT

A woman in her 60s admitted our hospital with a symptomless, incidentally detected pancreatic cystic lesion. Initial computed tomography (CT) imaging revealed a 2.2 cm unilocular cystic pancreas lesion in the body and tail of the pancreas without accompanying wall enhancement and with no mural nodule. There was no evidence of narrowing of the main pancreatic duct or of acute pancreatitis (Fig. 1A). The initial laboratory findings were unremarkable, including normal levels of γ -GT (13 IU/L; normal range, 5 to 36 IU/L), amylase (65 U/L; normal range, 30 to 110 U/L), and lipase (37 U/L; normal range, 13 to 60 U/L). Suspecting either a pseudocyst or MCN, the patient was regularly followed up. After 6 years of follow-up, the cystic lesion had increased in size to 3.5 cm (Fig. 1B). As a result, the patient underwent a distal pancreatectomy. On gross examination, a 3.5 cm-sized unilocular cyst was observed in the body and tail of the pancreas. The cyst wall was irregularly thickened, firm, and fibrotic (Fig. 1C). The inner surface of the cyst was yellowish white and

rough, with multifocal hemorrhagic spots. The cyst contained sticky mucinous fluid. The remaining pancreatic parenchyma away from the cystic neoplasm was unremarkable, and there was no dilatation of the main pancreatic duct.

Low-power magnification images revealed that the cystic wall was surrounded by dense spindle cell clusters, with numerous lymphoid follicles observed in a fibrotic background (Fig. 1D). The thin sections of the cyst wall were lined by a single layer of epithelial cells that were mostly non-mucinous or focally mucinous (Fig. 1E). The epithelial cells were pseudostratified without showing pleomorphism or prominent nucleoli, and the surrounding dense spindle cells were closely packed, showing ovarian-type spindle cells. Nuclear progesterone receptor labeling showed these spindle cells to be dense (Fig. 1F). The irregularly thickened portions of the cyst wall observed in the gross examination contained multiple lymphoid follicles in a background of chronic inflammatory cell infiltrations, predominantly lymphoplasmacytic (Fig. 1G). Some areas contained dense periductal lymphoplasmacytic infiltrations (Fig. 1H). Several foci of obliterative

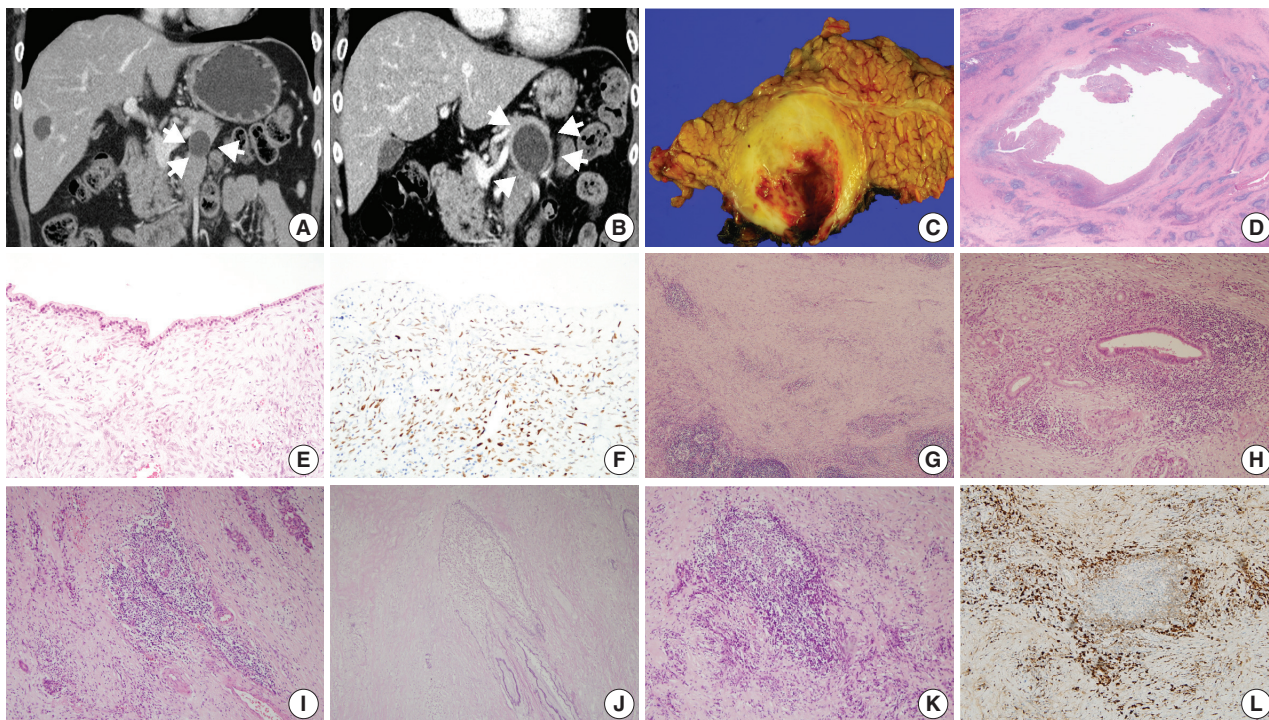


Fig. 1. (A) Coronal contrast-enhanced computed tomography image showing a unilocular cyst in the pancreas tail. (B) Six years later, the cyst had grown, with its longest diameter increasing from 2.2 to 3.5 cm, as well as thickening of the cyst wall (arrowheads). (C) The unilocular cyst in the body and tail of the pancreas showing irregular thickening of the cyst wall. (D) Scanning power image showing lymphoid follicles and lymphoplasmacytic infiltration around the cyst wall. (E) The cyst wall was lined mostly by non-mucinous and focally mucinous epithelial cells with mild cytologic atypia. (F) Progesterone receptor nuclear labeling highlighted ovarian-type stromal cells. (G) The irregularly thickened cyst wall contained multiple lymphoid follicles in a background of chronic inflammatory cell infiltrations. (H) Some areas showed dense periductal lymphoplasmacytic infiltrations. (I, J) Several foci of obliterative phlebitis were noted by hematoxylin and eosin staining (I) and elastic staining (J). (K, L) Areas of dense lymphoplasmacytic infiltrations (K) showed numerous IgG4-positive plasma cell infiltrations (L).

Table 1. Comparisons of clinicopathologic characteristics of MCN in association with AIP1 with previously reported cases

Study	Age (yr)	Sex	Dysplasia	Fibrosis	Obliterative phlebitis	IgG4+plasma cells/HPF	IgG4/IgG (%)	Serum IgG4 level (mg/dL)
Yakirevich et al. ¹²	33	Female	High-grade	Storiform	Present	75	42	97.5
DiCarlo et al. ¹³	26	Female	Low-grade	Dense band	Present	160	NA	NA
Present case	60	Female	Low-grade	Storiform	Present	215	57	0.4 ^a

MCN, mucinous cystic neoplasm; AIP1, type 1 autoimmune pancreatitis; NA, not applicable; HPF, high-power field.

^aSampled on postoperative day 6.

phlebitis were revealed by H&E and elastic staining (Fig. 1I, J). Areas of dense lymphoplasmacytic infiltrations (Fig. 1K) included numerous IgG4-positive plasma cell infiltrations (Fig. 1L). As many as 215 IgG4-positive plasma cells were observed in the most active area. The IgG4/IgG ratio was about 57%. Serum IgG4 measured 6 days after the distal pancreatectomy was within the normal range (0.4 mg/dL). The patient was diagnosed with low-grade MCN associated with AIP1.

All procedures performed in the current study were approved by Institutional Review Board approval (approval No. 2018-1160) for waiver of the informed consent in accordance with the 1964 Helsinki declaration and its later amendments.

DISCUSSION

MCN is a precursor lesion of pancreatic ductal adenocarcinomas, whereas AIP is a tumor mimicker. This case was interesting because the patient underwent distal pancreatectomy after the MCN increased in size. In addition to low-grade MCN, we observed features of AIP1 in the irregularly thickened periphery of the cyst wall. This case exhibited a range of histologic features considered to be pathologic diagnostic criteria of AIP1,⁷ including lymphoplasmacytic infiltration, stromal storiform fibrosis, and obliterative phlebitis, along with > 50 IgG4-positive plasma cell infiltrations (with up to 215 IgG4-positive plasma cells observed). Thus, this case was histologically highly suggestive of AIP1.

However, other histologic, imaging and serologic features consistent with AIP1, such as diffuse pancreatic enlargement and pancreatic ductal strictures without significant ductal dilatation, were not observed in the present case. The patient's serum IgG4 level 6 days postoperatively was not significantly elevated.

It is rare for the histologic features of AIP1 to be reported in association with pancreatic cystic lesions, including IPMNs and pseudocysts. All the reported cases exhibited the histologic features of AIP1; in addition, some cases showed increased serum IgG4 levels,^{8,9,11} whereas another did not.¹⁰ There has been only one English-language report of a case of MCN accompanied by the histologic features of AIP1, and that case had an elevated serum IgG4 level.¹²

In the present case, the histologic features of AIP1 were observed in a limited area, the periphery of the cyst wall, and did not extend into the surrounding pancreatic parenchyma. With the normal pancreatic ductal system observed on radiologic imaging, these features can be interpreted as indicating a localized form of AIP1. Similar features were reported in the previous case.¹² Comparisons of clinicopathologic characteristics of MCN in association with AIP1 with previously reported cases and the present case are summarized in Table 1.

The pathogenesis of AIP1 in association with MCN is not fully understood. The most plausible explanation is the co-existence of two lesions, the AIP1 and the MCN.¹³ Other possibilities include a secondary inflammatory response to a pre-existing MCN due to the use of fine needle aspiration biopsy or cytology of the MCN for histologic confirmation, or a secondary immune reaction of the periphery of the cyst wall of the pancreas to inspissated extracellular mucin from the MCN.¹²

In summary, we report a case of low-grade MCN coexisting with AIP1. This case exceptionally demonstrated the presence of both a cystic tumor and a tumor mimicker in the same pancreas.

ORCID

Mee-Jeong Kim: <https://orcid.org/0000-0001-7466-7586>

Tae Jun Song: <https://orcid.org/0000-0002-6156-8746>

Hyoung Jung Kim: <https://orcid.org/0000-0003-3391-5621>

Song-Cheol Kim: <https://orcid.org/0000-0003-4552-4169>

Myung-Hwan Kim: <https://orcid.org/0000-0003-0992-6734>

Seung-Mo Hong: <https://orcid.org/0000-0002-8888-6007>

Author Contributions

Conceptualization: SMH.

Data curation: MJK, SCK, MHK.

Formal analysis: TJS, HJK, SMH.

Investigation: MJK, SMH.

Validation: MJK, SMH.

Visualization: MJK, HJK, SMH.

Writing—original draft: MJK, SMH.

Writing—review & editing: MJK, HJK, SMH.

Conflicts of Interest

The authors declare that they have no potential conflicts of interest.

Acknowledgments

This study was funded by a grant (1320200) from National R&D Program for Cancer Control, Ministry of Health & Welfare, Republic of Korea.

REFERENCES

1. Bosman FT, Carneiro F, Hruban RH, Theise ND. WHO classification of tumours of the digestive system. 4th ed. Lyon: International Agency for Research on Cancer, 2010.
2. Basturk O, Hong SM, Wood LD, et al. A revised classification system and recommendations from the Baltimore Consensus Meeting for Neoplastic Precursor Lesions in the Pancreas. *Am J Surg Pathol* 2015; 39: 1730-41.
3. Hong SM, Park JY, Hruban RH, Goggins M. Molecular signatures of pancreatic cancer. *Arch Pathol Lab Med* 2011; 135: 716-27.
4. Hruban RH, Pitman MB, Klimstra DS. AFIP atlas of tumor pathology, series IV. Tumors of the pancreas. Washington, DC: Armed Forces Institute of Pathology, 2007.
5. Hart PA, Zen Y, Chari ST. Recent advances in autoimmune pancreatitis. *Gastroenterology* 2015; 149: 39-51.
6. Shimosegawa T, Chari ST, Frulloni L, et al. International consensus diagnostic criteria for autoimmune pancreatitis: guidelines of the International Association of Pancreatology. *Pancreas* 2011; 40: 352-8.
7. Deshpande V, Zen Y, Chan JK, et al. Consensus statement on the pathology of IgG4-related disease. *Mod Pathol* 2012; 25: 1181-92.
8. Gompertz M, Morales C, Aldana H, Castillo J, Berger Z. Cystic lesions in autoimmune pancreatitis. *Case Rep Gastroenterol* 2015; 9: 366-74.
9. Nakaji S, Hirata N, Fujii H, et al. A case of focal autoimmune pancreatitis (AIP) mimicking an intraductal papillary mucinous neoplasm (IPMN). *Clin J Gastroenterol* 2013; 6: 329-33.
10. Urata T, Naito Y, Izumi Y, et al. Localized type 1 autoimmune pancreatitis superimposed upon preexisting intraductal papillary mucinous neoplasms. *World J Gastroenterol* 2013; 19: 9127-32.
11. Vaquero EC, Salcedo MT, Cuatrecasas M, et al. Autoimmune pancreatitis type-1 associated with intraduct papillary mucinous neoplasm: report of two cases. *Pancreatology* 2014; 14: 316-8.
12. Yakirevich E, Henriksen KJ, Miner T, Resnick MB. Mucinous cystic neoplasm of the pancreas with increased IgG4+ plasma cells and histopathologic features of autoimmune pancreatitis/IgG4-related disease. *Pancreas* 2015; 44: 674-6.
13. DiCarlo C, Silverman J, Bunker M. Type 1 autoimmune pancreatitis associated with mucinous cystic neoplasm. *Am J Clin Pathol* 2016; 146(Suppl 1): 290 .

Adrenal Cortical Neoplasm with Uncertain Malignant Potential Arising in the Heterotopic Adrenal Cortex in the Liver of a Patient with Beckwith-Wiedemann Syndrome

Eun Na Kim · Dong Eun Song
Hee Mang Yoon¹ · Beom Hee Lee²
Chong Jai Kim

Departments of Pathology, ¹Radiology, and
²Pediatrics, Asan Medical Center, University of
Ulsan College of Medicine, Seoul, Korea

Received: September 9, 2018
Revised: November 10, 2018
Accepted: November 12, 2018

Corresponding Author

Chong Jai Kim, MD, PhD
Department of Pathology, University of Ulsan
College of Medicine, Asan Medical Center,
88 Olympic-ro 43-gil, Songpa-gu, Seoul 05505,
Korea
Tel: +82-2-3010-4516
Fax: +82-2-472-7898
E-mail: ckim@amc.seoul.kr

Patients with Beckwith-Wiedemann syndrome (BWS) are predisposed to developing embryonal tumors, with hepatoblastoma being the most common type. Our patient showed hemihypertrophy, macroglossia, and paternal uniparental disomy in chromosome 11 and was diagnosed with BWS. When the patient was 9 months old, a 2.5 × 1.5 cm oval hypoechoic exophytic mass was detected in the inferior tip of his right liver. Preoperative imaging identified it as hepatoblastoma; however, histologic, immunohistochemistry, and electron microscopic findings were compatible with adrenal cortical neoplasm with uncertain malignant potential. The origin of the adrenal tissue seemed to be heterotopic. Here, we describe for the first time an adrenal cortical neoplasm with uncertain malignant potential arising in the heterotopic adrenal cortex located in the liver of a patient with BWS.

Key Words: Beckwith-Wiedemann syndrome; Liver; Heterotopic; Adrenal gland neoplasms

Beckwith-Wiedemann syndrome (BWS, OMIM 130650).¹ characterized by hemihypertrophy, macroglossia, macrosomia, organomegaly, hyperinsulinism, and distinct facial features.² The genetic causes of BWS are complex but are mainly due to genomic imprinting disorders involving chromosome 11. In addition, patients with BWS are predisposed to developing tumors, with the incidence of the tumor being 4% to 21%. Most tumors consist of embryonal tumors such as Wilms tumor, hepatoblastoma, neuroblastoma, adrenal cortical carcinoma, or rhabdomyosarcoma.^{3,4} Given this disposition, a thorough tumor screening is recommended for BWS patients. We recently experienced a BWS patient who had adrenal cortical neoplasm with uncertain malignant potential arising in the heterotopic adrenal cortex located in his liver.

CASE REPORT

A male infant who was the third child of healthy parents was born at 36 weeks of gestation weighing 4,150 g. After birth, he was hospitalized in a neonatal intensive care unit for 10 days due to cyanosis and neonatal jaundice. Due to the presence of right hemihypertrophy and macroglossia, he was suspected of having BWS, and a genetic test for BWS confirmed paternal uniparental disomy (KvDMR/H19 aberrant methylation T0392241) in chromosome 11. At the time of birth, no mass was found in the imaging work-up.

At nine months, the infant's weight was in the 97th percentile at 11.7 kg, and his height was in the 95th percentile at 77 cm. Exercise development was average; however, due to leg length discrepancy by the prominent right hemihypertrophy,

the infant required an aid to move. There was no significant virilization.

During the tumor screening, abdominal ultrasonography revealed a 1.9×1.2 cm oval-shaped hypoechoic mass in the inferior tip of his right liver (Fig. 1A). A computed tomography (CT) scan showed an exophytic mass arising from the inferior tip of his right lobe of the liver (Fig. 1B). The mass had heterogenous

enhancement on the portal venous phase of contrast-enhanced abdominal CT scan. Apart from this, there were no abnormal findings in the kidneys, adrenal glands, lymph nodes, or other abdominal organs. Based on the ultrasound and CT imaging, hepatoblastoma of the liver was suspected. The levels of aspartate aminotransferase and alanine aminotransferase were in the normal range at 34 IU/L and 30 IU/L, respectively. Serology testing for

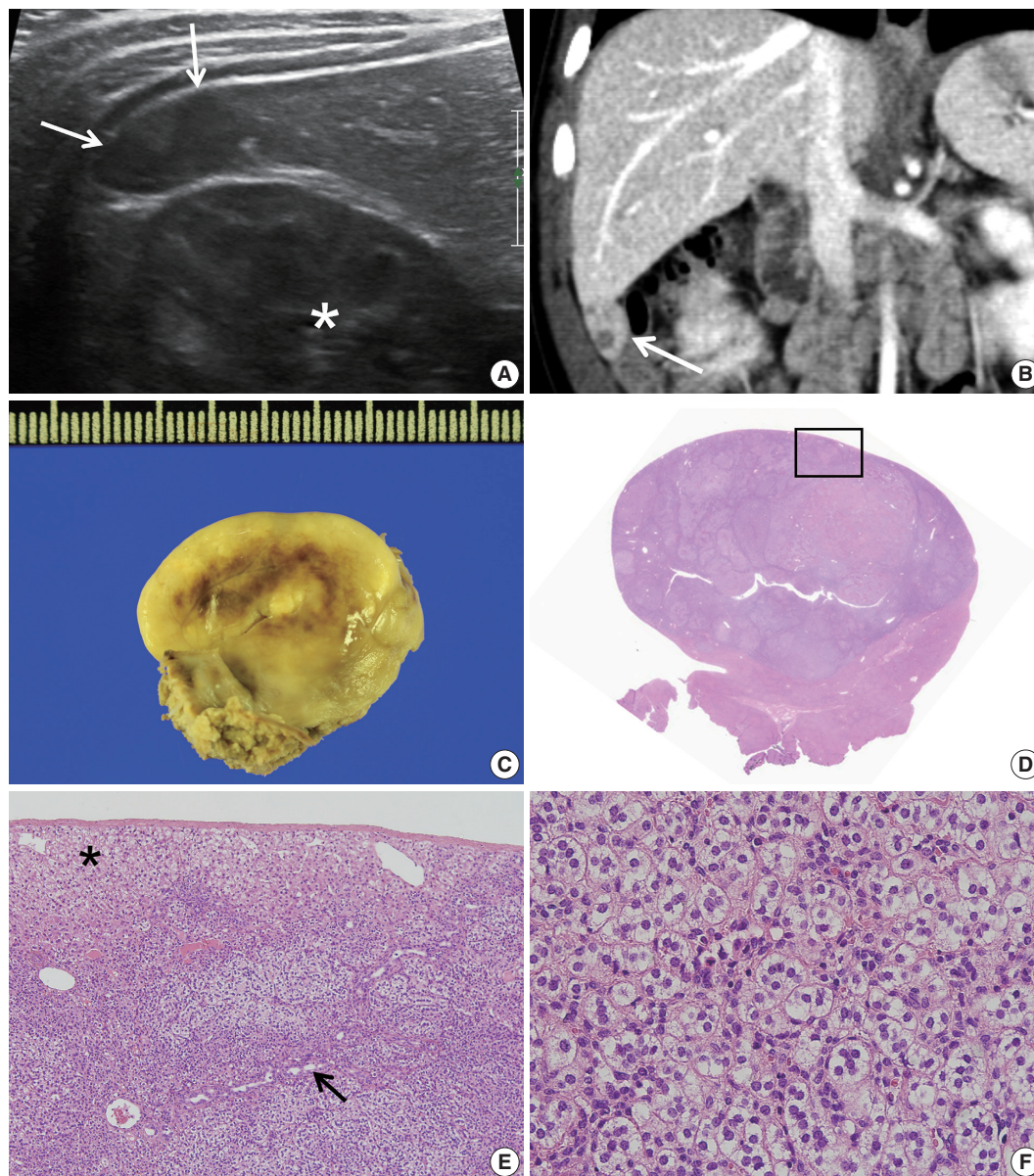


Fig. 1. (A) Axial ultrasound image showing an oval-shaped hypoechoic mass in the inferior tip of the right hemi liver (arrows). Asterisk indicates the right kidney. (B) Coronal computed tomography scan showing an exophytic mass arising from the inferior tip of the right hemi liver (arrow). (C) The cut surface of the tumor is grayish yellow with focal brown pigmentation and glistening. Necrosis and hemorrhage are absent. (D) The tumor shows exophytic growth (scan view). (E) The tumor is encased in a Glisson capsule and had remaining hepatocytes (asterisk). Bile ductules (arrow) were entrapped. (F) Tumor cells with nested growth pattern had plump clear cytoplasm, distinct and smooth cell membrane, bland and small nucleus, and micro nucleoli that resemble zona fasciculata of a normal adrenal gland.

(Continued on the next page)

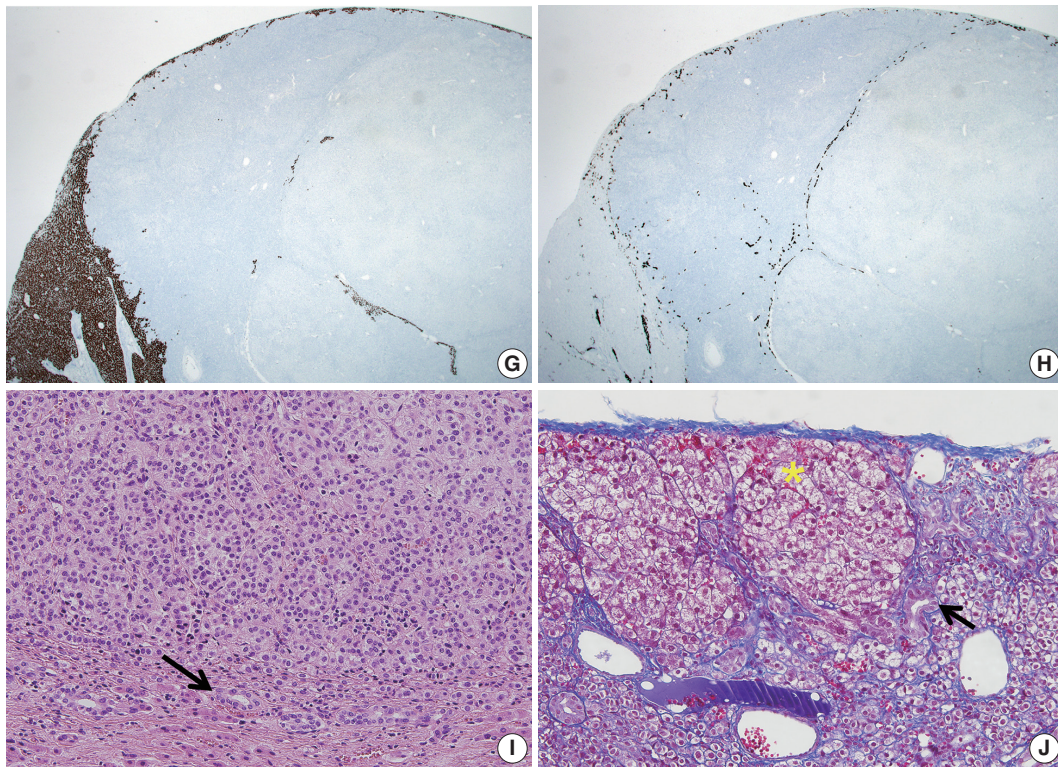


Fig. 1. (Continued from the previous page) (G) Hepar-1 immunohistochemical staining showing the remaining normal hepatocytes surrounding tumor cells. (H) Cytokeratin 7 immunohistochemical staining showing the entrapped bile ductules in the periphery of tumor cells. (I) The bile ducts (arrow) are not in contact with the tumor. (J) Remaining bile ducts (arrow) and hepatic parenchyma (asterisk) are pushed by the tumor. The Glisson capsule remains intact (Masson trichrome staining).

hepatitis was negative. The level of α -fetoprotein was slightly elevated at 57.4 ng/mL.

Suspecting hepatoblastoma, a laparoscopic partial hepatectomy was performed. Grossly, the resected tumor was accurately demarcated, revealing a solid mass measuring $2.5 \times 1.5 \times 0.6$ cm. The cut surface of the tumor was grayish white, yellow, and glistening (Fig. 1C). Microscopically, the tumor showed a nested growth pattern (Fig. 1D). The tumor cells had plump clear cytoplasm, distinct and smooth cell membranes, bland and small nuclei, and inconspicuous nucleoli which resembled the zona fasciculata of a normal adrenal gland (Fig. 1E, F). Mitosis was found in two out of 10 high-power fields, and there was no atypical mitosis. A Glisson capsule encased the tumor. Normal hepatic parenchyma and the remaining bile ducts were highlighted by Hepar-1 and cytokeratin 7 (Fig. 1G–J), and the remaining liver parenchyma was unremarkable (Fig. 1G–J).

We performed immunohistochemical staining using formalin-fixed, paraffin-embedded, 4- μ m-thick tissue sections with an OptiView DAB immunohistochemical detection kit.

The tumor cells did not exhibit immunoreactivity for arginase-1, hepatocyte (Hep par 1), α -1-fetoprotein, glypican 3, β -catenin,

or glutamine synthetase. INI-1 was expressed in the nucleus. The results showed that this was not a case of hepatoblastoma.

To confirm that the tumor originated from adrenal glands, immunohistochemistry for CD56, vimentin, Melan A, inhibin α , synaptophysin, and chromogranin was performed. The tumor cells showed strong diffuse immunoreactivity for CD56, vimentin, moderately intense immunoreactivity for Melan A, and weak and focal immunoreactivity for inhibin α . Synaptophysin immunoreactivity was weak and focal. The result of chromogranin immunohistochemistry was negative, and Ki-67 labeling index was 13.2% by manual count (Fig. 2A–F). Detailed information and results of the immunohistochemistry are described in Table 1. Reticulin histochemical staining was performed to evaluate the reticulin framework. As a result, reticulin staining demonstrated multifocal disruption of reticulin network within tumor cells (Fig. 2E, F), indicating that this tumor has uncertain malignant potential.

Electron microscope

Ultra-thin sections from formalin fixed tissue were examined with a transmission electron microscope (model GEM-1400,

Jeol, Tokyo, Japan). Electron microscopy revealed numerous mitochondria with tubular cristae and neurosecretory granules, which are compatible with the characteristics of adrenal cortical neoplasm (Fig. 2I, J). Histologic findings, immunohistochemical results, and electron microscopic findings all strongly suggested the possibility of adrenal cortical tumor present in the liver. The bilateral adrenal gland was normal, and there was no evidence of a primary tumor in the adrenal gland; therefore, we concluded that the origin of the adrenal tissue was of heterotopic nature.

Since only the pathologic findings of the tumor and only dei-

dentified personal information of the patient were used, formal written informed consent was not required with a waiver by the appropriate IRB of Asan Medical Center (IRB number: 2018-1042).

DISCUSSION

The heterotopic adrenal tissue is rarely found in the lungs, brain, ovaries, or placenta.⁵ Heterotopic adrenal tissue tends to occur in the abdominal cavity along the gonadal descent pathway

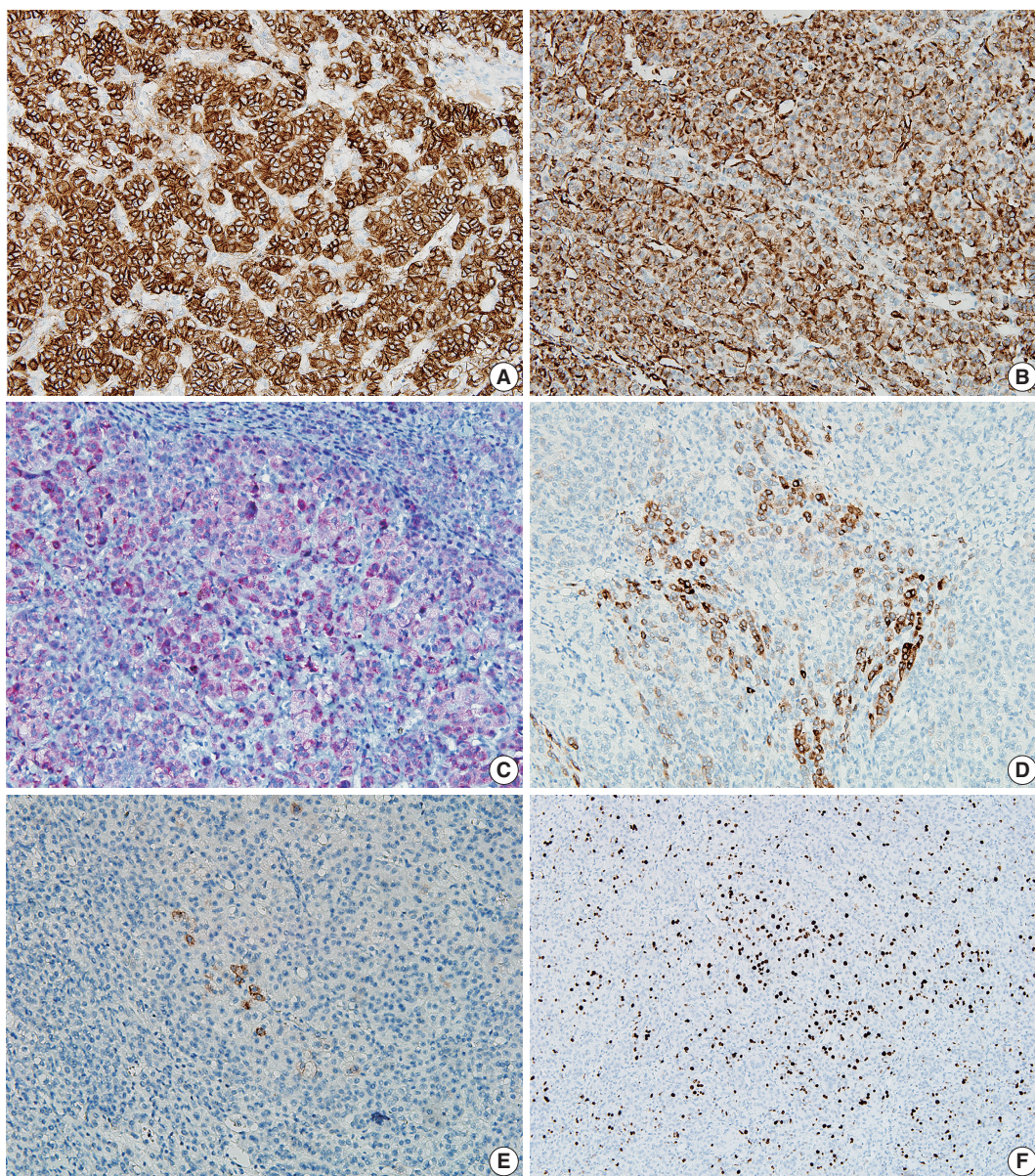


Fig. 2. The tumor cells show strong, diffuse immunoreactivity for CD56 (A), Vimentin (B), moderately intense immunoreactivity for Melan A (C), and weak focal immunoreactivity for inhibin α (D). (E) Synaptophysin immunoreactivity is very focal and weak. (F) Ki-67 labeling index is 13.2% in hot spot by manual count. *(Continued on the next page)*

or celiac axis.⁶ There are a few reports of heterotopic adrenal cortex in the liver.^{7,8}

There are two possible explanations for the mechanism of

heterotopic adrenal cortex in liver parenchyma.⁸ The first theory is a migration of adrenal gland tissue to the liver parenchyma along the mesogastrium during early developmental stage. The

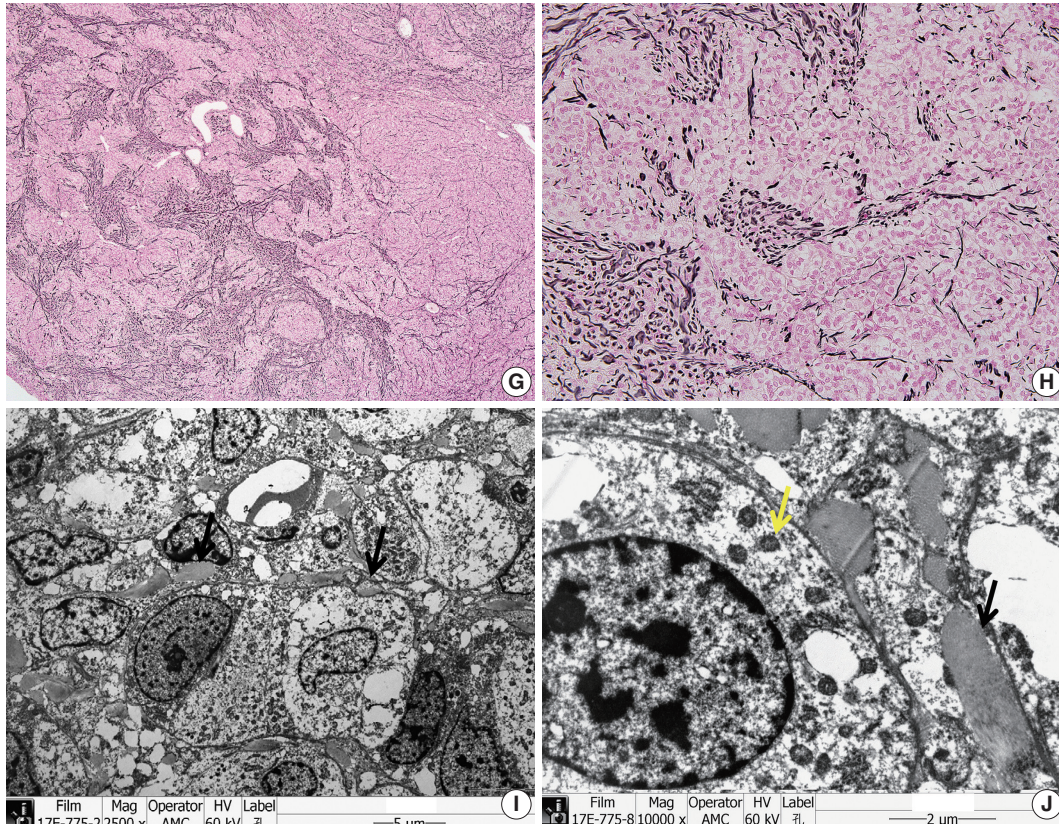


Fig. 2. (Continued from the previous page) (G, H) The tumor shows multifocal disruption of reticulin network. Electron microscopy shows numerous mitochondria with tubular cristae (I, $\times 2,500$; J, $\times 10,000$, black arrow) and neurosecretory granules (J, yellow arrow), which are compatible with adrenal cortical neoplasm.

Table 1. Detailed information and results of immunohistochemistry

Protein	Intensity	Localization	Pattern	Dilution	Code	Code and company
Arginase 1	-	-	-	1:200	080R-15	Cell Marque, Rocklin, CA, USA
Hepatocyte (Hep par 1)	-	-	-	1:200	M7158	Dako, Glostrup, Denmark
α -1-fetoprotein	-	-	-	1:500	RB-365-A	Neomarkers, Fremont, CA, USA
Glypican 3	-	-	-	1:200	261M-96	Cell Marque, Rocklin, CA, USA
β -catenin	-	-	-	1:500	610153	BD Pharmingen, Franklin Lakes, NJ, USA
Glutamine synthetase	-	-	-	1:500	AB73593	Abcam, Cambridge, UK
INI-1	+++	Nucleus	Diffuse	1:100	612111	Pharmingen, Franklin Lakes, NJ, USA
Vimentin	+++	Cytoplasm	Diffuse	1:500	18-0052	Zymed, Carlsbad, CA, USA
Cytokeratin 7	-	-	-	1:400	M7018	Dako, Glostrup, Denmark
Cytokeratin 19	-	-	-	1:100	319M-14	Cell Marque, Rocklin, CA, USA
CD56	+++	Cytoplasm membrane	Diffuse	1:100	NCL-L-CD56-504	Novocastra, Leica, Wetzlar, Germany
Vimentin	+++	Cytoplasm	Diffuse	1:500	18-0052	Zymed, Carlsbad, CA, USA
Melan A	++	Cytoplasm	Focal	1:50	NCL-L-MELAN A	Novo, Newcastle upon Tyne, UK
Inhibin α	+	Cytoplasm	Focal	1:100	MCA951S	Serotec, Kidlington, UK
Synaptophysin	+	Cytoplasm	Focal	1:200	336R-96	Cell Marque, Rocklin, CA, USA
Chromogranin	-	-	-	1:1,600	M0869	Dako, Glostrup, Denmark
Ki-67	++	Nucleus	13.2%	1:50	CMC27531021	Cell Marque, Rocklin, CA, USA

Intensity of staining: +, weak; ++, moderate; +++, strong.

Table 2. Neoplasm arising in ectopic adrenal tissue in BWS: clinical and pathological features as described in the literature

Reference	Age at diagnosis	Sex	Histologic diagnosis	Lesion location	Symptom	Management	Outcome	Associated disease
Wilkins et al. ⁷	2 yr 9 mo	M	Adrenocortical tumor	Liver	Virilism, Cushing syndrome	Right lobectomy	NED	No adrenal tissue in the usual location on the right
Cardinali et al. ¹¹	1 yr 5 mo	M	Myelolipoma	Renal hilum	Elevated blood level of cortisol, dehydroepiandrosterone	Adrenalectomy with ipsilateral renal hilar and intercaval-aortic lymph node dissection	NED	Adrenal cortical adenoma in adrenal gland
Giner et al. ¹²	2 yr	M	Adrenal cortical adenoma with oncocytic features	Spinal cord (L4-L5, extramedullary, intradural)	Abnormal gait	L3-S1 laminoplasty	1 Year later recurrence at the same level → second surgery → NED	

BWS, Beckwith-Wiedemann syndrome; NED, no evidence of disease.

second theory is an occurrence of adreno-hepatic fusion during the later stage. During the fusion, the mesenchyme encases the adrenal gland and liver, and after the mesenchyme is separated, adrenal gland fragments are entrapped in the liver parenchyma.^{2,9} Adreno-hepatic fusion is a relatively common phenomenon found in 9.9% of autopsy specimens,¹⁰ and is considered to be a part of the aging process as adreno-hepatic fusion is more often observed in older people. However, tumorous conditions arising from adreno-hepatic fusion are not common, and there is a partial capsule that separates the two organs.

In our current case, the tumor was encased by a Glisson capsule and hepatocytes and bile ductules found in the periphery of the tumor. And the patient was an infant. These characteristics suggest that the first theory discussed above regarding migration of adrenal gland tissue is likely the cause of the presence of heterotopic adrenal cortex in the liver of this patient.

For patients with BWS, many embryonal tumors occur due to the effects of growth factors and cyclin-dependent kinase. Although rare, various adrenal gland tumorous conditions (including cytomegaly of the fetal adrenal cortex, benign cyst, hyperplasia, adenoma, adenocarcinoma of the cortex, neuroblastoma, and pheochromocytoma) can develop in BWS patients. There were reports of neoplasms from the heterotopic adrenal cortex located in the liver,⁷ hilum of the kidney¹¹ and the spinal cord¹² of BWS patients (Table 2).

The incidence of childhood adrenal tumor is minimal (0.5%), and it is challenging to distinguish malignant adrenal tumor from a benign one, especially in child patients. The tumor of this patient was small, and there was no evidence of metastasis, as evidenced by the fact that the bilateral adrenal glands were normal. The mitotic count was low, and neither necrosis, atypical mitosis, nuclear atypia nor lymphovascular invasion was observed.

Only multifocal reticulin disruption was observed. Therefore, we concluded that the tumor was adrenal cortical neoplasm with uncertain malignant potential rather than adrenal cortical carcinoma or adrenal cortical adenoma, according to the diagnostic criteria of Wieneke, et al.¹³

Hepatoblastoma is the most common tumor in children with BWS. Therefore, it is possible that adrenal cortical neoplasm arising in the heterotopic adrenal cortex may be mistaken for hepatoblastoma in a usual clinical setting. To the best of our knowledge, our patient is the first case of adrenal cortical neoplasm with uncertain malignant potential arising from a heterotopic adrenal cortex observed in the hepatic parenchyma of a BWS patient. Pathologists will be able to avoid misdiagnosis if they know that tumors can occur from the heterotopic adrenal cortex in the liver especially in patients with BWS.

ORCID

Eun Na Kim: <https://orcid.org/0000-0003-2992-7881>

Dong Eun Song: <https://orcid.org/0000-0002-9583-9794>

Hee Mang Yoon: <https://orcid.org/0000-0001-6491-5734>

Beom Hee Lee: <https://orcid.org/0000-0001-9709-2631>

Chong Jai Kim: <https://orcid.org/0000-0002-2844-9446>

Author Contributions

Conceptualization: CJK.

Data curation: ENK.

Formal analysis: ENK, DES.

Investigation: ENK.

Methodology: ENK.

Resources: BHL, HMY.

Supervision: DES, CJK.

Visualization: ENK.

Writing—original draft: ENK, HMY.

Writing—review & editing: DES, CJK.

Conflicts of Interest

The authors declare that they have no potential conflicts of interest.

REFERENCES

1. Shuman C, Beckwith JB, Weksberg R. Beckwith-Wiedemann syndrome. In: Adam MP, Ardinger HH, Pagon RA, et al., eds. GeneReviews [Internet]. Seattle: University of Washington, c1993-2019 [cited 2018 Aug 2]. Available from: <https://www.ncbi.nlm.nih.gov/pubmed/20301568>.
2. Pettenati MJ, Haines JL, Higgins RR, Wappner RS, Palmer CG, Weaver DD. Wiedemann-Beckwith syndrome: presentation of clinical and cytogenetic data on 22 new cases and review of the literature. *Hum Genet* 1986; 74: 143-54.
3. Sotelo-Avila C, Gooch WM 3rd. Neoplasms associated with the Beckwith-Wiedemann syndrome. *Perspect Pediatr Pathol* 1976; 3: 255-72.
4. DeBaun MR, Tucker MA. Risk of cancer during the first four years of life in children from The Beckwith-Wiedemann Syndrome Registry. *J Pediatr* 1998; 132(3 Pt 1): 398-400.
5. Stocker JT, Dehner LP, Husain AN. Stocker and Dehner's pediatric pathology. 3rd ed. Philadelphia: Lippincott Williams & Wilkins, 2015.
6. Graham LS. Celiac accessory adrenal glands. *Cancer* 1953; 6: 149-52.
7. Wilkins L, Ravitch MM. Adrenocortical tumor arising in the liver of a three year old boy with signs of virilism and Cushing's syndrome: report of a case with cure after partial resection of the right lobe of the liver. *Pediatrics* 1952; 9: 671-81.
8. Vestfrid MA. Ectopic adrenal cortex in neonatal liver. *Histopathology* 1980; 4: 669-72.
9. Honore LH, O'Hara KE. Combined adrenorenal fusion and adrenohepatic adhesion: a case report with review of the literature and discussion of pathogenesis. *J Urol* 1976; 115: 323-5.
10. Honma K. Adreno-hepatic fusion: an autopsy study. *Zentralbl Pathol* 1991; 137: 117-22.
11. Cardinalli IA, de Oliveira-Filho AG, Mastellaro MJ, Ribeiro RC, Aguiar SS. A unique case of synchronous functional adrenocortical adenoma and myelolipoma within the ectopic adrenal cortex in a child with Beckwith-Wiedemann syndrome. *Pathol Res Pract* 2012; 208: 189-94.
12. Giner J, Esteban I, Carceller F, Saceda J, Regojo RM. Spinal adrenal cortical adenoma associated with Beckwith-Wiedemann syndrome: case report and review of the literature. *Childs Nerv Syst* 2017; 33: 1009-13.
13. Wieneke JA, Thompson LD, Heffess CS. Adrenal cortical neoplasms in the pediatric population: a clinicopathologic and immunophenotypic analysis of 83 patients. *Am J Surg Pathol* 2003; 27: 867-81.

Encapsulated Papillary Thyroid Tumor with Delicate Nuclear Changes and a *KRAS* Mutation as a Possible Novel Subtype of Borderline Tumor

Kenji Ohba^{1,2} · Norisato Mitsutake³
Michiko Matsuse³
Tatiana Rogounovitch³
Nobuhiko Nishino⁴ · Yutaka Oki²
Yoshie Goto¹ · Kennichi Kakudo⁵

¹Department of Internal Medicine, Enshu Hospital, Shizuoka; ²Department of Family and Community Medicine, Hamamatsu University School of Medicine, Shizuoka; ³Department of Radiation Medical Sciences, Atomic Bomb Disease Institute, Nagasaki University, Nagasaki; ⁴Department of Surgery, Maruyama Hospital, Shizuoka; ⁵Department of Pathology, Nara Hospital, Kindai University Faculty of Medicine, Nara, Japan

Received: November 8, 2018

Revised: December 5, 2018

Accepted: December 7, 2018

Corresponding Author

Kennichi Kakudo, MD, PhD
Department of Pathology, Nara Hospital, Kindai University Faculty of Medicine, 1248-1 Otoda-cho, Ikoma, Nara 630-0293, Japan
Tel: +81-743-77-0880
Fax: +81-743-77-0890
E-mail: kakudo@thyroid.jp

Although papillary thyroid carcinoma (PTC)-type nuclear changes are the most reliable morphological feature in the diagnosis of PTC, the nuclear assessment used to identify these changes is highly subjective. Here, we report a noninvasive encapsulated thyroid tumor with a papillary growth pattern measuring 23 mm at its largest diameter with a nuclear score of 2 in a 26-year-old man. After undergoing left lobectomy, the patient was diagnosed with an encapsulated PTC. However, a second opinion consultation suggested an alternative diagnosis of follicular adenoma with papillary hyperplasia. When providing a third opinion, we identified a low MIB-1 labeling index and a heterozygous point mutation in the *KRAS* gene but not the *BRAF* gene. We speculated that this case is an example of a novel borderline tumor with a papillary structure. Introduction of the new terminology “noninvasive encapsulated papillary *RAS*-like thyroid tumor (NEPRAS)” without the word “cancer” might relieve the psychological burden of patients in a way similar to the phrase “noninvasive follicular thyroid neoplasm with papillary-like nuclear features (NIFTP).”

Key Words: Borderline/precursor tumor; Observer variation; *RAS*-like tumor

A subset of thyroid tumors was classified as borderline/precursor tumors in the fourth edition of the *World Health Organization (WHO) Classification of Tumors of Endocrine Organs*.¹⁻³ This categorization was based on evidence from more than 150 publications on noninvasive follicular thyroid neoplasm with papillary-like nuclear features (NIFTP) and accompanied by a discussion of the incidence, diagnosis, and prognostic implications of this terminology in Nikiforov et al.⁴ However, these borderline thyroid tumors were defined only as encapsulated tumors with a follicular growth pattern, a category that included hyalinizing trabecular tumor (HTT), follicular tumor of uncertain malignant potential, well-differentiated tumor of uncertain malignant potential (WDT-Ump), and NIFTP.¹⁻³ Because papillary microcarcinoma was proposed to be renamed as papillary microtumor

(PMiT) by thyroid experts,⁵ there would be no reason to restrict borderline/precursor tumors to the follicular growth pattern.

Papillary thyroid carcinoma (PTC)-type nuclear changes are the most reliable morphological features in the diagnosis of PTC. However, the nuclear assessment used to identify these changes is highly subjective.⁶ In particular, the threshold for rendering a diagnosis between follicular adenoma (FA) and encapsulated follicular variant of PTC (FV-PTC) has varied greatly among pathologists.⁷ This issue is not restricted to follicular-growth patterned tumors. Issues with diagnosis using a nuclear assessment have also been seen in other cases. For example, the main differential diagnosis of encapsulated conventional PTCs is FAs with papillary hyperplasia,⁸ and distinguishing between these two types of tumors poses a challenge similar to that of

differentiating encapsulated FV-PTCs from FAs.

CASE REPORT

In September 2016, a 26-year-old man with no past medical history was found to have a nodule at the left lower lobe of the thyroid gland by palpation during an annual medical checkup exam. The patient visited our outpatient clinic at Enshu Hospital for further evaluation. There was no family history of thyroid disorders. Thyroid function tests indicated that the patient had euthyroid status with normal thyroid stimulating hormone (4.18 mIU/L; reference range, 0.50 to 5.00), FT4 (16.5 nmol/L; reference range, 11.6 to 21.9), and FT3 levels (4.7 pmol/L; reference range, 3.5 to 6.6) as measured by Elecsys (Roche Diagnostics K.K., Tokyo, Japan). Serum thyroglobulin was 18.7 µg/L (reference range, ≤33.7) and anti-thyroglobulin antibodies were undetectable. B-mode ultrasonography (US) revealed a hypoechoic, heterogeneous nodule 23 mm at its largest diameter with a slightly jagged border (Fig. 1A). Color Doppler US showed increased intranodular vascularity. Although fine-needle aspiration cytology (FNAC) showed a benign cytological diagnosis, the patient preferred to undergo a left lobectomy of the thyroid rather than continuing with an annual US follow-up. Unexpectedly, the nodule was diagnosed as an encapsulated PTC on histology by a local pathologist. However, when a second opinion was obtained, the nodule was diagnosed as a FA with papillary hyperplasia because of the lack of well-developed PTC-type nuclear features. To determine whether he would benefit from additional resection (completion thyroidectomy), cytological specimens and stored formalin-fixed, paraffin-embedded tissue blocks were analyzed in a third opinion consultation.

FNAC revealed a number of crowded groups of follicular cells with slight nuclear enlargement and mild nuclear overlapping (Fig. 1B). Diagnosis by the doctors providing a third opinion was high-risk indeterminate nodule (follicular neoplasm). The cut surface of the left lobe obtained from hemithyroidectomy demonstrated a well-circumscribed solid tumor. A low-power view showed an encapsulated nodule comprising two types of papillary lesions: one covered with follicular cells containing small hyperchromatic nuclei (adenomatous nodule-like lesion) and the other covered with larger follicular cells having large nonhyperchromatic vesicular nuclei (Fig. 1C, D). Only a trace amount of follicular pattern was noted in this tumor. In high-power view (Fig. 1E, F), the second type of papillary lesion showed nuclear enlargement, irregularity, elongation, and overlapping as well as a few nuclear grooves. Nuclear pseudoinclu-

sions were absent and chromatin characteristics were insufficient. As PTC-type nuclear features were equivocal (with a nuclear score of two according to Nikiforov et al.,⁴ the doctors providing a third opinion consultation did not endorse the previously suggested diagnoses of encapsulated PTC and FA with papillary hyperplasia. Additionally, these pathological findings did not fulfil the diagnostic criteria for new borderline tumor entities (i.e., NIFTP and WDT-UMP) according to the WHO classification, which not only are intended to be applied to encapsulated follicular-patterned lesions, but also have exclusion criteria that included the papillary growth pattern.^{1-4,9}

Immunohistochemical analysis demonstrated that the adenomatous nodule-like lesion, papillary-patterned lesion with equivocal PTC-type nuclear features, and the surrounding thyroid tissue were all negative for cytokeratin 19 (clone b170, Novocastra, Newcastle upon Tyne, UK) (Fig. 2A) and *BRAF*V600E (clone VE1, Spring Bioscience, Pleasanton, CA, USA) (Fig 2B). The MIB-1 labeling index was estimated to be approximately 1%–2% in all three tested tumor areas (clone MIB-1, Dako, Glostrup, Denmark) (Fig. 2C). Subsequent mutational analysis of *KRAS*, *NRAS*, *HRAS* (codons 12, 13, and 61), *BRAF* (exon 15), and *TERT* promoter (C250T and C228T), as described previously,¹⁰ demonstrated that none of the three tissue samples had the *BRAF* mutation or the *TERT* promoter mutation. Interestingly, a heterozygous point mutation in exon 2 of the *KRAS* gene (GGT to GCT) resulting in the replacement of glycine with alanine at codon 12 (G12A), was detected in tissue samples from both the adenomatous nodule-like lesion and the papillary-patterned lesion (Fig. 2D). In contrast, the surrounding thyroid tissue was found to contain wild-type *KRAS*. Therefore, the nodule was found to be a clonal neoplasm but not a non-neoplastic (hyperplastic) nodule. *NRAS* and *HRAS* mutations were not detected in any of the three tumor areas.

After completing the tests described above, we speculated that this tumor (noninvasive encapsulated papillary thyroid tumor with *RAS* mutation) may be an example of a novel borderline tumor with papillary architecture, which does not qualify as either NIFTP or WDT-UMP under the current WHO criteria. The patient decided not to undergo additional surgery and developed no recurrence or distant metastasis during 24 months of follow-up.

Prior to June 2017, the Institutional Review Board of the Enshu Hospital waived the need for ethics approval when only archived tissue specimens were used in a retrospective manner. This study was performed in accordance with the principles of the Declaration of Helsinki. Written informed consent was obtained from the patient for the publication of this case report.

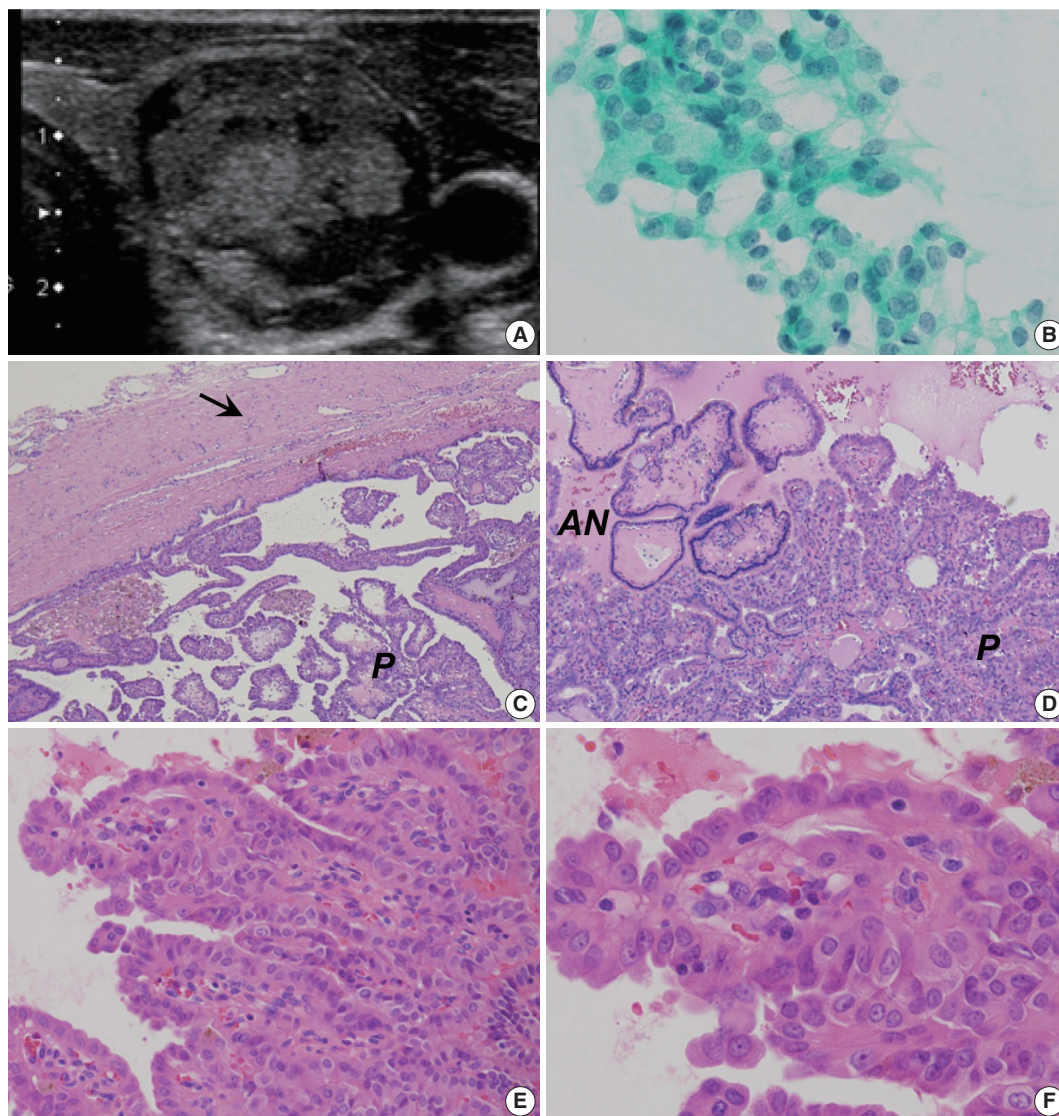


Fig. 1. Encapsulated papillary growth-patterned tumor with equivocal papillary thyroid carcinoma (PTC)-type nuclear features in a 26-year-old man (nuclear score 2 according to Nikiforov et al.⁴) (A) B-mode ultrasonography showing a hypoechoic, heterogeneous nodule with a largest diameter of 23 mm and a slightly jagged border. (B) Fine-needle aspiration cytology revealing a number of crowded groups of follicular cells with slight nuclear enlargement and mild nuclear overlapping (Papanicolaou stain). (C, D) The resected solid tumor showing a capsule (arrow) and two types of papillary lesions: one covered with follicular cells containing small hyperchromatic nuclei (adenomatous nodule-like lesion, AN) and the other covered with larger follicular cells having nonhyperchromatic nuclei (P). (E, F) High-power views of the second type of papillary lesion showing nuclear elongation and overlapping as well as a one- to two-fold enlargement of nuclei size with granular chromatin. Nuclear grooves are not abundant, and pseudoinclusions are absent. Chromatin characteristics of PTC-type nuclear features are insufficient.

DISCUSSION

We report an encapsulated thyroid tumor with a papillary growth pattern, nuclear score of 2, and a *KRAS* mutation. The patient underwent surgery for a supposedly benign thyroid nodule that was initially diagnosed as an encapsulated PTC by a local pathologist but then as a FA with papillary hyperplasia by a second opinion consultation. Our third opinion diagnoses

were high-risk indeterminate nodule (follicular neoplasm) based on FNAC, and borderline/precursor tumor based on histological findings. These discrepancies likely exist due to equivocal PTC-type nuclear changes, as NIFTP and WDT-UPT generally fall into one of the indeterminate diagnostic categories by preoperative FNAC.^{2,3}

This study further reports that this tumor is not a *BRAF*-mutant tumor, but rather a clonal tumor with a *RAS* mutation.

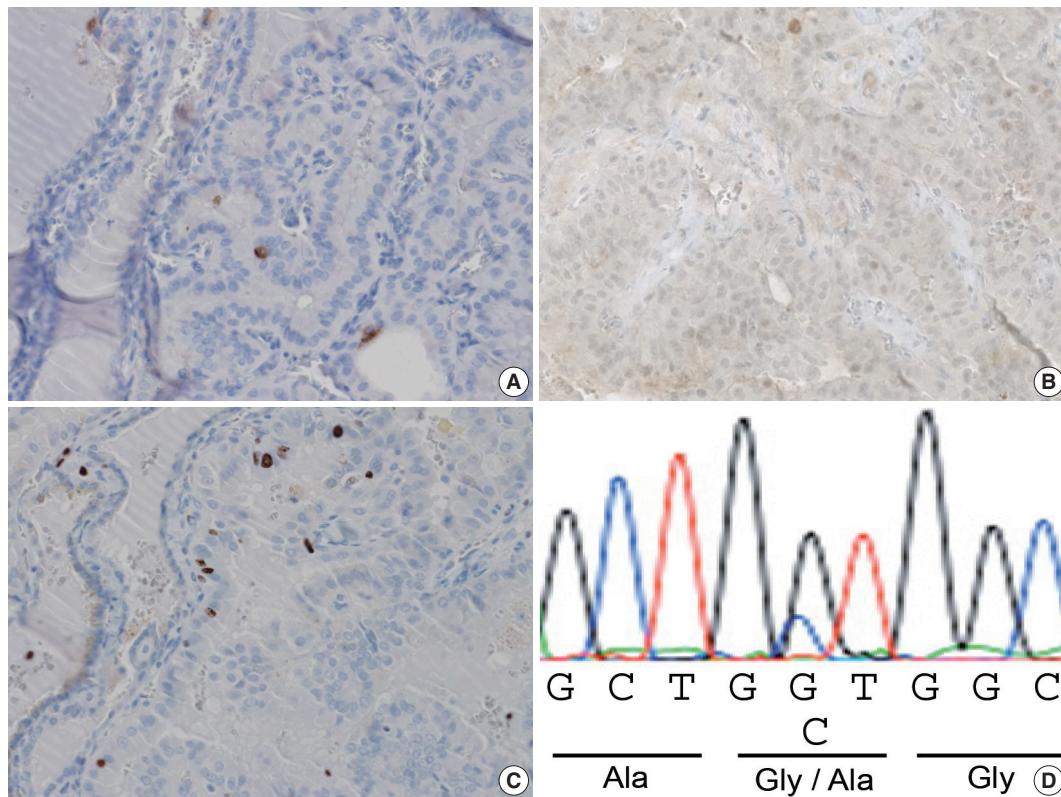


Fig. 2. Immunohistochemical and mutational analyses. (A, B) Immunohistochemical staining with cytokeratin 19 and *BRAFV600E* led to negative results in the cytoplasm of the tumor cells. (C) The MIB-1 labeling index was approximately 1%–2%. (D) Sequence analysis revealed a heterozygous point mutation of the *KRAS* gene in exon 2 (GGT to GCT) resulting in the substitution of alanine for glycine at codon 12 (G12A) in the tissue sample from the papillary lesion with a nuclear score of two and an adenomatous nodule-like lesion (D).

A *RAS*-mutant tumor became its own category when it was separated from conventional PTCs with a dominant papillary growth pattern featuring a *BRAF*-positive profile.⁴ There are PTCs in the literature that have been reported to have *RAS* mutations that were diagnosed as either invasive encapsulated or noninvasive encapsulated FV-PTCs.^{11–13} There are no detailed morphological studies of noninvasive encapsulated conventional-type PTC with a *RAS* mutation, and there are no available prognostic analyses. Recently, Radkay et al.¹⁴ investigated the cytopathologic features of common *RAS* mutation subtypes *NRAS*, *HRAS*, and *KRAS*. Out of 204 *RAS*-mutant thyroid tumors, 24 cases (11.8%) had *KRAS* mutations like the one reported here. Although the surgical resection specimen demonstrated conventional PTC in two cases, detailed information on either the presence of capsulation or the degree of PTC-type nuclear changes is not available. From a review of The Cancer Genome Atlas (TCGA) study database,¹² we identified four cases of PTC with *KRAS* mutations. Papillary growth pattern or classic type PTC was recorded in two of those cases. Case 1 (TCGA-EM-A4FV) was diagnosed as invasive encapsulated PTC. The disease

was stage N0 and the patient was disease-free 12 months post-operatively. Case 2 (TCGA-BJ-A0ZE) was diagnosed as invasive follicular variant PTC but not classic type PTC and was stage N0. The other two cases with *KRAS* mutations were FV-PTCs. Further studies are needed to evaluate the biological and clinical characteristics of noninvasive encapsulated tumors with a papillary growth pattern and *KRAS* mutations, although the frequency of such cases seems to be rare based on a survey of the current literature.^{12,14}

Two important histological findings (encapsulated and non-invasive) and two clinical parameters (no metastasis at diagnosis and no recurrence after a long-term follow-up) are used for borderline tumor classification (i.e., HTT and NIFTP).^{1,3,4} Although our case demonstrated three out of four features (encapsulated, noninvasive, and no metastasis at diagnosis), the absence of recurrence after a long-term follow up is still unknown. Because of the expected low frequency of this disease, we propose that an international working group be created to confirm the extremely low grade or biologically benign nature of a possible novel subtype of borderline tumor with a papillary structure. This pro-

posed working group study would be similar to the one conducted by the NIFTP international working group.

After the introduction of borderline thyroid tumors in the latest WHO classification,¹⁻³ pathologists have three choices for the characterization of thyroid tumors with a follicular growth pattern: benign, borderline, and malignant. For papillary thyroid tumors, pathologists are still forced to select from either benign or malignant, which may cause significant observer variation in the diagnosis of thyroid carcinomas like the one presented in this report. Welch and Black estimated the probability of overdiagnosis of thyroid cancer to be more than 99%.¹⁵ Therefore, the introduction of borderline tumors in papillary-patterned lesions is an urgent issue to reduce the overdiagnosis and overtreatment of indolent thyroid tumors.

The modified initial risk stratification system, published by the American Thyroid Association (ATA) in 2016,¹⁶ was incorporated into the 2017 WHO classification.¹⁻³ In contrast, borderline tumors were still listed as “cancer” with a very low risk of structural disease recurrence (<2%) in the 2015 ATA management guideline.¹⁶ These low-risk tumors include (1) papillary microcarcinoma, proposed as PMiT by thyroid experts;⁵ (2) intrathyroidal encapsulated FV-PTC (the majority of which have been downgraded to WDT-UMP or NIFTP when they are found to have no definite invasion); and (3) a <4 cm intrathyroidal *BRAF* wild-type PTC.^{17,18} In addition to these three options, there is potential for more borderline/precursor thyroid tumors with a very low risk of disease recurrence after complete excision. Since there would be no reason for restricting borderline/precursor tumors to the follicular growth pattern, we suggest an extension of the classification for novel borderline tumors with a papillary growth pattern. Prior to the introduction of the borderline tumor category by the 2017 WHO classification, our group proposed a new prognostic classification of thyroid tumors, in which extremely low-risk tumors with both follicular and papillary architectures were grouped into borderline/precursor tumors.¹⁹ Accordingly, we propose a new term to relieve the psychological burden of patients: “noninvasive encapsulated papillary *RAS*-like thyroid tumor” (NEPRAS).

For providing simplified and reproducible diagnostic criteria for nuclear features, Nikiforov et al.⁴ developed a three-point scoring scheme, in which each category of nuclear feature is assigned a score of either 0 or 1, yielding a summation nuclear score of 0–3. A score of 0–1 is diagnostic of a benign nodule, whereas a score of 2–3 is required for diagnosing PTC-type nuclear changes. Since even delicate nuclear changes (for example, a score of two, as presented in this case) led to a categorization

of PTC-type, the introduction of the borderline category in papillary growth pattern tumor classification could reduce the overdiagnosis and overtreatment of patients with indolent thyroid nodules. We would like to propose that tumors be diagnosed as FA with papillary hyperplasia, NEPRAS, and encapsulated PTC when nuclear scores are 0–1, 2, and 3, respectively. As a consequence, a subset of FAs with papillary hyperplasia and encapsulated PTC could potentially be up- or down-graded to NEPRAS. *RAS* mutations were reported to correlate with significantly less developed PTC-type nuclear features and indolent clinical behaviours,²⁰ indicating that the molecular profile of tumor cells may also play an important role in determining borderline tumors with a papillary growth pattern.

In conclusion, we report significant observer variation in a noninvasive encapsulated papillary growth-patterned tumor of more than 1 cm in diameter with a nuclear score of 2 and a *KRAS* mutation. Although further studies are required, we believe that the introduction of a borderline tumor classification for tumors with papillary structure would affect the psychological and clinical consequences related to the diagnosis of thyroid tumors.

ORCID

Kenji Ohba: <https://orcid.org/0000-0001-8538-8742>

Norisato Mitsutake: <https://orcid.org/0000-0002-2744-8046>

Michiko Matsuse: <https://orcid.org/0000-0001-6178-3342>

Tatiana Rogounovitch: <https://orcid.org/0000-0002-0616-3383>

Kennichi Kakudo: <https://orcid.org/0000-0002-0347-7264>

Author Contributions

Conceptualization: KK.

Investigation: NM, MM, TR, KK.

Methodology: NM, MM, TR.

Project administration: KO.

Resources: NN, YO, YG.

Supervision: KK.

Writing—original draft: KO.

Writing—review & editing: KO, NM, KK.

Conflicts of Interest

The authors declare that they have no potential conflicts of interest.

Acknowledgments

The authors are grateful to all the doctors who provided us with the opportunity to study the clinical course of this patient.

The authors also thank Dr. Hiroki Mori for his valuable comments and Enago (www.enago.jp) for the English language review.

REFERENCES

- Pappotti M, Volante M. Hyalinizing trabecular tumour. In: Lloyd RV, Osamura RY, Kloppel G, Rosai J, eds. WHO classification of tumours of endocrine organs. 4th ed. Lyon: International Agency for Research on Cancer, 2017; 73-4.
- Chan JK, Tallini G. Tumours of uncertain malignant potential. In: Lloyd RV, Osamura RY, Kloppel G, Rosai J, eds. WHO classification of tumours of endocrine organs. 4th ed. Lyon: International Agency for Research on Cancer, 2017; 76-7.
- Nikiforov YE, Ghossein RA, Kakudo K, et al. Non-invasive follicular thyroid neoplasm with papillary-like nuclear features. In: Lloyd RV, Osamura RY, Klöppel G, Rosai J, eds. WHO classification of tumours of endocrine organs. 4th ed. Lyon: International Agency for Research on Cancer, 2017; 78-80.
- Nikiforov YE, Seethala RR, Tallini G, et al. Nomenclature revision for encapsulated follicular variant of papillary thyroid carcinoma: a paradigm shift to reduce overtreatment of indolent tumors. *JAMA Oncol* 2016; 2: 1023-9.
- Rosai J, LiVolsi VA, Sobrinho-Simoes M, Williams ED. Renaming papillary microcarcinoma of the thyroid gland: the Porto proposal. *Int J Surg Pathol* 2003; 11: 249-51.
- Hirokawa M, Carney JA, Goellner JR, et al. Observer variation of encapsulated follicular lesions of the thyroid gland. *Am J Surg Pathol* 2002; 26: 1508-14.
- Chan J. Strict criteria should be applied in the diagnosis of encapsulated follicular variant of papillary thyroid carcinoma. *Am J Clin Pathol* 2002; 117: 16-8.
- Chan JK, Tsang WY. Endocrine malignancies that may mimic benign lesions. *Semin Diagn Pathol* 1995; 12: 45-63.
- Williams ED. Guest editorial: two proposals regarding the terminology of thyroid tumors. *Int J Surg Pathol* 2000; 8: 181-3.
- Mitsutake N, Fukushima T, Matsuse M, et al. *BRAF*(V600E) mutation is highly prevalent in thyroid carcinomas in the young population in Fukushima: a different oncogenic profile from Chernobyl. *Sci Rep* 2015; 5: 16976.
- Zhu Z, Gandhi M, Nikiforova MN, Fischer AH, Nikiforov YE. Molecular profile and clinical-pathologic features of the follicular variant of papillary thyroid carcinoma: an unusually high prevalence of ras mutations. *Am J Clin Pathol* 2003; 120: 71-7.
- Cancer Genome Atlas Research Network. Integrated genomic characterization of papillary thyroid carcinoma. *Cell* 2014; 159: 676-90.
- Rivera M, Ricarte-Filho J, Knauf J, et al. Molecular genotyping of papillary thyroid carcinoma follicular variant according to its histological subtypes (encapsulated vs infiltrative) reveals distinct *BRAF* and *RAS* mutation patterns. *Mod Pathol* 2010; 23: 1191-200.
- Radkay LA, Chiosea SI, Seethala RR, et al. Thyroid nodules with *KRAS* mutations are different from nodules with *NRAS* and *HRAS* mutations with regard to cytopathologic and histopathologic outcome characteristics. *Cancer Cytopathol* 2014; 122: 873-82.
- Welch HG, Black WC. Overdiagnosis in cancer. *J Natl Cancer Inst* 2010; 102: 605-13.
- Haugen BR, Alexander EK, Bible KC, et al. 2015 American Thyroid Association management guidelines for adult patients with thyroid nodules and differentiated thyroid cancer: the American Thyroid Association Guidelines Task Force on Thyroid Nodules and Differentiated Thyroid Cancer. *Thyroid* 2016; 26: 1-133.
- Elisei R, Viola D, Torregrossa L, et al. The *BRAF*(V600E) mutation is an independent, poor prognostic factor for the outcome of patients with low-risk intrathyroid papillary thyroid carcinoma: single-institution results from a large cohort study. *J Clin Endocrinol Metab* 2012; 97: 4390-8.
- Kakudo K, Bychkov A, Bai Y, Li Y, Liu Z, Jung CK. The new 4th edition World Health Organization classification for thyroid tumors, Asian perspectives. *Pathol Int* 2018; 68: 641-64.
- Kakudo K, Bai Y, Katayama S, et al. Classification of follicular cell tumors of the thyroid gland: analysis involving Japanese patients from one institute. *Pathol Int* 2009; 59: 359-67.
- Adeniran AJ, Zhu Z, Gandhi M, et al. Correlation between genetic alterations and microscopic features, clinical manifestations, and prognostic characteristics of thyroid papillary carcinomas. *Am J Surg Pathol* 2006; 30: 216-22.

Crystal-Storing Histiocytosis with Plasma Cell Neoplasm in the Setting of Chronic Carbamazepine Exposure

Woo Cheal Cho · Safina Hafeez · Peter Shen

Department of Pathology and Laboratory Medicine, Hartford Hospital, Hartford, CT, USA

Crystal-storing histiocytosis (CSH) is an uncommon phenomenon in which crystalline material accumulates within the cytoplasm of histiocytes, and is typically associated with an underlying lymphoproliferative or plasma cell disorder with monoclonal immunoglobulin expression, such as multiple myeloma (MM), lymphoplasmacytic lymphoma (LPL), and monoclonal gammopathy of undetermined significance (MGUS).^{1,2} With a few exceptions, the crystalline materials are almost exclusively composed of κ immunoglobulin light chains.^{2,3} Recently, other less common variants of CSH in which the crystalline material is not of an immunoglobulin origin have also been described, including clofazimine-induced CSH.^{4,5} Here, we describe a case of CSH with plasma cell myeloma in the setting of chronic carbamazepine exposure.

CASE REPORT

A 72-year-old woman with a history of chronic renal insufficiency, hypothyroidism, peripheral neuropathy, hypercholesterolemia, anxiety, and tremor was referred from her primary care physician's office to the emergency department for evaluation of pancytopenia. Her peripheral neuropathy had been managed with carbamazepine for several years. Bone marrow biopsy revealed infiltration and near-total replacement by cells filled with eosinophilic crystalloid material (Fig. 1A, B). Hematopoietic cells

were virtually undetectable, and extensive reticulin fibrosis was noted. CD138-positive, κ -restricted plasma cells (Fig. 1C) were highlighted to form collections and aggregates in the marrow, comprising at least 30% of total cellularity. No definitive IgG, IgA, or IgM was observed within the plasma cells. Histiocytes comprised the remainder of the cell population and were highlighted by CD68 (Fig. 1D) and CD163. κ expression (Fig. 1E) was also noted within the histiocytes. CD34 and CD117 failed to reveal a significant blast population. Other than occasional expressions, no significant myeloid population was highlighted by CD15. No CD1a expression was observed within histiocytes/macrophages. No metastatic carcinoma was revealed by cytokeratin. CD61 also failed to reveal the presence of megakaryocytes.

By polychromatic flow cytometry, approximately 58% of cells in the specimen displayed the phenotypic and light scatter properties of lymphocytes. Most of these were T cells, without specific phenotypic abnormalities, including CD4-positive and CD8-positive subsets (CD4:CD8 ratio of 2.5:1). B cells comprised approximately 12% of cells. No normal B-cell precursors (hematogones) were seen. Phenotypically mature B cells comprised a mixture of κ - and λ -bearing cells, without evidence of light chain restriction. Cells with the phenotypic and light scatter properties characteristic of plasma cells comprised 4% of cells, and included predominantly a cytoplasmic κ -restricted plasma cell population. No definitive expression for IgA, IgG, IgD, and IgM was noted within the plasma cells. CD34-positive myeloblasts comprised approximately < 1% of cells. Very few granulocytic cells were observed (17% of total cells), and 5% nucleated red blood cells were seen.

Further workup including serum protein and immunofixation electrophoresis showed hypogammaglobulinemia and markedly elevated monoclonal free κ light chains with a free κ : λ ratio of

Corresponding Author

Woo Cheal Cho, MD
Department of Pathology and Laboratory Medicine, Hartford Hospital, 80 Seymour Street, Hartford, CT 06102-5037, USA
Tel: +1-860-972-2488, Fax: +1-860-545-2204
E-mail: WooCheal.Cho@hhchealth.org

Received: April 10, 2018 Revised: May 24, 2018

Accepted: May 25, 2018

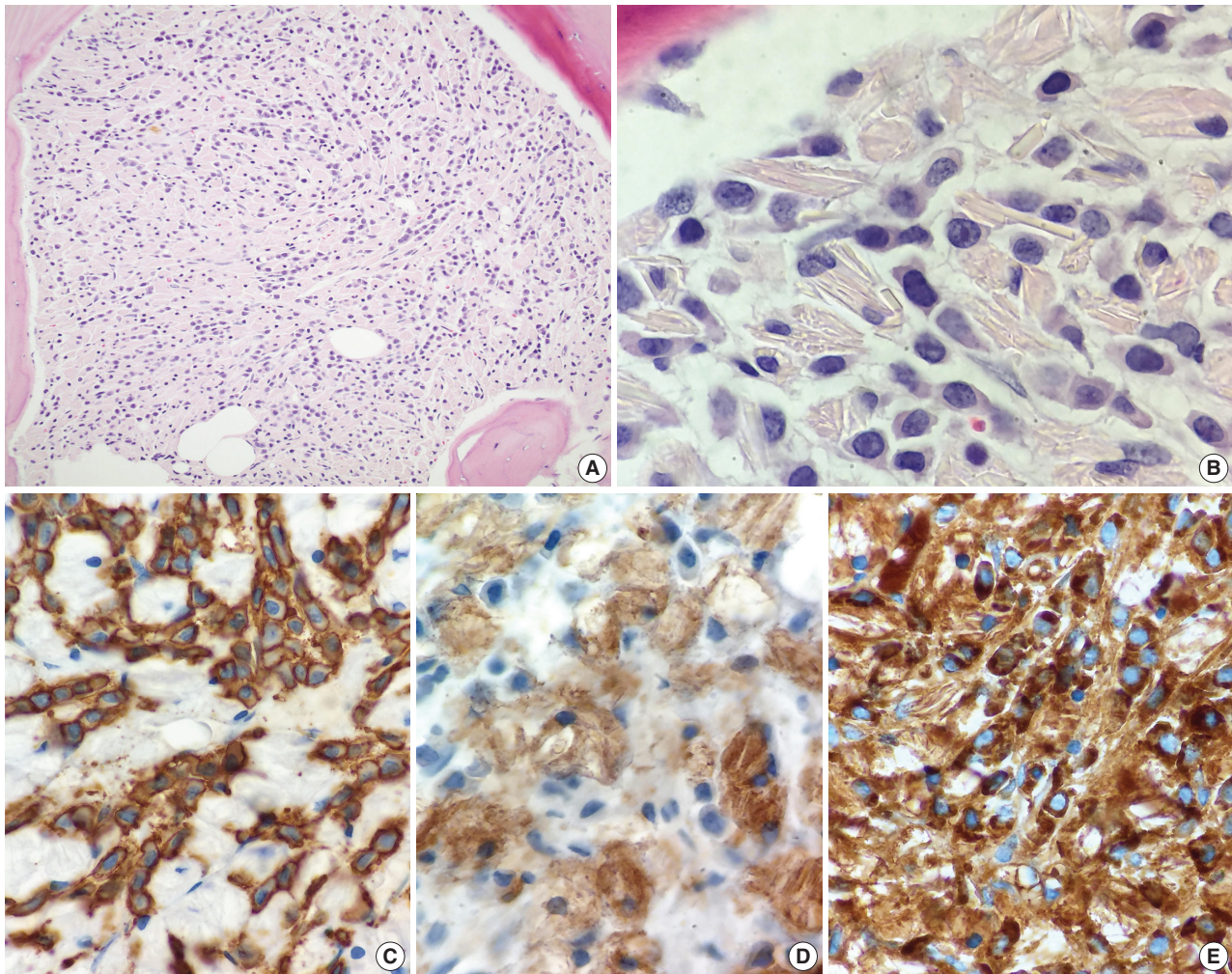


Fig. 1. Histologic findings of bone marrow biopsy. (A, B) Bone marrow biopsy showed infiltration and near-total replacement by cells filled with eosinophilic crystalloid material. The neoplastic cells were CD138-positive (C), kappa-restricted plasma cells, while the remainder of the cell population were histiocytes highlighted by CD68 (D) and CD163 (not shown). (E) Kappa expression was also noted within the histiocytes.

more than 700:1. These findings were most consistent with CSH associated with plasma cell myeloma. The patient was immediately placed on bortezomib and dexamethasone. Subsequent skeletal survey revealed no significant evidence of lytic lesions.

Formal written informed consent was not required with a waiver by the appropriate Institutional Review Board of Hartford Hospital (FWA00021932).

DISCUSSION

CSH is a rare, but well-documented phenomenon most frequently seen in patients with an underlying lymphoproliferative or plasma cell disorder with monoclonal immunoglobulin expression, such as MM, LPL, and MGUS.^{1,2} Other less common variants of CSH that are not of an immunoglobulin origin, including

clofazimine-induced CSH, have also recently been described.^{4,5} Clofazimine is a drug used to treat leprosy with frequent side effects including red to brownish discoloration of the skin and gastrointestinal disturbances. Reportedly, prolonged treatment with higher-dose clofazimine can also lead to CSH, albeit rare, in which clofazimine crystals accumulate in the lamina propria of the small bowel and may result in a severe enteropathy.⁴ Clofazimine crystals appear clear in routine histologic sections, as they dissolve in alcohol and other organic solvents, and in the presence of background plasmacytosis, may simulate histologically other immunoglobulin-associated CSHs.⁴ Our patient in the presented case had been taking carbamazepine, an antiepileptic drug, for several years for management of peripheral neuropathy. Currently, there is no known evidence of a direct link between prolonged carbamazepine exposure and development of CSH. However,

immune abnormalities are well-documented long-term adverse effects of antiepileptic drugs; and, in fact, development of hematologic disorders, including non-Hodgkin's lymphoma and MM, following a prolonged treatment with antiepileptic therapy, particularly phenytoin, has previously been reported.⁶ The potential carcinogenic effect of carbamazepine is still unclear, although pancytopenia as in our patient has been rarely observed in patients receiving carbamazepine. Carbamazepine can alter the immune system by increasing the production of various interleukins (ILs), including IL-6, which is known to play a key role in the pathogenesis of MM. IL-6 not only serves as a growth factor, but it also serves as a survival factor in MM, ultimately inhibiting apoptosis of myeloma cells.^{7,8} Recently, there have been a few case reports raising the possibility of a causal relationship between carbamazepine exposure and subsequent development of hypogammaglobulinemia, MGUS or MM.^{9,10} These reports are still anecdotal and few in number, and further studies are needed to fully understand the potential carcinogenicity of carbamazepine and its possible link with plasma cell neoplasms.

In conclusion, we report a unique case of CSH with plasma cell myeloma thought to have developed following prolonged carbamazepine therapy. Although plasma cell neoplasms have been reported in patients with prolonged exposure to carbamazepine, to the best of our knowledge, no case of CSH with plasma cell neoplasm in the setting of chronic carbamazepine exposure has been previously described.

ORCID

Woo Cheal Cho: <https://orcid.org/0000-0001-5867-1403>

Author Contributions

Conceptualization: WCC.

Data curation: WCC, PS.

Formal analysis: WCC, SH, PS.

Investigation: WCC, SH.

Methodology: PS.

Project administration: WCC, PS.

Resources: SH.

Supervision: PS.

Validation: WCC.

Writing—original draft: WCC.

Writing—review & editing: WCC, PS.

Conflicts of Interest

The authors declare that they have no potential conflicts of interest.

REFERENCES

- Kapadia SB, Enzinger FM, Heffner DK, Hyams VJ, Frizzera G. Crystal-storing histiocytosis associated with lymphoplasmacytic neoplasms: report of three cases mimicking adult rhabdomyoma. *Am J Surg Pathol* 1993; 17: 461-7.
- Lebeau A, Zeindl-Eberhart E, Müller EC, et al. Generalized crystal-storing histiocytosis associated with monoclonal gammopathy: molecular analysis of a disorder with rapid clinical course and review of the literature. *Blood* 2002; 100: 1817-27.
- Jones D, Bhatia VK, Krausz T, Pinkus GS. Crystal-storing histiocytosis: a disorder occurring in plasmacytic tumors expressing immunoglobulin kappa light chain. *Hum Pathol* 1999; 30: 1441-8.
- Sukpanichnant S, Hargrove NS, Kachintorn U, et al. Clofazimine-induced crystal-storing histiocytosis producing chronic abdominal pain in a leprosy patient. *Am J Surg Pathol* 2000; 24: 129-35.
- Dogan S, Barnes L, Cruz-Vetrano WP. Crystal-storing histiocytosis: report of a case, review of the literature (80 cases) and a proposed classification. *Head Neck Pathol* 2012; 6: 111-20.
- Olsen JH, Schulgen G, Boice JD Jr, et al. Antiepileptic treatment and risk for hepatobiliary cancer and malignant lymphoma. *Cancer Res* 1995; 55: 294-7.
- Gado K, Domjan G, Hegyesi H, Falus A. Role of INTERLEUKIN-6 in the pathogenesis of multiple myeloma. *Cell Biol Int* 2000; 24: 195-209.
- Verrotti A, Basciani F, Trotta D, Greco R, Morgese G, Chiarelli F. Effect of anticonvulsant drugs on interleukins-1, -2 and -6 and monocyte chemoattractant protein-1. *Clin Exp Med* 2001; 1: 133-6.
- Moreno-Ancillo A, Cosmes Martin PM, Dominguez-Noche C, et al. Carbamazepine induced transient monoclonal gammopathy and immunodeficiency. *Allergol Immunopathol (Madr)* 2004; 32: 86-8.
- Günaldı M, Paydaş S, Usul Afşar C, Bozkurt Duman B, Erçolak V, Haksöyler V. Carbamazepine and multiple myeloma: possible interaction. *Turk J Haematol* 2013; 30: 83-4.

Wharton Jelly Hair in a Case of Umbilical Cord Stricture and Fetal Death

Eun Na Kim · Jae-Yoon Shim¹ · Chong Jai Kim

Departments of Pathology and ¹Obstetrics and Gynecology, Asan Medical Center, University of Ulsan College of Medicine, Seoul, Korea

Placenta forms the intrauterine environment that supplies oxygen and nutrients to the fetus during pregnancy. The umbilical cord is the lifeline of the fetus that connects the fetus to the placenta. An abnormally thin umbilical cord is associated with adverse pregnancy outcomes such as oligohydramnios, fetal growth restriction, and fetal distress.^{1,2} Critical events occurring in the umbilical cord, especially stricture, knots, hemorrhage, and strangulation, often lead to fetal death.^{3,4} Here, we report for the first time an autopsy case of fetal death caused by umbilical cord stricture accompanied by hair growth in the Wharton jelly.

CASE REPORT

A 28-year-old primigravida woman presented with severe fetal growth restriction and oligohydramnios at 23 weeks of gestational age. Five days later, the ultrasound examination revealed fetal death in utero, and a macerated female fetus weighing 350 g (< 3rd percentile) was delivered.⁵ The circumference of the head was 18.0 cm (< 3rd percentile),⁶ and that of the abdomen was 14.4 cm (< 3rd percentile).⁶ Infantogram showed mildly hypoplastic thoracic cage (Fig. 1A), and chest circumference was 14.6 cm (10th–25th percentile).⁷ Chromosomal analysis by amniocentesis performed at 18 weeks showed normal findings.

Fetal autopsy and placental biopsy revealed hypocoiling of the umbilical cord (Fig. 1B) with a rather abrupt stricture located 6.5 cm from the placental insertion. Localized edema of the umbilical cord was associated with the stricture. The diameter of the umbilical cord at the stricture was 4 mm, which was

lower than the 10th percentile of the normal range (Fig. 2).¹ Microscopic examination of the umbilical cord stricture revealed hair follicles including hair shafts and papillary mesenchymal body in the firm and fibrotic Wharton jelly. Capillary vessel formation was also found in the peripheral region of the Wharton jelly (Fig. 3). Squames were detected in the alveoli of fetal lungs, and chorionic villi showed increased syncytial knots and distal villous hypoplasia. Overall, the umbilical cord stricture associated with unusual development of hair follicles and fibrotic Wharton jelly seems to have significantly contributed to the fetal demise.

The mother has provided written informed consent for autopsy prior to the postmortem examinations. Since only the pathology and autopsy findings of an already deceased fetus and only de-identified personal information of the mother and the fetus were used, the Institutional Review Board (IRB) of Asan Medical Center determined exemption (IRB number: 2017-1192).

DISCUSSION

The Wharton jelly is the umbilical cord stroma that originates from the extraembryonic mesoderm of allantois. The Wharton jelly is rich in mucopolysaccharides such as hyaluronic acid and chondroitin sulfate and thus protects umbilical vessels from compression.⁸ Loss of protection by the Wharton jelly can lead to compromised fetoplacental circulation and subsequent fetal death.⁹ Umbilical cord stricture is a known cause of fetal death.³ Hypocoiling also renders umbilical cord vessels susceptible to kinking and acute obstruction.

The Wharton jelly has been extensively studied as a reservoir of mesenchymal stem cells (MSCs) in the field of regenerative medicine. The Wharton jelly MSCs show a differentiation spectrum covering ectodermal and endodermal lineages.¹⁰ To the best of our knowledge, the current case is the first example of hair growth and follicle formation in the umbilical cord. It should

Corresponding Author

Chong Jai Kim, MD, PhD
Department of Pathology, Asan Medical Center, University of Ulsan College of Medicine, 88 Olympic-ro 43-gil, Songpa-gu, Seoul 05505, Korea
Tel: +82-2-3010-4516, Fax: +82-2-472-7898, E-mail: ckim@amc.seoul.kr

Received: August 13, 2018 Revised: September 29, 2018

Accepted: October 24, 2018

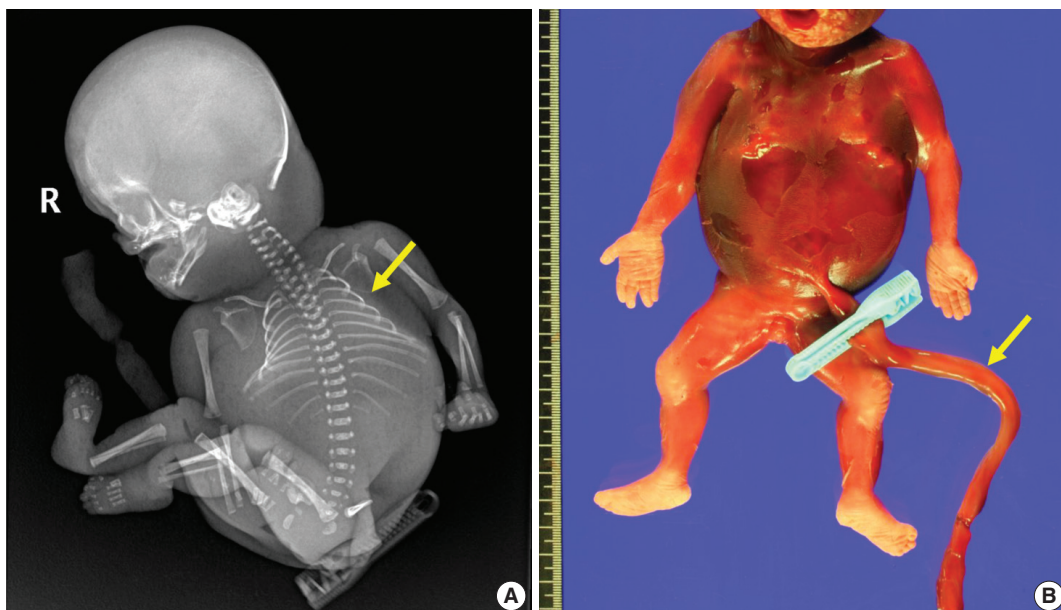


Fig. 1. Major characteristics of the fetus. (A) Infantogram shows hypoplastic small rib cage (arrow). (B) The stillborn macerated fetus has no coiling of the umbilical cord (arrow).



Fig. 2. Gross features of the placenta and the umbilical cord. (A) The umbilical cord is marginally inserted, and the connecting chorionic plate vasculature is tortuous and prominent (red arrow). The umbilical cord shows abrupt constriction (white arrow) and associated segmental edema of the Wharton jelly (yellow arrow). (B) A view from the maternal side of the placenta shows a constriction in the umbilical cord (white arrow). The placental parenchyma is pale and edematous (red arrow).

also be mentioned that hair formation overlaps with a fibrotic change in the Wharton jelly and the development of capillaries. Capillaries are not normally observed in the Wharton jelly, and the anatomical location of the stricture is apart from the umbilicus, where fetal skin tissue can coexist. It is unclear at this point whether the hair and capillaries are products of *de novo* differentiation of pluripotent Wharton jelly MSCs. The development of multiple capillaries in the periphery and fibrosis of Wharton jelly may be secondary consequences of stricture, and the capillaries can be considered collaterals for compensating for chronically compromised umbilical circulation.

In addition to developmental uniqueness, lessons from the

current case include that thorough histologic examination is necessary to determine the cause of fetal death and document significant findings.

ORCID

Eun Na Kim: <https://orcid.org/0000-0003-2992-7881>

Jae-Yoon Shim: <https://orcid.org/0000-0003-1881-8436>

Chong Jai Kim: <https://orcid.org/0000-0002-2844-9446>

Author Contributions

Conceptualization: CJK.

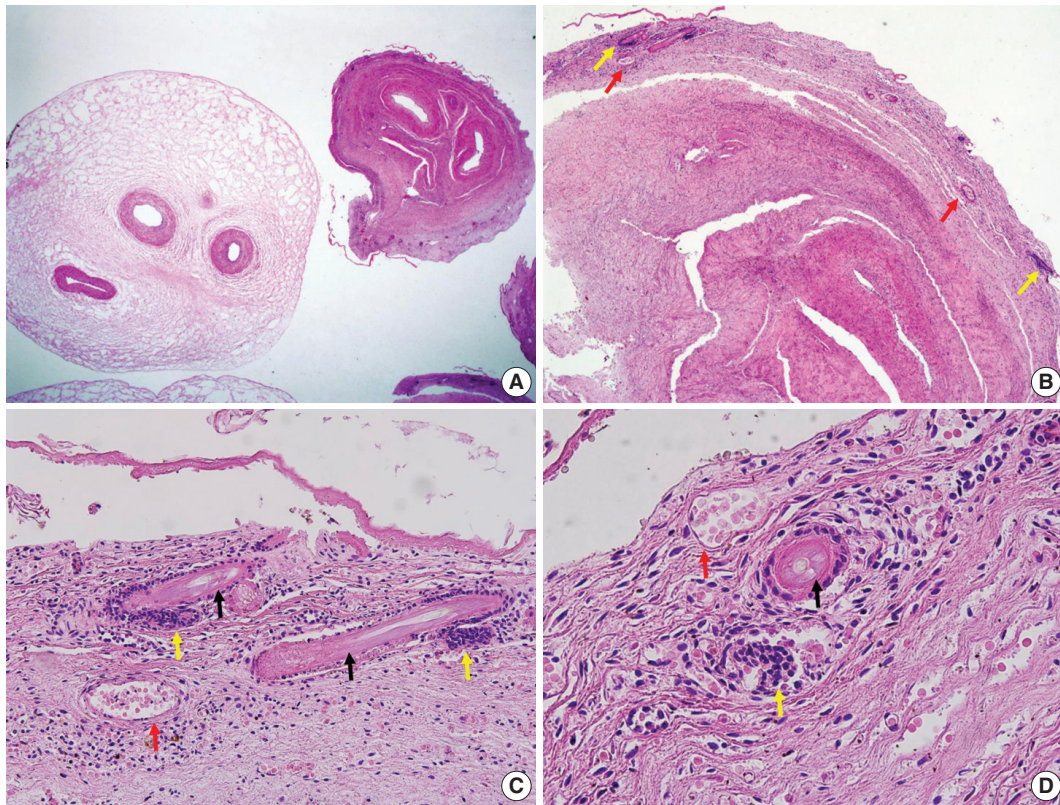


Fig. 3. Microscopic features of the umbilical cord at the stricture. (A) Dense fibrosis of the Wharton jelly at the site of constriction (right) and adjacent edematous Wharton jelly (left). (B) Multiple hair follicles (yellow arrows) and capillaries (red arrows). (C, D) Hair shafts (black arrows) with adjacent papillary mesenchymal body of the hair follicles (yellow arrows) and capillaries (red arrows).

Data curation: ENK.

Investigation: ENK.

Methodology: ENK.

Resources: JYS.

Supervision: CJK.

Visualization: CJK.

Writing—original draft: ENK.

Writing—review & editing: CJK, JYS.

Conflicts of Interest

The authors declare that they have no potential conflicts of interest.

REFERENCES

1. Proctor LK, Fitzgerald B, Whittle WL, et al. Umbilical cord diameter percentile curves and their correlation to birth weight and placental pathology. *Placenta* 2013; 34: 62-6.
2. Baergen RN. Cord abnormalities, structural lesions, and cord "accidents". *Semin Diagn Pathol* 2007; 24: 23-32.
3. Horn LC, Faber R, Stepan H, Simon E, Robel R, Wittekind C. Umbilical cord hypercoiling and thinning: a rare cause of intrauterine death in the second trimester of pregnancy. *Pediatr Dev Pathol* 2006; 9: 20-4.
4. Benirschke K. Obstetrically important lesions of the umbilical cord. *J Reprod Med* 1994; 39: 262-72.
5. Lee JK, Jang HL, Kang BH, et al. Percentile distributions of birth weight according to gestational ages in Korea (2010-2012). *J Korean Med Sci* 2016; 31: 939-49.
6. Jung SI, Lee YH, Moon MH, et al. Reference charts and equations of Korean fetal biometry. *Prenat Diagn* 2007; 27: 545-51.
7. Chitkara U, Rosenberg J, Chervenak FA, et al. Prenatal sonographic assessment of the fetal thorax: normal values. *Am J Obstet Gynecol* 1987; 156: 1069-74.
8. Benirschke K, Burton GJ, Baergen RN. *Pathology of the human placenta*. 6th ed. New York: Springer-Verlag, 2016; 403.
9. Peng HQ, Levitin-Smith M, Rochelson B, Kahn E. Umbilical cord stricture and overcoiling are common causes of fetal demise. *Pediatr Dev Pathol* 2006; 9: 14-9.
10. Aljotawi OS, Xiao Y, Zhang D, et al. Generating CK19-positive cells with hair-like structures from Wharton's jelly mesenchymal stromal cells. *Stem Cells Dev* 2013; 22: 18-26.

Metastatic Insulinoma Presenting as a Liver Cyst

Hua Li · Tony El Jabbour · Ankesh Nigam¹ · Hwajeong Lee

Departments of Pathology and Laboratory Medicine and ¹General Surgery, Albany Medical Center, Albany, NY, USA

Insulinoma is usually detected early in the disease course as a benign form due to clinical manifestations associated with hyperinsulinism.¹ Malignant insulinoma presenting as a hepatic cystic metastasis has not been described in the literature.

CASE REPORT

A 74-year-old woman with no significant past medical history presented with abdominal pain and vomiting. Abdominal computed tomography scan showed five enhancing hepatic masses measuring up to 7.6 cm in greatest dimension, and a cyst, measuring 6.2 cm in greatest dimension, in the medial segment of the left hepatic lobe (Fig. 1). One of the mass lesions was biopsied and showed a well-differentiated neuroendocrine tumor. Subsequent octreotide scan showed an additional focus of uptake in the pancreatic tail measuring 2.1 cm.

The patient was placed under active surveillance. Three months later, she developed worsening diaphoretic episodes and tremors. Initial blood testing showed: proinsulin 1,290 pmol/L (range, 1.7 to 12 pmol/L), glucose 42 mg/dL (range, 65 to 99 mg/dL), insulin 40.3 µIU/mL (range, 2.6 to 24.9 µIU/mL), and C-peptide 10.4 ng/mL (range, 1.1 to 4.4 ng/mL). Initial conservative management failed. Therefore, the patient underwent distal pancreatectomy with splenectomy and resection of the hepatic tumors and cyst.

Grossly, the pancreatic tail displayed a 2.6-cm-sized, ill-defined, firm and tan solid nodule. The resected hepatic segments

exhibited multiple well-demarcated lobulated tan nodules, measuring up to 6.5 cm in greatest dimension. A portion of the hepatic cyst wall measuring 2.4 cm was also received.

Microscopic examination of the pancreatic tail nodule showed a proliferation of neoplastic cells arranged in nested and trabecular patterns (Fig. 2). The neoplastic cells were relatively uniform and cuboidal, with finely granular, amphophilic to eosinophilic cytoplasm and centrally located round to oval nuclei. A “salt and pepper” chromatin pattern was noted. The mitotic rate was less than 2 mitoses/10 high power fields and the Ki67 proliferation index was 0.05%. A diagnosis of well-differentiated neuroendocrine tumor, World Health Organization (WHO) grade 1, was rendered. Given the clinical history, the overall findings were consistent with functioning pancreatic neuroendocrine tumor (PanNET), insulinoma. The liver masses were metastatic well-differentiated neuroendocrine tumor from the pancreas with the Ki67 proliferation index 1.75%, WHO grade 1.

The liver cyst was lined by neoplastic cells, which were morphologically identical with those in the pancreatic tumor. Scattered tumor nests were noted in the cyst wall. These cells were positive for synaptophysin and cytokeratin AE1/AE3, confirming the diagnosis of cystic metastasis of pancreatic well-differentiated neuroendocrine tumor (Fig. 3).

The postoperative course was uneventful. The postoperative insulin level dropped to normal. The patient has been free of symptoms for 3 months and is doing well.

This study was approved by the Institutional Review Board of Albany Medical Center with a waiver of informed consent (IRB Protocol #5036, Date 1/16/2018) and performed in accordance with the principles of the Declaration of Helsinki.

Corresponding Author

Hwajeong Lee, MD
Department of Pathology and Laboratory Medicine, Albany Medical Center, 47 New Scotland Ave., MC81, Albany, NY 12208, USA
Tel: +1-518-2626903, Fax: +1-518-2623663, E-mail: LeeH5@amc.edu

Received: December 11, 2018 Revised: January 7, 2019

Accepted: January 14, 2019

DISCUSSION

PanNETs, also known as islet cell tumors, account for 1%–2%



Fig. 1. Computed tomography shows one of the metastatic nodules (*) and a cyst (**) in the liver.

of pancreatic tumors.² PanNETs are classified as functioning or non-functioning depending on the secretion of bioactive peptides. Functioning PanNETs secrete one or more biologically active peptides such as insulin, gastrin, glucagon, somatostatin, and vasoactive intestinal peptide, and induce corresponding clinical symptoms, while non-functioning PanNETs are usually asymptomatic.² Due to the clinical symptoms resulting from the secretion of biologically active peptides, functioning PanNETs tend to present earlier in the disease course, whereas non-functioning tumors remain silent until metastasis and associated symptoms ensue.³

In about 40%–80% of patients with PanNETs, metastases are detected at diagnosis, commonly in the liver.⁴ Cystic PanNETs demonstrate indolent clinical behavior compared to solid tumors.⁵ Metastatic neuroendocrine tumors are usually solid; however, cystic hepatic metastases of ileal neuroendocrine tumor have been re-

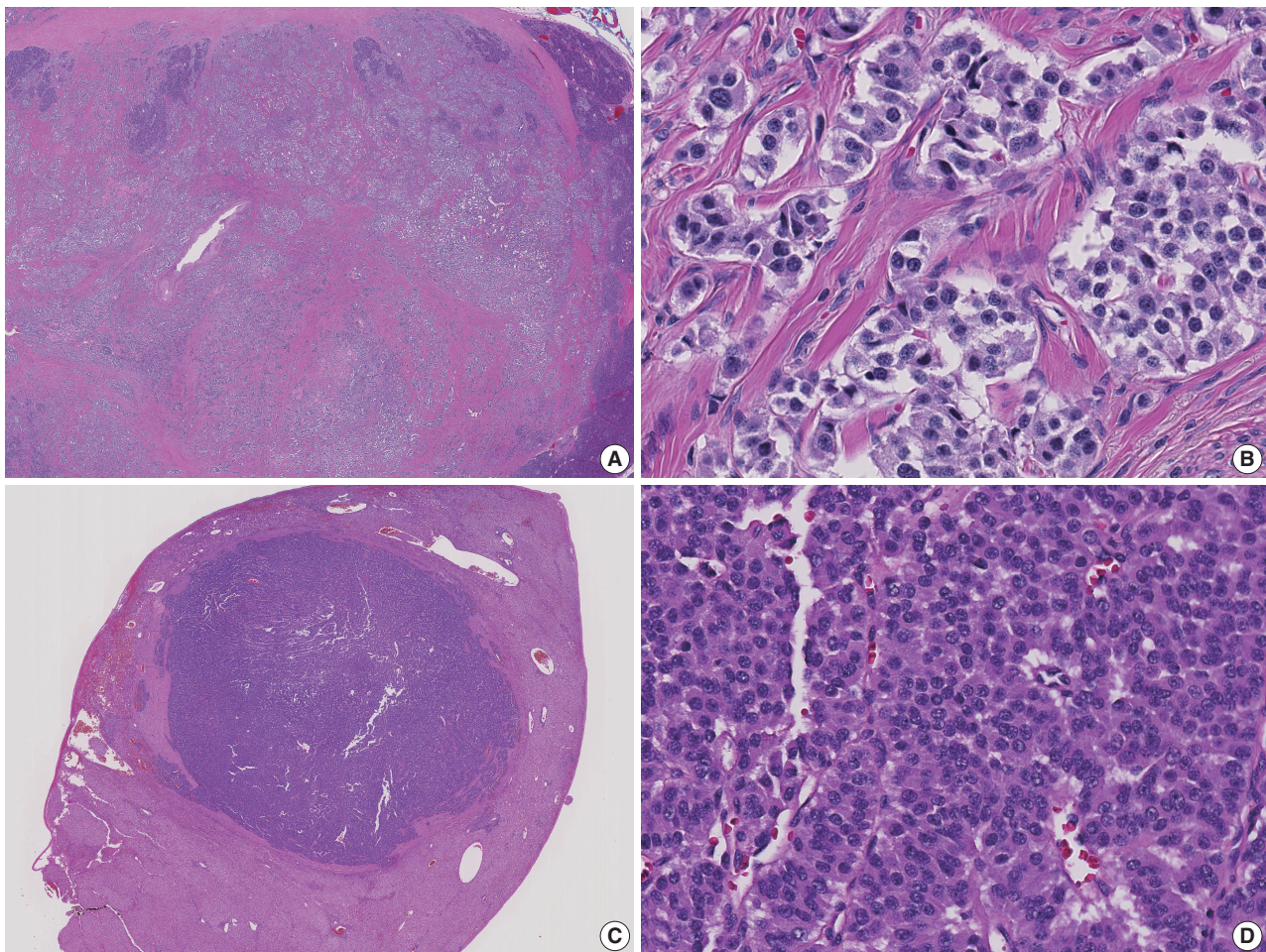


Fig. 2. Primary pancreatic neuroendocrine tumor and hepatic metastasis. (A) Scanning view of the tumor in the pancreas. (B) Higher magnification view shows "salt and pepper" chromatin pattern of the tumor cells. (C) Scanning view of the solid hepatic metastasis. (D) Higher magnification view of the hepatic metastasis shows trabecular growth pattern.

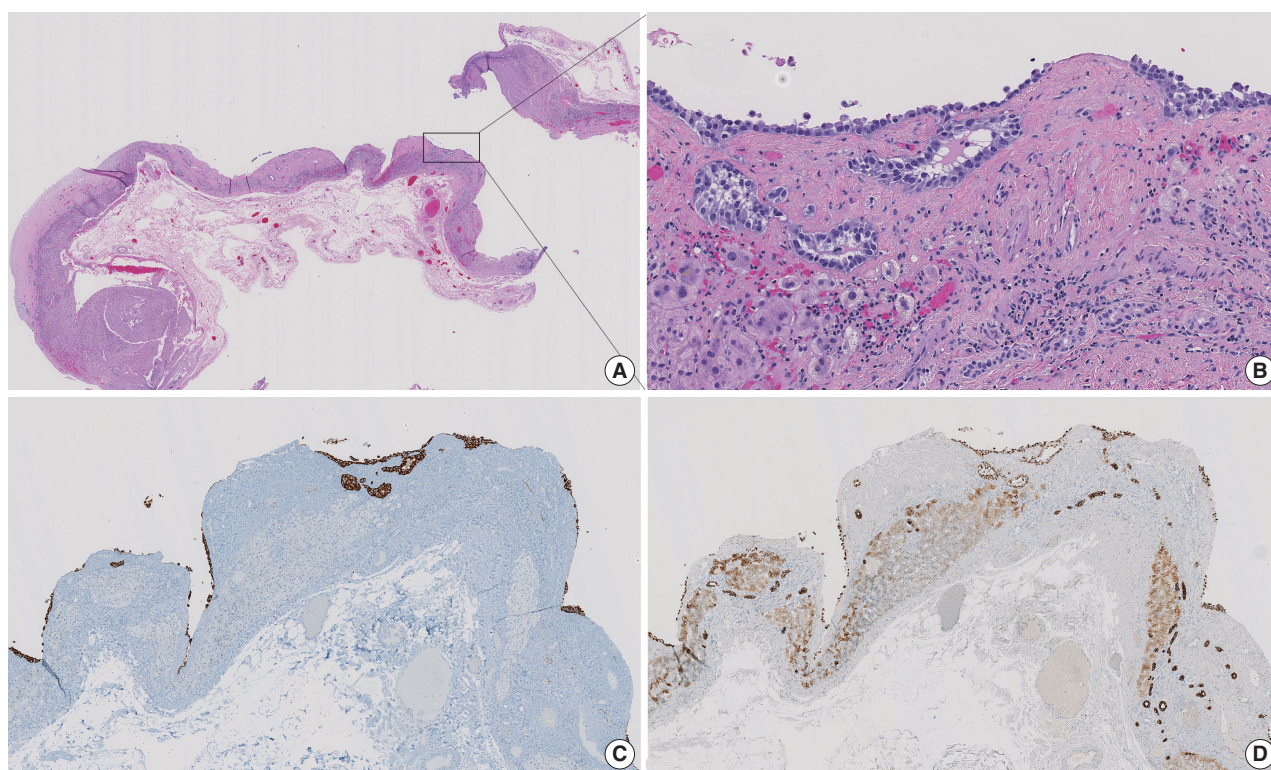


Fig. 3. Hepatic cystic metastasis of pancreatic well-differentiated neuroendocrine tumor. (A) Scanning view shows cyst walls. (B–D) Medium-power view demonstrates neoplastic cells lining the cyst (B) that are positive for synaptophysin (C) and cytokeratin AE1/AE3 (D).

ported.^{6,7} Metastatic PanNET presenting as a liver cyst has not been reported in the literature.

Insulinoma is the most common functioning PanNET and constitutes 30%–45% of the cases.¹ Insulinoma is usually smaller (<2 cm in diameter) than non-functioning PanNETs (often larger than 5 cm in diameter), due to the early diagnosis of insulinoma secondary to symptoms associated with hyperinsulinism.² Interestingly, however, symptoms related to hypoglycemia manifested late in the disease course in our patient, 3 months after the confirmation of liver metastasis. Our case illustrates that the tumor burden of functioning PanNET may not always correlate with the severity of the symptoms. Alternatively, a neuroendocrine tumor may acquire functionality during the disease progression and a nonfunctioning tumor may transition into a functioning tumor.⁸

Our objective is to present a unique case of cystic hepatic metastasis of a functioning PanNET. Moreover, metastatic insulinoma is rare (range, 2.4% to 17.9%; average, 8.4%).^{2,9} Cystic lesions of the liver encompass a variety of pathologic entities. Although rare, cystic metastasis of neuroendocrine tumor needs to be considered as a differential diagnosis when evaluating hepatic cysts. Notably, cystic metastasis of neuroendocrine tumor in the liver would be a diagnostic pitfall when the primary lesion is occult, as have often been described.¹⁰

ORCID

Hua Li: <https://orcid.org/0000-0001-7481-3942>

Tony El Jabbour: <https://orcid.org/0000-0002-6823-1919>

Ankesh Nigam: <https://orcid.org/0000-0002-7565-6333>

Hwajeong Lee: <https://orcid.org/0000-0001-7005-6278>

Author Contributions

Conceptualization: HL (Hwajeong Lee).

Data curation: HL (Hua Li).

Formal analysis: HL (Hua Li), TEJ.

Investigation: HL (Hua Li), TEJ, AN, HL (Hwajeong Lee).

Methodology: HL (Hua Li), TEJ, HL (Hwajeong Lee).

Project administration: HL (Hwajeong Lee).

Resources: AN, HL (Hwajeong Lee).

Supervision: HL (Hwajeong Lee).

Validation: AN, HL (Hwajeong Lee).

Visualization: HL (Hua Li), TEJ.

Writing—original draft: HL (Hua Li).

Writing—review & editing: HL (Hua Li), TEJ, AN, HL (Hwajeong Lee).

Conflicts of Interest

The authors declare that they have no potential conflicts of interest.

REFERENCES

1. Halfdanarson TR, Rubin J, Farnell MB, Grant CS, Petersen GM. Pancreatic endocrine neoplasms: epidemiology and prognosis of pancreatic endocrine tumors. *Endocr Relat Cancer* 2008; 15: 409-27.
2. Bosman FT, Carneiro F, Hruban RH, Theise ND. WHO classification of tumours of the digestive system. 4th ed. Lyon: International Agency for Research on Cancer, 2010; 322-6.
3. Halfdanarson TR, Rabe KG, Rubin J, Petersen GM. Pancreatic neuroendocrine tumors (PNETs): incidence, prognosis and recent trend toward improved survival. *Ann Oncol* 2008; 19: 1727-33.
4. Zhang X, Song J, Liu P, et al. A modified M-stage classification based on the metastatic patterns of pancreatic neuroendocrine neoplasms: a population-based study. *BMC Endocr Disord* 2018; 18: 73.
5. Cloyd JM, Kopeccky KE, Norton JA, et al. Neuroendocrine tumors of the pancreas: degree of cystic component predicts prognosis. *Surgery* 2016; 160: 708-13.
6. Fiori S, Del Gobbo A, Gaudioso G, et al. Hepatic pseudocystic metastasis of well-differentiated ileal neuroendocrine tumor: a case report with review of the literature. *Diagn Pathol* 2013; 8: 148.
7. Isomura T, Kojiro M, Kawano Y, et al. Small multiple carcinoid tumors occurring in the ileum with a pseudocystic liver metastasis. *Acta Pathol Jpn* 1980; 30: 137-43.
8. Yoshioka M, Shibata S, Uchinami H, et al. The transformation of a nonfunctioning islet cell tumor of the pancreas into a proinsulinoma under conditions of lung metastasis. *Intern Med* 2015; 54: 785-90.
9. Bozkirli E, Bakiner O, Abali H, et al. A case of inoperable malignant insulinoma with resistant hypoglycemia who experienced the most significant clinical improvement with everolimus. *Case Rep Endocrinol* 2013; 2013: 636175.
10. Alexandraki K, Angelousi A, Boutzios G, Kyriakopoulos G, Rontogianni D, Kaltsas G. Management of neuroendocrine tumors of unknown primary. *Rev Endocr Metab Disord* 2017; 18: 423-31.

